10-19-2015

Reactivity of 1,2,5,6-Tetrathiocines

Justin David Wrixon
University of Windsor

Reactivity of 1,2,5,6-Tetrathiocines

By

Justin D. Wrixon

A Thesis
Submitted to the Faculty of Graduate Studies
through the Department of Chemistry and Biochemistry
in Partial Fulfillment of the Requirements for
the Degree of Master of Sciences
at the University of Windsor

Windsor, Ontario, Canada

2015

Reactivity of 1,2,5,6-Tetrathiocines

by

Justin D. Wrixon

APPROVED BY:

_____

B. S. Zielinski
Department of Biological Sciences

_____

C. L. B. Macdonald
Department of Chemistry and Biochemistry

_____

J. M. Rawson, Advisor
Department of Chemistry and Biochemistry

September 21, 2015

DECLARATION OF CO-AUTHORSHIP / PREVIOUS PUBLICATION

I. Co-Authorship Declaration

I hereby declare that this thesis incorporates some material that is the result of joint research, as follows:

For all the structures presented in Chapters 2 – 5 of this thesis, crystallographic data collection and refinement was performed by both Dr. Jeremy Rawson and myself. All elemental analysis and high resolution mass spectrometry were performed by Dr. Janeen Auld. Figures of cyclic voltammograms presented in Chapters 2 and 3 were generated by Yassine Beldjoudi. The DFT calculations presented in this thesis were undertaken by Dr J.J. Hayward.

The starting material *N,N′*-dimethylbenzimidazole and some samples of bis-(dimethoxybenzo)-1,2,5,6-tetrathiocine were prepared by Dr. John Hayward and Mr O. Raza respectively.

The work presented in Chapter 5 of this thesis incorporates the results of research undertaken in collaboration with two undergraduate students, Mr Osman Raza and Mr Mohamed Harb. Crystals of DOXBDTA˙ and DOXEBDTA˙ suitable for X-ray diffraction were provided by Mohamed Harb and Osman Raza respectively.

I am aware of the University of Windsor Senate Policy on Authorship and I certify that I have properly acknowledged the contribution of other researchers to my thesis, and have obtained written permission from each of the co-author(s) to include the above material(s) in my thesis.

I certify that, with the above qualification, this thesis, and the research to which it refers, is the product of my own work.

II. Declaration of Previous Publication

At the time of submission of this thesis, some of the work originating from the studies described in this thesis have already been published or have been submitted for publication as follows:

"Oxidative addition chemistry of tetrathiocines: synthesis, structures and properties of group 10 dithiolate complexes", J. D. Wrixon, J. J. Hayward, O. Raza and J. M. Rawson, *Dalton Trans.*, 2014, **43**, 2134-2139.

DFT calculations were performed by Dr. J. Hayward and the tetrathiocine starting material was synthesized by Mr. O. Raza. Preparation of the manuscript was performed by myself, Dr. Hayward and Dr. Rawson.

"*Phosphine-control of the oxidative addition chemistry of tetrathiocines to Pd(0): Characterisation of mono-, di- and hexa-nuclear Pd(II) dithiolate complexes*", J. D. Wrixon, J. J. Hayward and J. M. Rawson, *Inorg. Chem.*, 2015, accepted.

DFT calculations were performed by Dr. J. Hayward. Preparation of the manuscript was performed by myself, Dr. Hayward and Dr. Rawson.

"Oxidative Addition of Bis-(dimethoxybenzo)-1,2,5,6-Tetrathiocines to $Pt(PPh_3)_4$: Synthesis and Structures of Mono- and Di-metallic Platinum Dithiolate Complexes, $(dmobdt)Pt(PPh_3)_2$ and $[(dmobdt)Pt(PPh_3)]_2$", Justin D. Wrixon, Zeinab Ahmed, M. Usman Anwar, Yassine Beldjoudi, Nabila Hamidouche, John, J. Hayward and Jeremy M. Rawson, *Polyhedron*, 2015, accepted.

Preparation of the manuscript was performed by myself, Dr. Hayward and Dr. Rawson.

I certify that I have obtained a written permission from the copyright owner(s) to include the above published material(s) in my thesis. I certify that the above material describes

work completed during my registration as a graduate student at the University of Windsor.

I declare that, to the best of my knowledge, my thesis does not infringe upon anyone's copyright nor violate any proprietary rights and that any ideas, techniques, quotations, or any other material from the work of other people included in my thesis, published or otherwise, are fully acknowledged in accordance with standard referencing practices. Furthermore, to the extent that I have included copyrighted material that surpasses the bounds of fair dealing within the meaning of the Canada Copyright Act, I certify that I have obtained a written permission from the copyright owner(s) to include such material(s) in my thesis.

I declare that this is a true copy of my thesis, including any final revisions, as approved by my thesis committee and the Graduate Studies office, and that this thesis has not been submitted for a higher degree to any other University or Institution.

ABSTRACT

This thesis describes selected chemistry of 1,2,5,6-tetrathiocines, 8-membered heterocycles containing four S atoms which can be considered as bis(disulfides). Chapter 1 provides a literature review of the existing chemistry of 1,2,5,6-tetrathiocines. Chapters 2 – 4 examine the oxidative addition chemistry of tetrathiocines to zero-valent group 10 metal complexes in the presence of an auxiliary phosphine ligand under microwave conditions to afford nickel, palladium and platinum dithiolate complexes. These chapters probe the effect of the metal (Chapter 2), the auxiliary phosphine (Chapter 3) and the tetrathiocine (Chapter 4) on the outcome of the chemical reaction, leading to a range of mono-, di- and hexa-metallic complexes which have been fully characterized by multinuclear NMR, mass spectroscopy and X-ray diffraction. Finally, Chapter 6 describes the use of tetrathiocines as precursors to 1,3,2-benzodithiazyl (BDTA) radicals and two new dithiazolyl radicals have been isolated and characterized by X-ray diffraction and EPR spectroscopy.

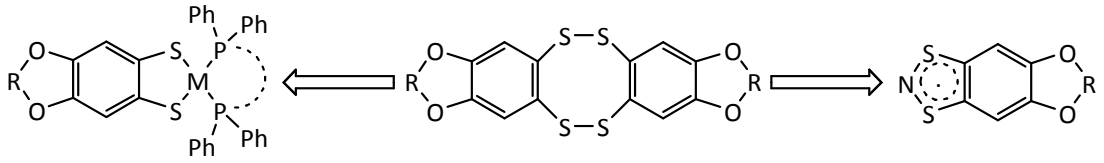

Metal Dithiolate | 1,2,5,6 - Tetrathiocine | 1,3,2- Benzodithiazolyl Radical

DEDICATION

I would like to dedicate this work to my loving fiancé, Stephanie, my parents, Dave and Diane, my sister, Kristen and my entire family who continue to support and believe in me every day.

ACKNOWLEDGEMENTS

First off I would like to thank my supervisor, Dr. Jeremy Rawson, for allowing me the opportunity to join his lab back in 2011 without any prior experience or understanding of what it meant to perform research. You have always been patient, understanding, extremely helpful, and provided me with the opportunity to discover my true passion for chemistry. Since my very first day in the lab, four years ago, your door has always been open for me and I will forever be grateful.

I would like to thank Dr. John Hayward for putting up with me and my ridiculous questions. You were a pivotal part of making my transition into the lab very easy and enjoyable. If it were not for your expertise in microwave reactions, NMR spectroscopy, and knowing the boiling point of every solvent, I would not have been able to accomplish half of what I have today.

I would like to thank Dr. Usman Anwar (aka the Crystal King) for his continuous help in the lab and making every day enjoyable with his humour. Thank you for all of your help and guidance in expanding my knowledge of crystal growing techniques.

Over the last few years, I have made a lot of great friends working in the Rawson lab. I want to thank each and every one of them for the part that they played in making my experience enjoyable. Although some have come and go, it has been wonderful to see all you all accomplish great things.

I would like to thank Dr. Janeen Auld for all of her help with Elemental Analysis and Mass Spectroscopy and Dr. Matt Revington for his help with NMR spectroscopy. I would also like to thank the entire staff within the Department of Chemistry and Biochemistry, without all of you, my experience would not have been as smooth and enjoyable as it was.

I would like to extend a large thank you to Dr. Charles Macdonald for serving as my departmental examiner and taking the time to read both my undergraduate and master's thesis over the last few years. I would also like to thank Dr. Barbara Zielinski

for graciously agreeing to serve as my external department examiner and reading my work.

Last but definitely not least, I would like to thank my Fiancé, Stephanie, and my entire family for their ongoing support and patience. Without their support and motivation, completing this thesis would not have been possible. I owe all of my life successes to each and every one of you.

TABLE OF CONTENTS

LIST OF TABLES

LIST OF FIGURES

LIST OF SCHEMES

LIST OF ABBREVIATIONS, SYMBOLS, AND NOMENCLATURE

B3LYP	Hybrid DFT functional comprising Becke's exchange functional and Lee Yang Parr correlation functional.
BDTA	the benzo-1,3,2-dithiazolyl radical, $C_6H_4S_2N$
$bdtH_2$	1,2-benzene dithiol, $C_6H_4(SH)_2$
CCDC	Cambridge Crystallographic Data Centre
COD	cyclo-octadiene
15-crown-5	1,4,7,10,13-pentaoxacyclopentadecane
CSD	Cambridge Structural Database
Cy	cyclohexyl, $C_6H_{11}^-$
d	Doublet
dba	Dibenzylideneacetone
dd	doublet of doublets
DFT	density functional theory
$dmobdtH_2$	4,5-dimethoxy-benzo-1,2-dithiol, $(MeO)_2C_6H_4(SH)_2$
dppe	diphenylphosphinoethane, $Ph_2PCH_2CH_2PPh_2$
dppf	diphenylphosphinoferrocene, $Ph_2PC_5H_4FeC_5H_4PPh_2$
dppm	diphenylphosphonomethane, $Ph_2PCH_2PPh_2$
dt	doublet of triplets
DTA	Dithiazolyl
EPR	electron paramagnetic resonance
ESI-TOF	electro-spray-ionisation time-of-flight (mass spectroscopy)
Et	ethyl, CH_2CH_3
FT-IR	Fourier-transform infra-red
HOMO	highest occupied molecular orbital
HRMS	High resolution mass spectroscopy
Hz	Hertz
^{I}Pr	*iso*-propyl, $CH(CH_3)_2$
IR	infra-red

LACV3P*	The LACVP basis set extended to triple zeta quality with an additional polarisation function.
LACVP	The LACVP basis set which comprises Slater type orbitals (6-31G) for elements H – Ar and a LANL2DZ basis set for heavier atoms.
LANL2DZ	A computational basis set of double zeta quality which uses an effective core potential basis set for non-valence electrons.
LUMO	lowest unoccupied molecular orbital
m	Multiplet
MBDTA	4-methyl-benzo-1,3,2-dithiazolyl radical, $H_3C{\cdot}C_6H_3S_2N$
M'BDTA	the 3-methyl-benzo-1,3,2-dithiazolyl radical, $H_3C{\cdot}C_6H_3S_2N$
MCPBA	metachloroperbenzoic acid
Me	methyl, CH_3
MHz	Megahertz
mnt^{2-}	maleonitrile dithiolate dianion, $[(NC)_2C_2S_2]^{2-}$
^{n}Bu	*neo*-butyl, $(CH_2)_3CH_3$
NMR	nuclear magnetic resonance
^{n}Pr	*neo*-propyl, $(CH_2)_2CH_3$
o-tol	*ortho*-tolyl, $H_3C{\cdot}C_6H_4$
Ph	phenyl, C_6H_5
ppm	parts per million
R	alkyl group
s	Singlet
t	Triplet
^{t}Bu	*tert*-butyl, $C(CH_3)_3$
$tdtH_2$	4-methyl-benzene-1,2-dithiol (toluenedithiol), $H_3C{\cdot}C_6H_3(SH)_2$
TLC	thin layer chromatography
tmeda	tetramethylethylenediamine, $(H_3C)_2NCH_2CH_2N(CH_3)_2$

CHAPTER 1

Introduction

1.1 An Introduction to Tetrathiocine Chemistry

Tetrathiocines are 8-membered heterocycles containing four S atoms. Many possible structural isomers exist of which the 1,2,3,4-tetrathiocines (**I.1**, **Figure 1.1**) can be formed from lithiation of organics followed by treatment with elemental sulfur[1] and have chemistries akin to polysulfides. The 1,2,5,6-tetrathiocine isomers can be considered as bis(disulfides) and a number of structural studies have been reported and comprise families in which the carbon atoms are variously saturated (**I.2a**)[2,5] or unsaturated (**I.2b**)[3] (**Figure 1.1**). In the latter case the C atoms often form part of a conjugated ring such as a benzo group or other heterocycle. It is this latter group which is particularly relevant to this thesis and their chemistry is reviewed here.

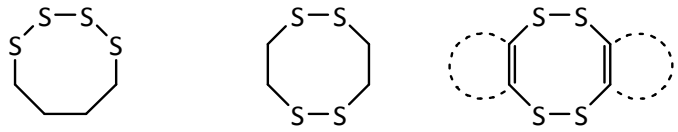

I.1 **I.2a** **I.2b**

1,2,3,4-tetrathiocine 1,2,5,6-tetrathiocines

Figure 1.1 Structures of 1,2,3,4-tetrathiocine (left) and 1,2,5,6-tetrathiocine (right) rings

1.2. Preparation of 1,2,5,6-tetrathiocines

1.2.1 Oxidation of 1,2-dithiols.

Chivers *et al*. reported the oxidation of both fluorinated and chlorinated benzene dithiols 1,2-$C_6X_4(SH)_2$ (X = F, Cl) with SO_2Cl_2 and I_2 respectively led to formation of the 1,2,5,6-tetrathiocines **I.3** and **I.4** (**Figure 1.2**) in yields greater than 85%.[4] Notably the dithiol precursors are not commercially available and need to prepared by sequential lithiation of $C_6X_4H_2$ (X = F, Cl) and treatment with elemental sulfur.[4]

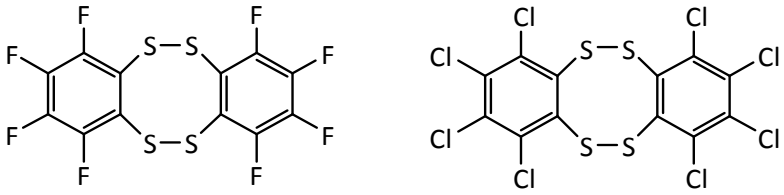

I.3 **I.4**

Figure 1.2 Molecular structure of $(C_6F_4S_2)_2$ (left) and $(C_6Cl_4S_2)_2$

1.2.2 Oxidation of dithiolates

An alternative synthetic strategy to access 1,2,5,6-tetrathiocines is the oxidation of *s*-, *p*- and *d*-block 1,2-dithiolate complexes using oxidants such as I_2, SO_2Cl_2 or MCPBA. Nakata *et al*.[5] carried out a 2-step procedure (**Scheme 1.1**) to prepare a 1,2-dithiol containing a saturated backbone; The reaction of cis-cyclo-octene with S_8O in refluxing CS_2 yielded a mixture of products which included 1,2,3-trithiolane (**I.5**) as a yellow oil in 10% yield. Reduction of **I.5** with $LiAlH_4$ in ether afforded *cis*-cyclooctane-1,2-dithiol (**I.6**) in 76% yield. Subsequent treatment of **I.6** with NaH forms the disodium salt which upon oxidation with MCPBA produced the tri-cyclic 1,2,5,6-tetrathiocine (**I.7**), albeit in very low yield (~ 5%).

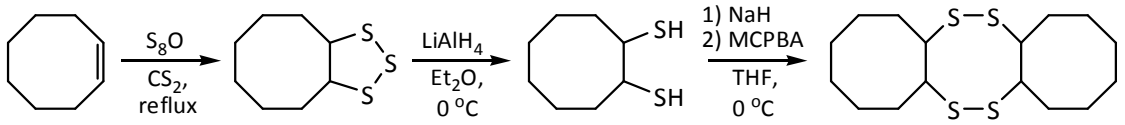

I.5 **I.6** **I.7**

Scheme 1.1 Four-step synthesis of Bis(cyclooctane)-1,2,5,6-tetrathiocine developed by Nakata.[5]

Similar work by Kamigata *et al*.[6] described the oxidation of a *cis*-di-sodium ethene-1,2-dithiolate with iodine/potassium iodide at -10 °C to produce a 1,2,5,6-tetrathiocine (**I.8**) in 14% yield along with small amounts of a bicyclic trimer (**I.9**) and tetramer (**I.10**) (**Scheme 1.2**).

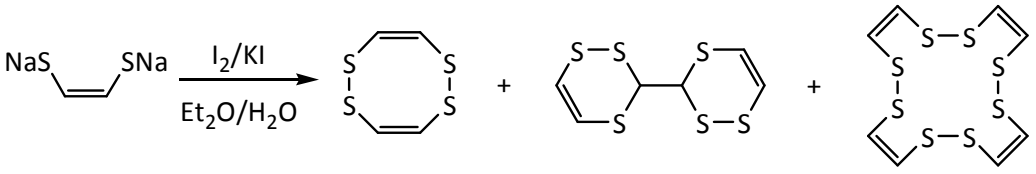

I.8 **I.9** **I.10**

Scheme 1.2 Synthetic products of the oxidation of cis-disodium ethene-1,2-dithiolate with I_2/KI.

The synthesis of tetrathiocines from *p*-block dithiolates has been reported by Sato and coworkers, who showed that the heavier Se analogues could also be prepared in this manner.[7] Their studies used tin(IV) dithiolate complexes which were treated with BuLi and H^+ followed by aerobic oxidation to afford the tetrathiocines in 66% yield.

Due to the known complexity involved in the formation of appropriate substituted ethene-1,2-dithiolate precursors,[8] an alternative approach was used by Kamigata[6] to prepare both mono- and di-substituted tetrathiocines via oxidation of a titanocene dithiolene complex containing one methoxycarbonyl substituent (**I.11**) and two methoxycarbonyl substituents (**I.14**) respectively, with sulfuryl chloride (**Scheme 1.3**). The multi-step synthesis of **I.14** was carried out by following a known literature method.[9] Oxidation of **I.14** resulted in a

mixture of a 1,2-dithiete (**I.15**) (66% yield) along with small amounts of a 1,2,5,6-tetrathiocine (**I.16**) (1.6%), and a substituted tetramer complex (**I.17**) (2.0%). However, oxidation of **I.11** with sulfuryl chloride afforded only 1,2,5,6-tetrathiocine derivatives **I.12** (22%) and **I.13** (17%) respectively.

Notably the propensity for formation of a range of oligomers from these reactions such as the monomeric dithiete (**I.15**), the dimeric tetrathiocine (**I.16**) and tetrameric (**I.17**), appears to hamper the isolation of pure tetrathiocine. Indeed tetrathiocine **I.8** was found to readily convert into tetramer **I.10** (**Scheme 1.2**) at room temperature when added to acetonitrile suggesting that, despite the strength of the S-S bond (~ 250 kJ.mol^{-1}),[10] there is some lability and potential equilibrium between oligomers.

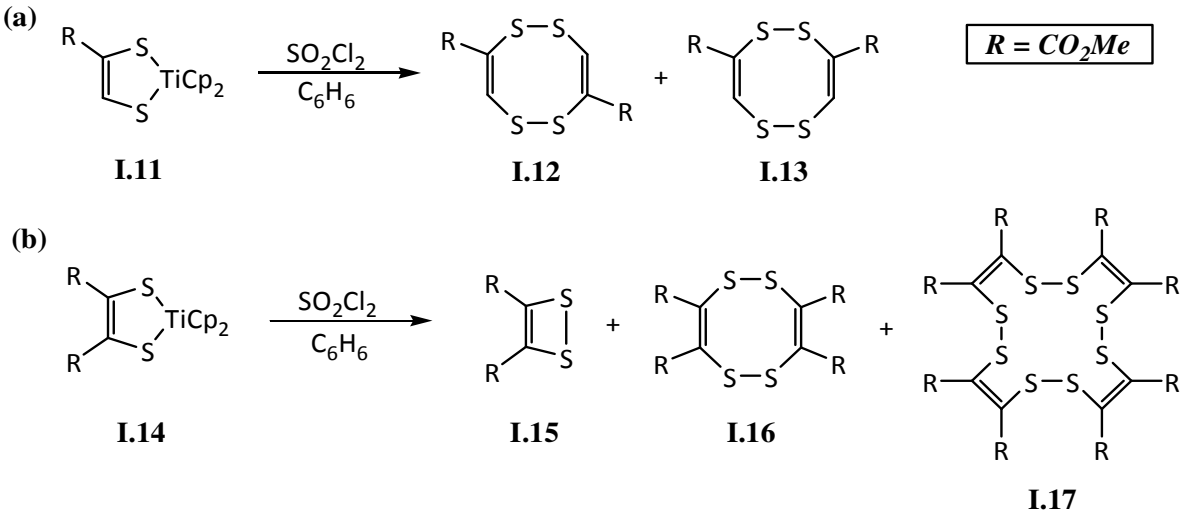

Scheme 1.3 Preparation of **(a)** mono-substituted and **(b)** di-substituted tetrathiocines via oxidation of a titanocene dithiolene complex.

Work by Deplano and coworkers showed that nickel dithiolene complexes could be oxidized with IBr to afford the tetrathiocine.[11] Similar work by Almeida found that monometallic thiophene-dithiolate complexes of Ni^{II} readily oxidized to give tetrameric Ni^{II} clusters and the thiophenotetrathiocine, albeit in low yield.[12] Rauchfuss reported the oxidation of the zinc dithiolate anion $[Zn(C_3S_5)_2]^{2-}$ with SO_2Cl_2 to afford the tetrathiocine C_6S_{10} as a crystalline material in 46% recovered yield.[13]

1.2.3 Reaction of 1,2-dialkoxybenzenes with S_2Cl_2

The synthetic methods described in section 1.2.1 and 1.2.3 typically involve multi-step reactions to form the dithiol/dithiolate precurors prior to mild oxidation, typically affording moderate to poor overall yields of tetrathiocine in multi-step reactions. Stender *et al.*[14] reported that the reaction of several dialkoxy-benzene derivatives with S_2Cl_2, yielded the corresponding tetrathiocines in a one-pot synthesis under mild conditions. Unlike previous methods outlined, formation of these tetrathiocines is believed to likely occur via electrophilic substitution which is promoted by using a polar, ionizing solvent such as glacial acetic acid and the activating nature of the π-donor alkoxy groups (**Scheme 1.4**). This one-step synthesis provides an alternative route to a variety of 1,2,5,6-tetrathiocines in good yields and multi-gram quantities (**Table 1.1**).

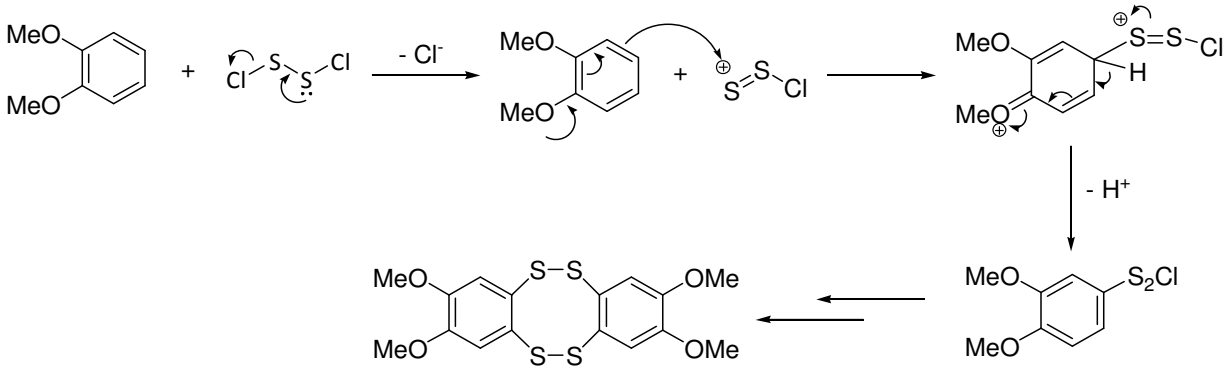

Scheme 1.4 Formation of dialkoxy-benzene tetrathiocines via electrophilic substitution in glacial acetic acid.

Table 1.1 Table of substituted dialkoxy-benzene tetrathiocines prepared by Stender and their respective yields.[14]

Substituent (R)	Recovered Yield (%)
Me	65
Et	16
n-Pr	29
i-Pr	65
½ CH_2	52
½ CH_2CH_2	52

1.2.4 Other synthetic strategies to afford tetrathiocines

An alternative but related strategy to that described in section 1.2.2 is disproportionation of dithiolate complexes. Work by Klar and coworkers describe the thermal decomposition of a Te^{IV} dithiolate to afford the di(methylbenzo)-tetrathiocine.[15] Rogers prepared pyrrole-functionalised tetrathiocines from reduction of bis-thiocyanates with $LiAlH_4$ or with NaOMe or hydrazine (see **Scheme 1.5**).[16] Attwood and coworkers found that reaction of *p*-phenylene diamine with $Na_2S_2O_3$ followed by an acid work up afforded the *p*-diaminobenzo-functionalised tetrathiocine,[17] a reaction originally reported in 1903 by Perkin and Green.[18]

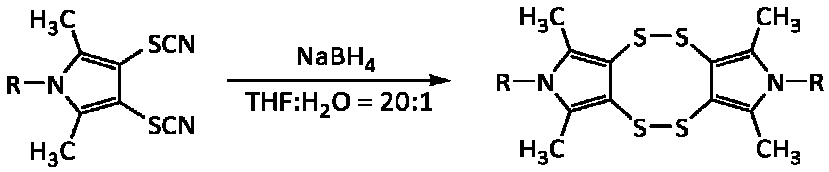

Scheme 1.5 Synthesis of pyrrole-functionalized tetrathiocines prepared by Rogers.

1.3 Structural Studies on 1,2,5,6-Tetrathiocines

Structural studies on 1,2,5,6-tetrathiocines reveal that these structures adopt either a 'chair' or 'twisted' conformation,[19] with the majority (3:1 ratio of the 24 reported structures in the CSD) adopting the chair conformation. The structures of $(C_6F_4S_2)_2$ (**I.3**), which adopts a chair conformation, and $(C_6Cl_4S_2)_2$ (**I.4**), which adopts a twisted conformation are shown in **Figure 1.2**.

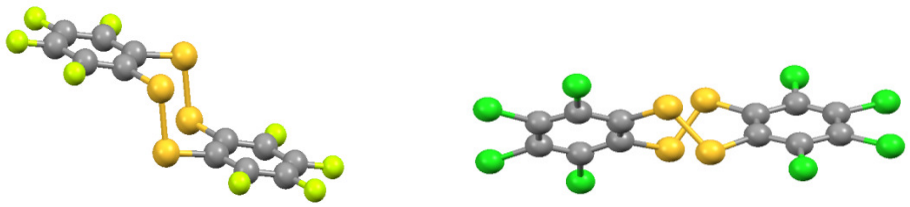

Figure 1.3 Crystal structure of $(C_6F_4S_2)_2$ (left) and $(C_6Cl_4S_2)_2$ (right)

1.4 Reactivity of 1,2,5,6-Tetrathiocines

The reaction chemistry of tetrathiocines is predominantly that of six reaction types; which are summarized below.

1.4.1 Cycloaddition.

A series of reports have shown that the tetrathiocine can act as a dithio-orthoquinone ('dithiete') in [4+2] cycloaddition reaction with alkynes, affording thianthrenes with recovered yields in the range 38 – 80%.[13, 20]

1.4.2 Oligomerisation

Despite the strength of the S-S bond (264 $kJ.mol^{-1}$),[21] tetrathiocines undergo a number of reactions which would indicate S-S bond cleavage is labile in solution. For example part of their chemistry appears to reflect dithiete character (section 1.4.1) and they undergo dimerization to form 16-membered heterocycles at ambient temperature in chloroform or acetonitrile (76% yield).[6b,22] Further work is necessary to fully understand the mechanistic aspects of these conversions between different oligomers. Given the strength of the S-S bond, it is likely that such transformations may be acid and/or base-catalyzed or proceed via a redox process. Indeed, in the presence of base, conversion of the parent tetrathiocine $(H_2C_2S_2)_2$ has been found to afford a series of trimeric $H_6C_6S_6$ rings differing in the nature of the *trans vs cis* conformations around the C=C bond.[23] In some cases disproportionation occurs with formation of both the 16-membered macrocycle as well as the dithiete.[22b]

1.4.3 Photolysis and Thermolysis

Photolysis of tetrathiocines occurs *via* S-atom abstraction leading to ring contraction under mild conditions (8 – 20 ^{o}C, 6 – 24 h) to form the 6-membered thianthrenes in high to quantitative yields (63- 98%).[7a,24] The intermediate 7-membered C_4S_3 ring generated after a single S-atom abstraction has been isolated in some instances in low yield (10%).[24b] In the case of **I.3** an unusual ring expansion occurs under irradiation leading to a 9-membered C_4S_5 heterocycle.[4] The 6-thianthrenes have been shown to be redox active.[24a]

In some circumstances this ring-contraction reaction has additionally been shown to be a thermally-driven process,[25] although polymerization has also been reported for $(C_6H_4S_2)_2$.[26] Further S atom abstraction has also been observed at elevated temperatures during [4+2] cyclisation reactions leading to highly-functionalised thiophene derivatives.[20b] An alternative decomposition route under irradiation is trithiole formation.[27]

1.4.4 Coordination Chemistry

Tetrathiocines undergo exchange reactions with transition metal thiolate complexes such as $[Me_4N][Mo(=O)(SPh)_4]$ in the presence of $NaBH_4$ to generate the corresponding dithiolate complexes and elimination of PhSSPh.[28] The Mo^V species is reduced by the borohydride anion in solution to produce the Mo^{IV} species. Similar complexes have been prepared with the group 12 metals (zinc, cadmium and mercury),[28b] as well as tungsten.[28d] Alternative transition metal precursors which have been employed include thiotungstates such as $[PPh_4]_2[WS_4]$.[29]

1.4.5 Chlorination, Reduction and Alkylation

Previous work in this group has shown that chlorination of tetrathiocines provides a convenient route to bis(sulfenyl chlorides) which are used as intermediates towards free radical synthesis (see Chapter 5).[30] Similar oxidation reactions have been reported for $[(F_3C)_2C_2S_2]_2$ although over chlorination can reduce the C=C double bond.[31]

Reduction of the tetrathiocine with HOC_2H_4SH in a methanol/water mix has been shown to drive formation of an equilibrium between the dithiol and the tetrathiocine.[32] Similarly H_3PO_2 can be used for this reduction process.[17]

Alkylation of tetrathiocines with MeI occurs with S-S bond cleavage, alkylation of the sulfur atom and elimination of I_2.[17]

1.4.6 Trithiole Generation

Treatment of tetrathiocines with NaSH affords the trithiole in good yields (77%).[33]

1.5 Overview of this Thesis

It is clear from these studies that ring expansion and contraction processes are prevalent under irradiation, thermolysis or in the presence of base. Under suitable conditions equilibria can be achieved between the dithiol and the tetrathiocine indicating the reaction chemistry has the potential to be complex in nature. However tetrathiocines appear potentially useful building blocks for the construction of coordination complexes as well as other organic heterocycles.

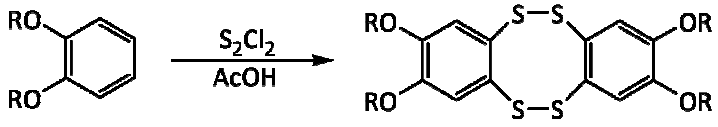

Scheme 1.6 Synthetic methodology for the formation of benzo-fused tetrathiocines.

In this thesis, Chapters 2 – 4 describe the oxidative addition reactions of the S-S bond of 1,2,5,6-tetrathiocines to zero-valent group 10 metals (Ni, Pd, Pt) in the presence of an auxiliary phosphine ligand to form metal dithiolate complexes. Chapter 2 examines the reactivity as a function of metal, Chapter 3 examines the effect of the auxiliary phosphine ligand and Chapter 4 examines the effect of the tetrathiocine on reactivity. Chapter 4 also extends the scope of tetrathiocines available by expanding the synthetic methodology developed by Stender (**Scheme 1.6**).[14] In Chapter 5 the oxidation of the disulfide bond to form a bis(sulfenyl chloride) is explored as a route to 1,3,2-dithiazolyl radicals. Both sets of reactions indicate that the chemistry of these tetrathiocines can be considered largely as the chemistry of a bis(disulfide).

1.6 References

1. T. Janosik, B. Stensland and J. Bergman, *J. Org. Chem.*, 2002, **67**, 6220.

2. For examples see; **(a)** M. H. Goodrow, M. M. Olmstead and W. K. Musker, *Tet. Lett.*, 1982, **32**, 3231; **(b)** G. Gafner and L. J. Admiraal, *Acta Cryst.*, 1969, **B25**, 2114; **(c)** C. Vinas, W. M. Butler, F. Teixidor and R. W. Rudolph, *Organomet.*, 1984, **3**, 503; **(d)** R.D. Adams, M. Huang and S. Johnson, *Polyhedron*, 1978, **17**, 2775.

3. **(a)** M.C.Aragoni, M.Arca, F.A.Devillanova, F.Isaia, V.Lippolis, A.Mancini, L.Pala, A.M.Z.Slawin, J.D.Woollins, *Chem.Comm.*, 2003, 2226; **(b)** F.Bigoli, P.Deplano, M.L.Mercuri, M.A.Pellinghelli, G.Pintus, E.F.Trogu, G.Zonnedda, H.H.Wang, J.M.Williams, *Inorg. Chim. Acta*, 1998, **273**, 175; **(c)** A.I.Kotov, S.V.Konovalikhin, R.V.Pisarev, G.V.Shilov, O.A.Dyachenko, E.B.Yagubskii, *Mendel. Comm.*, 1994, 180; **(d)** A.Penicaud, K.Boubekeur, A.I.Kotov, E.B.Yagubskii, *Acta. Cryst.*, 2000, **C56**, 497; **(e)** F.Bigoli, P.Deplano, F.A.Devillanova, J.R.Ferraro, V.Lippolis, P.J.Lukes, M.L.Mercuri, M.A.Pellinghelli, E.F.Trogu, J.M.Williams, *Inorg. Chem.*, 1997, **36**, 1218; **(f)** H.Sugimoto, M.Tarumizu, K.Tanaka, M.Miyake, H.Tsukube, *Dalton Trans.*, 2005, 3558; **(g)** E.Fanghanel, R.Herrmann, J.Bierwisch, H.Hartung, U.Baumeister, G.Maier, H.P.Reisenauer, *J. Prakt Chem. Chem. Ztg.*, 1994, **336**, 444; **(h)** D.J.Mitchell, E.L.Lippert, *Acta Cryst.* 1965, **18**, 559; **(i)** E.J.Yearley, E.L.Lippert, D. J. Mitchell, A. A. Pinkerton, *Acta Cryst*., 2007, **C63**, 0576.

4. T. Chivers, M. Parvez, I. Vargas-Baca and G. Schatte, *Can. J. Chem.*, 1998, **76**, 1093.

5. A. Ishii, M. Suzuki, T. Sone and N. Nakata, *Phosphorus, Sulfur, and Silicon Relat. Elem.*, 2009, **184**, 1184.

6. **(a)** T. Shimizu, K. Iwata and N. Kamigata, *Angew. Chem. Int. Ed. Engl.*, 1996, **35**, 2357; **(b)** T. Shimizu, H. Murakami, Y. Kobayashi, K. Iwata and N. Kamigata, *J. Org. Chem.*, 1998, **63**, 8192.

7. **(a)** S. Ogawa, M. Sugawara, Y. Kawai, S. Nizuma, T. Kimura and R. Sato, *Tet. Lett.*, 1999, **40**, 9101; **(b)** T. Yamamoto, S. Ogawa, M. Sugawara, Y. Kawai and R. Sato, *Bull. Chem. Soc. Jpn*., 2006, **79**, 460.

8. W. E. Truce, M. M. Boudakian, R. F. Heine and R. J. McManimie, *J. Am. Chem. Soc.*, 1956, **78**, 2743.

9. C. M. Bolinger and T. B. Rauchfuss, *Inorg. Chem.*, 1982, **21**, 3947.

10. *An Introduction to Organosulfur Chemistry*, R. J. Cremlyn, John Wiley and Sons: Chichester, 1996.

11. F. Bigoli, P. Deplano, M. L. Mercuri, M. A. Pellinghelli, G. Pintus, E. F. Trogu, G. Zonnedda, H. H. Wang and J. M. Williams, *Inorg. Chim. Acta*, 1998, **273**, 175

12. A. I. S. Neves, I. C. Santos, L. C. J. Pereira, C. Rovira, E. Ruiz, D. Belo and M. Almeida, *Eur. J. Inorg. Chem.*, 2011, 4807.

13. X. Yang, T. B.Rauchfuss and S.Wilson, *Chem.Commun.*, 1990, 34.

14. K. W. Stender, N. Wolki and G. Klar, *Phosphorus, Sulfur, and Silicon Relat. Elem*., 1989, **42**, 111.

15. J. Kopf, K. von Deuten, B. Nakhdjavan and G. Klar, *Z. Naturforschung B*, 1979, **34**, 48.

16. K. Zong, W. Chen, M. P. Cava and R. D. Rogers, *J.Org.Chem.*, 1996, **61**, 8117.

17. M. V. Lakshmikantham, M. S. Raasch, M. P. Cava, S. G. Bott and J. L. Atwood, *J. Org. Chem.*, 1987, **52**, 1874.

18. A. G. Green and A. G. Perkin, *J. Chem. Soc*., 1903, **83**, 1201.

19. A search of the CSD (2013) revealed 24 structures of tetrathiocines with unsaturated carbon backbones of which 18 adopt a chair conformation and 6 adopt a twisted conformation.

20. **(a)** D. J. Harrison and U. Fekl, *Chem.Commun.*, 2009, 7572; **(b)** T. Shimizu, H. Murukami and N. Kamigata, *J. Org. Chem.*, 1999, **64**, 8489.

21. Chemistry Data Book, SI Edition, J.G. Stark and H.G. Wallace, J. Murray. Publ. (1980).

22. T. Shimizu, K. Iwata, N. Kamigata, *Angew. Chem. Int. Ed. Engl.* 1996, **108**, 2505.

23. T. Shimizu and N. Kamigata, *J. Organomet. Chem.*, 2000, **611**, 106.

24. **(a)** T. Kimura, K. Tsujimura, S. Mizusawa, S. Ito, Y. Kawai, S. Ogawa and R. Sato, *Tet. Lett.*, 2000, **41**, 1801; **(b)** T. Kimura, S. Mizusawa, A. Yoneshima, S. Ito, K. Tsujimura, T. Yamashita, Y. Kawai, S. Ogawa and R. Sato, *Bull. Chem. Soc. Jpn.*, 2002, **75**, 2647; **(c)** T. Kimura, T. Obonai, T. Nozaki, K. Matsui, T. Namauo, A. Yamakawa and Y. Takaguchi, *Heterocycles*, 2010, **80**, 183.

25. M. V. Stasevych, M. Y. Plotnikov, M. O. Platonov, S. I. Sabat, R. Y. Musyanovych and V. P. Novikov, *Heteroatom Chem.*, 2005, **16**, 205.

26. L. Field, W. Stephens and E. Lippert, Jr., *J. Org. Chem.*, 1961, **26**, 4782.

27. E. Fanghaenel, R. Herrmann, J. Bierwisch, H. Hartung, U. Baumeister, G, Maier and H. P. Reisenauer, *Chem. Zeitung*, 1994, **336**, 444.

28. **(a)** K. Baba, T.-A. Okamura, C. Suzuki, H. Yamamoto, T. Yamamoto, M. Ohama and N. Ueyama, *Inorg. Chem.*, 2006, **45**, 894; **(b)** K. Baba, T.-A. Okamura, H. Yamamoto, T. Yamamoto and N. Ueyama, *Inorg. Chem.*, 2008, **47**, 2837; **(c)** K. Baba, T.-A. Okamura, H. Yamamoto, T. Yamamoto, M. Ohama and N. Ueyama, *Chem. Lett.*, 2005, **34**, 44; **(d)** K. Baba, T.-A. Okamura, H. Yamamoto, T. Yamamoto, M. Ohama and N. Ueyama, *Inorg. Chem.*, 2006, **45**, 8365; **(e)** T.-A. Okamura, Y. Ushijima, Y. Omi and K. Onitsuka, *Inorg. Chem.*, 2013, **52**, 381.

29. X. Yang, G. K. W. Freeman, T. B. Rauchfuss and S. R. Wilson, *Inorg. Chem.*, 1991, **30**, 3034.

30. A. Alberola, D. Eisler, R. J. Less, E. Navarro-Moratalla and J. M. Rawson, *Chem. Commun.*, 2010, 6114.

31. S. Reimann-Anderson, H. Pritzkow and W. Sundermeyer, *Chem. Ber.*, 1994, **127**, 533.

32. J. Houk and G. M. Whitesides, *J. Am. Chem. Soc.*, 1987, **109**, 6825.

33. K. Rasheed and J. D. Warkentin, *J. Org. Chem.*, 1980, **45**, 4806.

CHAPTER 2

Synthesis, Structures and Properties of (dmobdt)M(dppe) (M = Ni, Pd and Pt).

2.1 Introduction

The chemistry of transition metal dithiolene complexes has continued to be a large active field of study since its first appearance in the early 1960's, due to the unique redox and structural properties which they exhibit.[1] Previous studies on nickel dithiolene complexes have indicated that the redox chemistry of these complexes is sensitive to the dithiolene ligand.[2] The non-innocent nature of the dithiolene ligand system provides us with two possible resonance structures for these C_2S_2M rings (see **Figure 2.1**). These ligands can be considered non-innocent due to the uncertainty in their oxidation state, which in turn makes it more difficult to define the oxidation state of the metal center when a complex is formed.[3] The oxidative addition of a dithiolene ligand to a metal(0) complex can result in a metal center in the +2 oxidation state resulting in the 1,2-dithiolate resonance form. Conversely, the dithiolene can be charge neutral, bonding in a dithioketone resonance form. Indication of which resonance form is likely observed can be determined upon further crystallographic study of these complexes. It has previously been reported[4] that the C–S single bond lengths for sp^2 hybridized carbon atoms typically range from 1.71 – 1.75 Å, whereas the C=S bond lengths typically range from 1.67 – 1.68 Å.

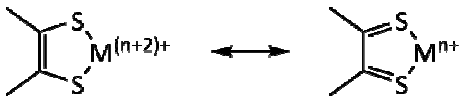

Figure 2.1 The possible resonance forms for a transition metal dithiolene complex: ene-1,2-dithiolate dianion (*left*) and neutral dithioketone (*right*).

2.1.1 Redox Properties

An understanding of the redox properties of group 10 dithiolene metal complexes is essential in determining their potential in future applications.[5] Nickel, palladium, and platinum have been observed to form stable complexes in the +2 oxidation state. Whilst complexes of Ni^{II} ions can be octahedral, tetrahedral or square planar, the larger ligand field and reduced inter-electron repulsion of the heavier group 10 elements favours exclusively the square planar conformation. Nevertheless with medium-strong field ligands, such as dithiolates, Ni^{II} also shows preponderance for square-planar coordination. Previous studies have indicated the ability of Ni(II) dithiolate complexes to undergo a reversible one-electron reduction resulting in the formation of the corresponding Ni(I) complex.[6] Yet in the same study, it was observed that both the corresponding Pd(II) and Pt(II) complexes did not undergo a reversible reduction, indicating the relative instability of Pd(I) and Pt(I) complexes compared to that of Ni(I). By holding the dithiolate ligand constant for all three group 10 complexes, the effect of changing the metal center on the redox properties and their relative stabilities can be determined through the use of cyclic voltammetry.

2.1.2 Structural Properties

Palladium and platinum have been found to undergo very similar chemistry when in the +2 oxidation state.[7] Both Pd(II) and Pt(II) are generally found to exhibit characteristic square planar geometries when forming tetra-coordinate complexes (see **Table 2.1**). However, this is not always the case with Ni(II) which is commonly observed to form both square planar and tetrahedral tetra-coordinate complexes (**Table 2.1**) as well as 5- and 6-coordinate geometries. It is generally observed that that the most noticeable difference between Ni(II) square planar and tetrahedral geometries are their magnetic properties.[8] Square planar complexes exhibit diamagnetic behaviour, whereas tetrahedral complexes exhibit paramagnetic behavior associated with the $e^4t_2^4$ configuration. Thus a combination of structure determination using X-ray crystallography, coupled with magnetic measurements on these complexes, provides complementary information on their geometric preference. A search of the CSD[9] revealed all reported nickel mono- and bis(dithiolene) complexes exhibit a square planar rather than tetrahedral conformation.

As expected, the same was determined to be true for both palladium and platinum, consistent with the known preference for square planar coordination for these tetra-coordinate metals, even in the presence of weak field ligands.

Table 2.1 Most common oxidation states and examples of tetra-coordinate group 10 metal complexes. *Table reproduced from data in reference 6*

Oxidation State	Coordination Number	Geometry	Examples
Ni(II)	4	Square Planar	$NiBr_2(PEt_3)_2$, $[Ni(CN)_4]^{2-}$
Ni(II)	4	Tetrahedral	$NiCl_4^{2-}$, $NiCl_2(PPh_3)_2$
Pd(II)	4	Square Planar	$[PdCl_2]_n$, $[Pd(CN)_4]^{2-}$
Pt(II)	4	Square Planar	$PtCl_4^{2-}$, $Pt(PEt_3)_2(C_6F_5)_2$

2.1.3 Synthesis of Group 10 Dithiolate Complexes

Dithiolene complexes are typically prepared from ligand exchange reactions of *s*-block metal dithiolates with *d*-block metal salts or *via* condensation of the free thiol with transition metal oxo, alkoxo, and amido precursors or the oxidative addition of 1,2-dithietes to low-valent transition metals.[1]

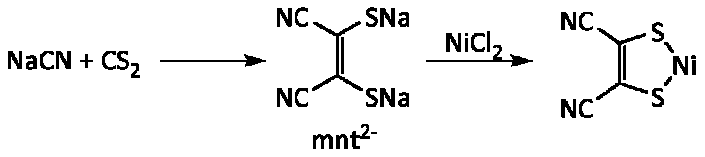

Scheme 2.1 Synthesis of disodium 1,2-maleonitrile-1,2-dithiolate (Na_2mnt) and subsequent transmetallation to afford a Ni^{II} complex.[10]

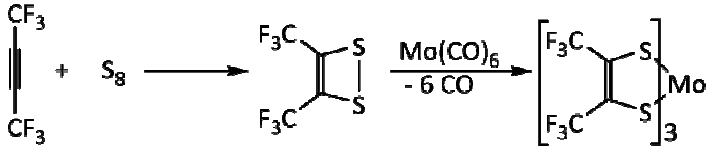

Scheme 2.2 Synthesis of bis(trifluoromethyl)dithiolates by oxidative addition.[11]

However the number of commercially available dithiols is small and much of the chemistry of benzo-fused dithiolate anions focuses on 3,4-dimercaptotoluene ($tdtH_2$) and 1,2-benzendithiol ($bdtH_2$). A search of the CSD (2013) revealed 639 structures containing the benzenedithiolate core. Of those complexes, 68% were comprised of either a benzene dithiolate or toluene dithiolate (53% and 15% respectively).

bdt^{2-} **tdt^{2-}**

Figure 2.2 Common derivatives used in the formation of metal benzo-dithiolene complexes 1,2-benzendithiolato (**bdt^{2-}**) and toluene-3,4-dithiolato (**tdt^{2-}**).

Alternative synthetic strategies to prepare dithiolates include the reaction of metal sulfides with alkynes[12] (which generates dithiolates of the type $R_2C_2S_2^{2-}$) and the oxidative addition of 1,2-dithietes and dithiins to low-valent metals.[13] Again these latter approaches tend to target non-benzo-fused dithiolates. As a consequence the development of new routes to benzo-fused dithiolates may lead to new derivatives in which the steric and electronic properties of the dithiolate can be tailored.

2.1.4. Project Objectives

Notably whilst dithiolate ligands such as mnt^{2-} and $(CF_3)_2C_2S_2^{2-}$ tend to be strongly electron-withdrawing, the presence of alkoxy groups in tetra-methoxy-dibenzo-1,2,5,6-tetrathiocine (**1, Scheme 2.3**) and related systems offers electron-rich, π-donating, dithiolate complexes, thereby moderating the electronic properties of the ligand and in stark contrast to the electron-withdrawing nature of the mnt^{2-} and $(F_3C)_2C_2S_2^{2-}$ dianions.

The goal of the project was to determine an alternative general synthetic pathway to access a variety of different derivatives from readily available starting materials in order to tailor the electronic properties for materials applications. By keeping the tetrathiocine **1** and phosphine co-ligand dppe constant, we can determine the trends in reactivity for

the group 10 metals. Trends in reactivity due to the variation of the tetrathiocine and phosphine co-ligand were investigated in subsequent chapters.

2.2 Results and Discussion

2.2.1 Synthesis of 2',3 ',8 ',9 ' -tetramethoxy-dibenzo-1,2,5,6-tetrathiocine $[(MeO)_2C_6H_2S_2]_2$ (1).

Previous research in the Rawson group has focused on specific methodologies to access 1,2-dithiols and/or 1,2-dithiolate precursors for the synthesis of stable free radicals (see **Chapter 5**). One such methodology proceeds *via* the formation of tetrathiocines from 3,4-dialkoxybenzenes.[14] Implementing the synthetic pathway developed by Stender *et al.*[15], the target tetrathiocine **1** was synthesized from the reaction of 1,2-dimethoxybenzene with S_2Cl_2 in glacial acetic acid under ambient conditions over a period of 18 hrs. Formation of the tetrathiocine is likely to occur *via* electrophilic substitution by ClS_2^+ *para* to the π-donating methoxy group, a site activated to such electrophilic attack. Dissociation of S_2Cl_2 to ClS_2^+ and Cl^- is promoted in the polar, ionizing solvent glacial acetic acid (see **Scheme 2.3**). The initial blue colour of the crude product was discharged by treatment with a few drops of methanoic $SnCl_2$, ultimately affording **1** as a pale yellow solid in moderate recovered yields (~ 40 - 45%, *cf* literature value of 65%, **Table 1.1**).

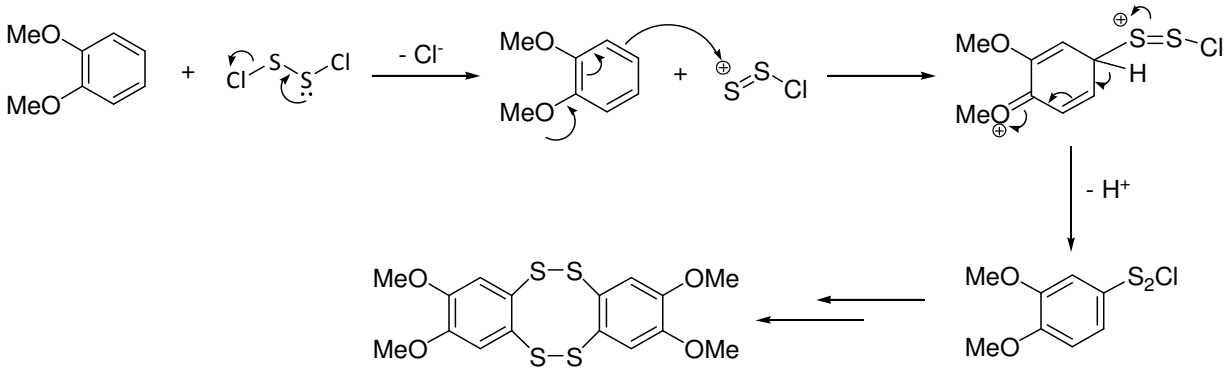

Scheme 2.3 Formation of the tetrathiocine (**1)** via electrophilic substitution.

The low solubility of **1** (and related tetrathiocines) in organic solvents made full characterization difficult, but **1** provided satisfactory elemental analysis.

2.2.2 Synthesis of Group 10 Metal Dithiolene Complexes via Oxidative Addition

Despite the advantages of π-delocalization and conjugation, very few benzo-fused dithiol derivatives have been reported and the chemistry of benzo-fused-1,2-dithiolato metal complexes focuses predominantly on derivatives of commercially available 1,2-benzene-dithiol and toluene-3,4-dithiol (see **Figure 2.2**).[16] Our recent forays into the chemistry of tetrathiocines[6] prompted us to examine the oxidative addition chemistry of such tetrathiocines to low oxidation state transition metals as an alternative two-step synthetic strategy to dithiolate complexes (**Scheme 2.4**).[17]

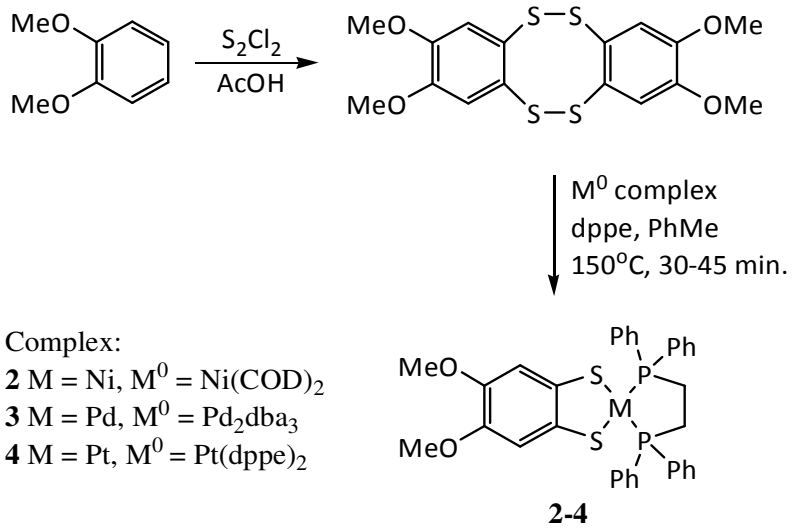

2-4

Scheme 2.4 Two-step synthesis of group 10 dithiolene complexes.

Initial studies examined the reactivity of **1** towards zero-valent group 10 transition metals at ambient temperature, specifically $Ni(COD)_2$, $Pd_2(dba)_3$ and $Pt(PPh_3)_4$, typically in the presence of the chelate phosphine ligand dppe. However, the low solubility of the tetrathiocines in a range of organic solvents led to very slow reactivity. Increasing the reaction temperature afforded a mixture of products which were monitored by ^{31}P NMR (see **Figure 2.3a** for example).

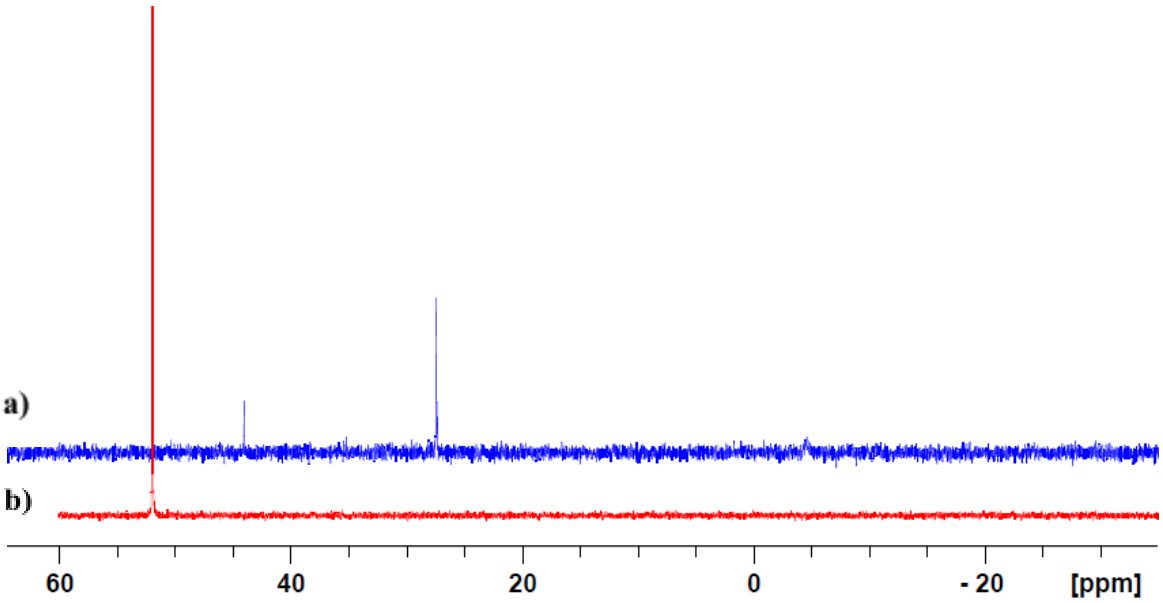

Figure 2.3 Example of *ex situ* ^{31}P NMR spectra for the reaction of Pd_2dba_3 with **1** in the presence of dppe: **a)** after 48 h stirring at 125 °C, **b)** after micro-wave irradiation at 150 °C for 30 mins. [free dppe resonates at -19 ppm]

The use of microwave irradiation has been shown to afford higher selectivity and faster reaction times in many transformations.[18] Reaction of the tetrathiocine with zero-valent group 10 transition metal complexes $Ni(COD)_2$ or Pd_2dba_3 in the presence of 1 equivalent of dppe per metal center or with $Pt(dppe)_2$ in toluene at 150ºC under microwave irradiation for 30 – 45 min afforded complexes (dmobdt)M(dppe) [M = Ni, Pd, Pt], **2-4** respectively, in very good recovered yields (77 – 89%). Examination of the resultant ^{31}P NMR spectra (see **Figure 2.3b** for example) revealed singlet spectra for all three complexes (with satellites arising from $^1J_{Pt\text{-}P}$ coupling in **4**) consistent with a unique ^{31}P environment and ^{31}P chemical shift comparable[19] to other square-planar group 10 M^{II} complexes with MP_2S_2 ligand sets.

In order to confirm formation of complexes **2-4**, high resolution mass spectrometry measurements were obtained by positive ion ESI-TOF indicating the presence of the expected $[M + H]^+$ ion peaks with three replicate acquisitions completed with better than 0.5 ppm mass accuracy. Elemental analysis confirmed the correct carbon and hydrogen compositions for **2-4** within 0.5%. In the case of **3** and **4**, one molecule of CH_2Cl_2 was

included in the expected composition calculated as these complexes were observed to crystallize as solvates. Further analysis by ^{1}H NMR indicated the presence of the desired complexes along with a trace amount of solvent impurities.

Complex **3** was recrystallized from a saturated CH_2Cl_2 solution first layered with toluene and secondly with hexanes, allowing slow diffusion of both layers into the saturated CH_2Cl_2 producing large red-purple needles suitable for characterization by X-ray diffraction. Similarly, complexes **2** and **4** were recrystallized from a saturated CH_2Cl_2 solution layered with hexanes to afford dark purple needle-like and yellow plate-like crystals respectively.

2.2.3 Crystal Structures of Complexes 2, 3 and 4.

The crystal structures of **2 – 4** all reveal square-planar coordination geometries for all three group 10 metals (**Figure 2.4**). Complex **2** crystallized in the orthorhombic space group $P2_12_12_1$ without any solvent molecules, whereas complexes **3** and **4** crystallized in the tetragonal *I-42d* space group as CH_2Cl_2 solvates with half a molecule in the asymmetric unit. There were no exceptional bond lengths in any of these structures and the C–S and aryl C–C bond lengths (see **Table 2.2**) indicated that the best representation of the dithiolene ligand for these complexes was a M^{II}-dithiolate complex as opposed to the M^0-dithioketone representation.

Table 2.2 Selected bond lengths and angles for complexes **2-4**.

	2	**3**	**4**
M-P bond length (Å)	2.1619(7) 2.1661(7)	2.2739(6)	2.2552(7)
M-S bond length (Å)	2.1490(7) 2.1613(7)	2.2977(6)	2.3042(7)
C-S bond length (Å)	1.758(3) 1.755(2)	1.754(2)	1.751(2)
C-C bond length (Å)	1.383(3)	1.388(3)	1.395(3)
P-M-P bond angle (°)	86.64(3)	84.98(3)	85.31(4)
S-M-S bond angle (°)	92.88(3)	88.85(3)	88.46(4)

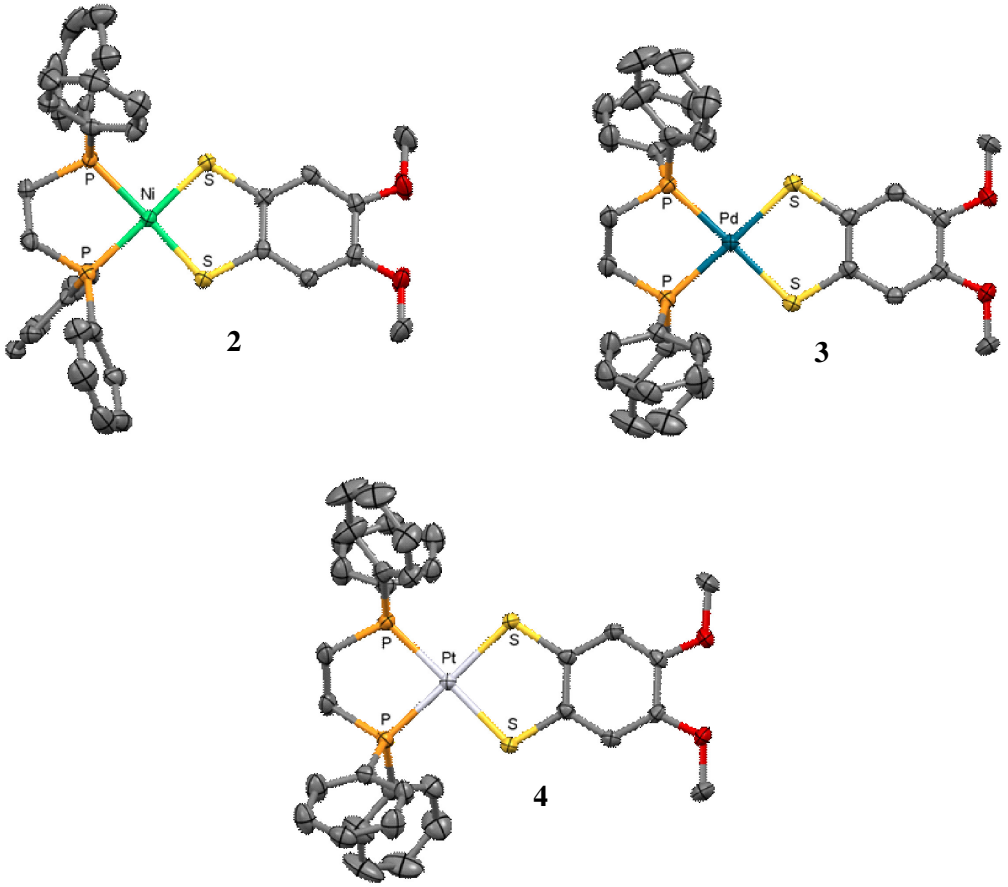

Figure 2.4 Crystal structures of complexes **2**, **3** and **4** (bottom) with thermal ellipsoids drawn at 75% probability. *Note that all hydrogen atoms (and solvate molecules for **3** and **4**) have been removed for clarity.*

As expected, both **3** and **4** formed four-coordinate square planar complexes which are typical for second and third-row transition metals with a d^8 configuration. However, this trend is often not observed by first-row transition metals as the electronic preference for these complexes to form four-coordinate square planar complexes is smaller than that of the second and third-row metals due to a smaller crystal field and larger inter-electron repulsion.[20] This results in four-coordinate first-row transition metal complexes adopting both tetrahedral and square planar geometries with tetrahedral favoured for weak field and bulky ligands. In this context the angles between MP_2 and MS_2 planes for both **3** and **4** are within 0.5° of coplanarity (0.11° for **3** and Pd and 0.47° for **4**) whereas **2** is not. For complex **2**, there is a marked twisting between NiP_2 and NiS_2 planes (13.14°) that occurs at the metal center that prevents the complex from exhibiting a perfectly square planar

geometry (**Figure 2.5**). Nevertheless this angle is much closer to perfectly planar ($\theta = 0^o$) than idealized tetrahedral ($\theta = 90^o$).

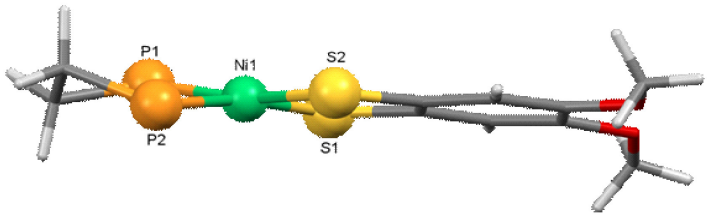

Figure 2.5 Crystal structure of complex **2** illustrating pseudo square planar geometry. *Note that all hydrogen atoms and phenyl groups have been removed for clarity.*

2.2.4 Cyclic Voltammetry Studies on Complexes 2, 3 and 4.

Cyclic voltammetry studies were made on solutions of **2 – 4** in CH_2Cl_2 using 0.1 M [^{n}Bu$_4$N][PF$_6$] as the supporting electrolyte, in order to compare and contrast the effects of changing the metal center on the redox properties of the complexes and to probe the nature of the frontier orbitals in conjunction with DFT studies. The cyclic voltammograms are illustrated in **Figure 2.6**, and the resultant data collated in the form of half-wave potentials ($E_{1/2}$) relative to Ag/Ag^+, and peak-to-peak potentials (ΔE_{pp}) in **Table 2.3**.

As discussed in section 2.1.1, previous studies on nickel dithiolate complexes has shown that the redox chemistry is sensitive to the nature of the dithiolate ligand.[2] For example the half-wave reduction potential of Ni(mnt)(dppe) is -1.20 V with a peak-to-peak separation of 59 mV expected for a reversible 1 e^- process. The resultant [Ni(mnt)(dppe)]$^-$ anion was sufficiently stable to be detected by EPR spectroscopy. The electrochemistry of the related Ni(tdt)(dppe) dithiolate complex was reported to have a reduction wave at $E_{1/2}$ = -1.50 V. However the much larger peak-to-peak potential was scan-rate dependent (130 mV at 100 mV/s and 200 mV at 200 mV/s), consistent with a quasi-reversible process in which electron transfer is a slow rate-limiting step, whilst decomposition of the initial electro-generated product to form one or more daughter

products is rapid. The lifetime of the $[Ni(tdt)(dppe)]^{-}$ radical anion is insufficiently long to be detected by EPR spectroscopy, and appears to be undergoing rapid disproportionation at a rate comparable with the timescale of the electrochemical experiment.[5] Although **2** was found to exhibit a seemingly reversible one-electron reduction (-1.61 V), the peak-to-peak potential (0.37 V at 100 mV/s) was consistent with the short-lived species, analogous to that generated from Ni(tdt)(dppe). All attempts to identify a paramagnetic species by *in situ* EPR spectroscopy proved unsuccessful, supporting the short-lived nature of the electrochemically generated species.

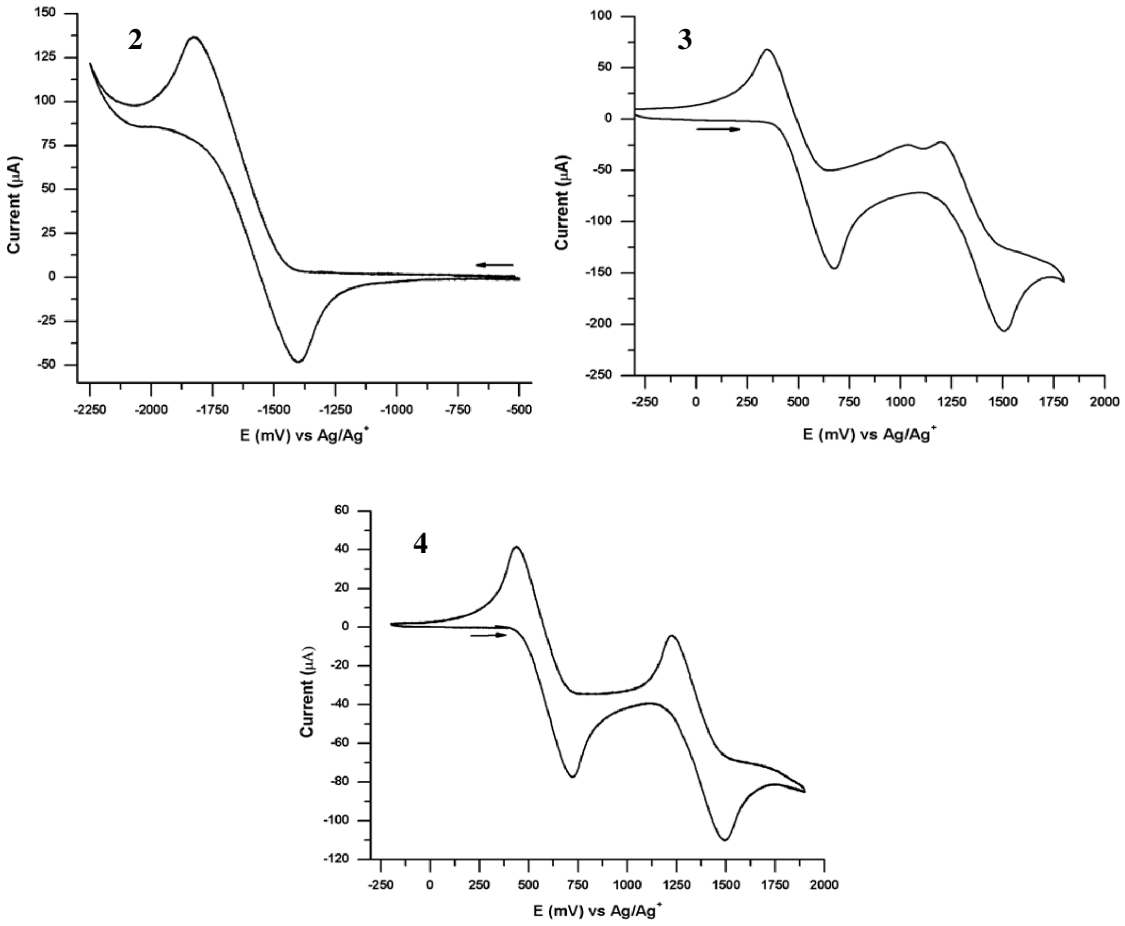

Figure 2.6 CV scans of complexes **2-4** using 0.1M $[^{n}Bu_4N][PF_6]$ supporting electrolyte in CH_2Cl_2 (scan rate 100 mV/s).

Table 2.3 Electrochemical data for complexes **2-4**.

	Complex 2	**Complex 3**	**Complex 4**
$E_{1/2}^{red}$ (V)	-1.61	-	-
$E_{1/2}^{ox}$ (V)	+0.73	+0.51, +1.35	+0.58, +1.36
ΔE_{pp} (V)	0.37	0.33, 0.29	0.29, 0.26

Both complexes **3** and **4** exhibited two quasi-reversible one-electron oxidations, the first of which appears close to the oxidation potential of ferrocene (+0.73 V). These are marginally easier oxidations than those observed for $(Ph_2C_2S_2)$Pd(dppe) and $(Ph_2C_2S_2)$Pt(dppe) (which are +0.43 and +0.45 V respectively).[6] In a similar fashion to **2**, the peak-to-peak separation indicated electrochemically generated oxidation products with a short lifetime. Attempts to selectively chemically oxidize both **3** and **4** also failed to generate any long-lived EPR-active species.

2.2.5 Computational Studies of Complexes 2, 3 and 4.

In order to evaluate the differing nature of the redox processes observed for **2** in relation to **3** and **4**, a series of single point calculations on **2 – 4** were undertaken using hybrid density functional theory methods using both B3LYP and BP86 functionals and triple-zeta quality basis set with additional polarization (LACV3P*) which implements an effective core potential for the *d*-block metal.[21] These calculations were undertaken by Dr J. Hayward. No significant change to the relative energies or characteristics of the frontier orbitals were observed with changes to the functional employed.

In all three cases the LUMO is predominantly a σ* anti-bonding MO centered on the metal-phosphine and metal-dithiolate core with both the nickel and palladium LUMOs involving substantial metal-sulfur σ* character (**Figure 2.7a**) with a metal $d_{x^2-y^2}$ contribution. The LUMO of the Pt complex comprises predominantly dppe π* character. Conversely the HOMOs of the series are all highly dithiolate ligand-based, as shown for **3** (**Figure 2.7b**) with a small amount of electron density on the metal comprising a d_{xz}–d_{yz} admixture. Thus reduction of **2** is likely to be a metal-based reduction and lead to

weakening of the Ni-S and Ni-P bonds whereas the oxidation of **3** and **4** are best considered to be ligand-based redox processes, consistent with conversion of the dithiolate dmobdt^{2-} to the dmobdt$^{\bullet -}$ radical anion, reflecting the non-innocent nature of this ligand. The similarity in $E_{1/2}^{ox}$ for both **3** and **4** is also consistent with a predominantly ligand based oxidation process.

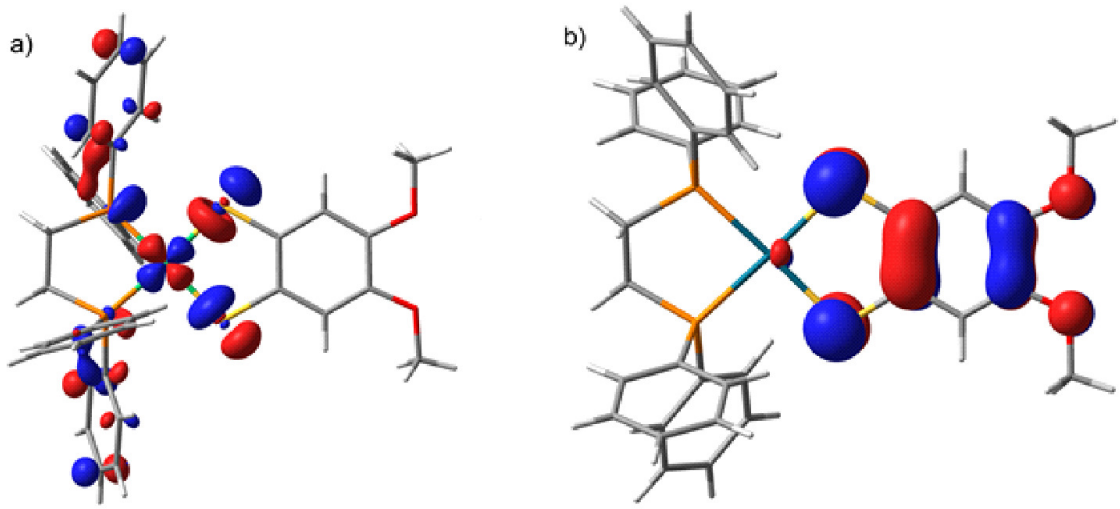

Figure 2.7 DFT calculations: a) LUMO of complex **2** and b) HOMO of complex **3**.

2.3 Conclusions

In this chapter, the one-pot synthesis of metal dithiolate complexes has been achieved *via* oxidative addition of tetrathiocine **1** to zero-valent group 10 metals in very good yields (> 75%) under microwave conditions. Structural studies have allowed us to gain an understanding of the nature of the dithiolene ligand which is best described by the 1,2-dithiolate representation for all three complexes. Electrochemical studies combined with DFT have provided an insight of the redox properties of all three complexes. Whilst complex **2** exhibited a quasi-reversible one-electron metal-based reduction, both **3** and **4** were observed to exhibit two sequential quasi-reversible one-electron ligand-based oxidations.

This is a potentially versatile route to a broad cross-section of *d*-block metal complexes, permitting tuning of the phosphine co-ligand, transition metal and tetrathiocine. In the next chapter, the effect of substituting the phosphine co-ligand on the structure and properties of these complexes is investigated.

2.4 Experimental

2.4.1 Electrochemistry

Cyclic voltammetry measurements were made on solutions of **2 – 4** in CH_2Cl_2 using 0.1 M [^{n}Bu$_4$N][PF_6] as the supporting electrolyte. (electrochemical grade, Fluka) using a BAS 100B Electrochemical Analyzer with BAS 100W software using a sweep rate of 100 mV s^{-1} with glassy carbon working electrode, Pt wire auxiliary electrode and an Ag/AgCl reference electrode against which the Fc/Fc^+ couple appeared at +0.73 V.

2.4.2 Computational Studies

Single point DFT calculations were undertaken on the structures of **2-4** determined by X-ray diffraction using the LACVP3* basis set and both B3LYP and BP86 functionals[21] within Jaguar.[22] The LACVP3* basis set uses an effective core potential for the metal atom and provides triple split-valence zeta quality (6-311+G*) for all atoms with an additional polarization function.[23] Such basis sets have been previously employed to study a range of organometallic/coordination chemistry complexes including Pd and Ru phosphines.[24] Changes in the functional did not lead to significant changes to the energies of the HOMOs and LUMOs or indeed the nature of the frontier orbitals.

2.4.3 Crystallographic Studies

Crystals were mounted on a cryoloop with paratone oil and examined on a Bruker SMART or Bruker APEX-II diffractometer equipped with a CCD area detector and an Oxford Cryostream cooler. Data were measured at 150(2) K using graphite-monochromated Mo-Kα radiation (λ = 0.71073 Å) using the APEX-II software.[25] Final cell constants were determined from full least squares refinement of all observed reflections. The data were collected for absorption (sadabs)[26] and the structures solved by direct methods to reveal most non-H atoms. Remaining heavy atom positions were located in subsequence difference maps and the structure refined with full least squares

refinement on F^2 within the SHELXTL suite.[27] Hydrogen atoms were placed at calculated positions and refined isotropically with a riding model. In the case of **3** and **4** both the complex and the CH_2Cl_2 solvate lay about a crystallographic 2-fold axis with the CH_2Cl_2 exhibiting some evidence for disorder which was modeled over two sites. In addition all three complexes crystallized in acentric space groups. In all cases there was some degree of merohedral twinning. In the case of **3** and **4** the twin was *ca*. 50:50 making assignment of the absolute structure meaningless. However, in the case of **2**, the crystal chosen exhibited a 90:10 twin and the Flack parameter (0.094(10)) permitted the correct absolute structure to be determined (as S for the crystal selected for the crystallographic study). In all cases the twinning was treated with the appropriate TWIN law and BASF parameter to refine the twin components. Structure solution, refinement and preparation of final cif files were undertaken using the SHELXTL package.

2.4.4 General Experimental Procedures

NMR spectra were recorded on a Bruker DPX300 UltraShield 300 MHz spectrometer with a Broadband AX Probe using $CDCl_3$ (^1H δ = 7.26 ppm, s) as an internal reference point relative to Me_4Si (δ = 0 ppm). ^{31}P NMR spectra were referenced to 85% H_3PO_4 (δ = 0 ppm). IR spectra were obtained using a Bruker Alpha FT-IR spectrometer equipped with a Platinum single reflection diamond ATR module. Elemental compositions were determined on a PerkinElmer 2400 Series II Elemental Analyzer. Mass spectra were recorded on a Waters Micromass LCT Classic Electrospray Ionization Time of Flight (ESI-TOF) mass spectrometer operated in positive mode**.**

2.4.5 Preparation of 2',3',8',9' -tetramethoxy-dibenzo-1,2,5,6-tetrathiocine, (1).[15]

Veratrole (3 mL, 23.5 mmol) was added to degassed glacial acetic acid (60 mL) in an inert nitrogen atmosphere. S_2Cl_2 (2 mL, 24.9 mmol) was added dropwise to the rapidly stirred solution. Upon complete addition the solution was left to stir at room temperature for 18 h. A blue precipitate was isolated *via* vacuum filtration and washed with two fractions of Et_2O (~ 10 mL). The solid was suspended in $CHCl_3$ (150 mL) and treated with a few drops of a methanolic tin solution (3 g of $SnCl_2$ in 5 mL of MeOH) until the

blue suspension turned pale yellow under a yellow solution. The yellow solid was isolated by vacuum filtration and washed with two aliquots of Et_2O (~ 10 mL), then dried in *vacuo* (1.92 g, 41% recovered yield).

Elemental analysis calc. for $C_{16}H_{16}O_4S_4 \cdot {}^1/_6\ CHCl_3$: C 46.18; H 3.88%; found: C 46.47; H 3.84% [small $CHCl_3$ contamination was observed due to included solvent in the lattice]

IR ν_{max} (cm^{-1}): 3069(w), 3010(w), 2998(w), 2976(w), 2973(w), 2837(w), 1573(m), 1484(s), 1457(m), 1435(s), 1347(m), 1314(m), 1255(vs), 1210(vs), 1179(s), 1024(vs), 884(m), 850(m), 790(m), 473(m), 430(m).

2.4.6 Preparation of Ni(dmobdt)(dppe), (2).

$Ni(COD)_2$ (0.150 g, 0.545 mmol), dppe (0.218 g, 0.545 mmol) and tetrathiocine **1** (0.109 g, 0.273 mmol) were combined in an oven-dried 5 mL microwave vial in the glove box. Dry toluene (5 mL) was added and the suspension was heated in the microwave for 40 min at 150 °C. The resultant dark brown solid was isolated from a pale yellow solution by filtration. The precipitate was washed with hexanes and dried in air (0.320 g, 89% yield). The solid was recrystallized from a saturated CH_2Cl_2 solution layered with hexanes to produce dark purple needle-shaped crystals suitable for X-ray diffraction.

NMR (ppm): δ_H ($CDCl_3$) = 7.83 (8H, 7.86–7.80, m, *m*-H), 7.47 (12H, 7.54–7.43, m, *o,p*-H), 6.95 (2H, s, benzo C–H), 3.74 (6H, s, CH_3), 2.36 (4H, d, $^2J_{PH}$ = 17.4 Hz, PCH_2); $\delta_P\{^1H\}$($CDCl_3$) = 59.83.

HRMS (ESI-TOF) *m/z*: $[M + H]^+$ calcd for $C_{34}H_{33}O_2P_2S_2Ni^+$ 657.0745; found 657.0723.

Elemental Analysis calc. for $C_{34}H_{32}O_2P_2S_2Ni$: C 62.12; H 4.91%; found: C 61.59; H 4.71%.

IR ν_{max} (cm^{-1}): 3052(w), 2997(w), 2929(w), 2829(w), 1584(w), 1483(s), 1469(s), 1434(vs), 1343(m), 1244(vs), 1199(s), 1174(m), 1100(s), 1043(s), 815(m), 782(m), 746(m), 690(vs), 531(vs), 482(m).

2.4.7 Preparation of Pd(dmobdt)(dppe), (3).

Pd_2dba_3 (0.100 g, 0.109 mmol), dppe (0.087 g, 0.218 mmol) and tetrathiocine **1** (0.044 g, 0.109 mmol) were combined in an oven dried 5 mL microwave vial in the glove box. Dry toluene (5 mL) was added and the suspension heated in the microwave for 30 min at 150 °C. The resultant bright pink solid was isolated from the clear-yellow solution by filtration. The precipitate was washed with a small amount of hexanes and dried in air (0.131 g, 85% yield). The solid was recrystallized from a saturated CH_2Cl_2 solution layered with toluene and hexanes to produce red-purple needles suitable for X-ray diffraction.

NMR (ppm) ($CDCl_3$)**:** δ_H = 7.83 (8H, 7.86–7.79, m, *m*-H), 7.46 (12H, 7.51–7.44, m, *o,p*-H), 6.91 (2H, s, benzo C–H), 3.75 (6H, s, CH_3), 2.50 (4H, d, $^2J_{PH}$ = 20.7 Hz, PCH_2); $\delta_P\{^1H\}$ = 51.94.

HRMS (ESI-TOF) ***m/z*:** $[M + H]^+$ calcd for $C_{34}H_{33}O_2P_2S_2Pd^+$ 705.0427; found 705.0462.

Elemental Analysis calc. for $C_{34}H_{32}O_2P_2S_2Pd \cdot CH_2Cl_2$: C 53.20; H 4.87%; found: C 53.26; H 4.39%.

IR ν_{max} (cm^{-1}): 3358(w), 3050(w), 2922(m), 2850(w), 2829(w), 1483(s), 1470(s), 1434(vs), 1339(m), 1240(vs), 1198(s), 1174(m), 1100(s), 1039(s), 846(m), 744(m), 703(s), 690(vs), 524(vs), 486(m).

2.4.8 Preparation of Pt(dmobdt)(dppe), (4).

$Pt(dppe)_2$ (0.100 g, 0.101 mmol) and tetrathiocine **1** (0.020 g, 0.050 mmol) were combined in an oven dried 5 mL microwave vial in the glove box. Dry toluene (5 mL) was added to the vial and the suspension heated in the microwave for 30 min at 150 °C. The resultant bright yellow microcrystalline solid was isolated from a clear-yellow solution by gravity filtration. The precipitate was washed with a small amount of hexanes and dried in air (0.062 g, 77% yield). The solid was recrystallized from a saturated CH_2Cl_2 solution layered with hexanes to produce bright yellow plate-like crystals suitable for X-ray diffraction.

NMR (ppm) ($CDCl_3$)**:** δ_H = 7.84 (8H, 7.87–7.81, m, *m*-H), 7.45 (12H, 7.46–7.44, m, *o,p*-H), 7.07 (2H, s, benzo C–H), 3.76 (6H, s, CH_3), 2.47 (4H, 2.54–2.39, m, PCH_2); $\delta_P\{^1H\}$ = 45.90 ($^1J_{Pt–P}$ = 3427 Hz).

HRMS (ESI-TOF) ***m/z*****:** $[M + H]^+$ calcd for $C_{34}H_{33}O_2P_2S_2Pt^+$ 794.1039; found 794.1037.

Elemental Analysis calc. for $C_{34}H_{32}O_2P_2S_2Pt \cdot CH_2Cl_2$: C 47.84, H 3.90%; found: C 47.53, H 3.66%.

IR ν_{max} (cm^{-1}): 3053(w), 2988(w), 2900(w), 2830(w), 1485(s), 1435(vs), 1341(m), 1241(vs), 1200(m), 1103(s), 1042(m), 748(m), 691(vs), 531(vs), 481(m).

2.5 References

1. *Dithiolene chemistry: Synthesis, properties, and applications,* ed. E. I. Stiefel, Interscience: Hoboken, New Jersey, 2003.

2. G. A. Bowmaker, P. D. W. Boyd, G. K. Campbell, J. M. Hope and R. L. Martin, *Inorg. Chem.*, 1982, **21**, 1152.

3. G. Periyasamy, N. A. Burton, I. H. Hillier, M. A. Vincent, H. Disley, J. McMaster and C. D. Garner, *Farad. Discuss.,* 2007, **135**, 469.

4. F. H. Allen, O. Kennard, D. G. Watson, L. Brammer, A. G. Orpen and R. Taylor, *J. Chem. Soc., Perkin Trans. II*, 1987, S1.

5. **(a)** K. Arumugam, M. C. Shaw, P. Chandrasekaran, D. Villagran, T. G. Gray, J. T. Mague and J. P. Donahue, *Inorg. Chem*., 2009, **48**, 10591; **(b)** N. Robertson and L. Cronin, *Coord. Chem. Rev*., 2002, **227**, 93; **(c)** J. Jones and J. Douek, *J. Inorg. Nucl. Chem*., 1981, **43**, 406; **(d)** P. Cassoux, L. Valade, H. Kobayashi, A. Kobayashi, R. A. Clark and A. E. Underhill, *Coord. Chem. Rev*., 1991, **110**, 115; **(e**) M. M. Ahmad, D. J. Turner, A. E. Underhill, C. S. Jacobsen, K. Mortensen and K. Carneiro, *Phys. Rev. B,* 1984, **29**, 4796; **(f)** H. Imai, T. Otsuka, T. Naito, K. Awaga and T. Inabe, *J. Am. Chem. Soc*., 1999, **121**, 8098; **(g)** M. Uruichi, K. Yakushi, Y. Yamashita and J. Qin, *J. Mater. Chem*., 1998, **8**, 141; **(h)** N. Venkatalakshmi, B. Varghese, S. Lalitha, R. F. X. Williams and P. T. Manoharan, *J. Am. Chem. Soc*., 1989, **111**, 5748.

6. G. A. Bowmaker, P. D. W. Boyd and G. K. Campbell, *Inorg. Chem.*, 1983, **22**, 1208.

7. *Advanced Inorganic Chemistry: A Comprehensive Text*, 2nd ed., F. A. Cotton, G. Wilkinson, Interscience: London, England, 1966.

8. *Transition Metal Chemistry: A series of advances*, ed. R. L. Carlin, Marcel Dekker, New York, New York, 1968.

9. A search of the CSD (2014) revealed 124 structures containing at least one nickel dithiolate [NiS_2C_2] unit, all of which were close to planarity.

10. J. A. McCleverty, *Prog. Inorg. Chem.* 1968, **10**, 49.

11. T. Shimizu, H. Murakami, Y. Kobayashi, K. Iwata and N. Kamigata, *J. Org. Chem.* 1998, **63**, 8192.

12. **(a)** C. M. Bolinger, T. B. Rauchfuss and S. R. Wilson, *J. Am. Chem. Soc.* 1981, **103**, 5620; **(b)** C. M. Bolinger, T. B. Rauchfuss and A. L. Rheingold, *J. Am. Chem. Soc.* 1983, **105**, 6321; **(c)** R. J. Pafford and T. B. Rauchfuss, *Inorg. Chem.* 1998, **37**, 1974; **(d)** H. Oku, N. Ueyama and A. Nakamura, *Inorg. Chem.* 1997, **36**, 1504.

13. K. Wang, J. M. McConnachie and E. I. Stiefel, *Inorg. Chem.*, 1999, **38**, 4334.

14. J. M. Rawson, A. Alberola, D. Eisler, R. J. Less, E. Navarro-Moratalla, *Chem. Comm.*, 2010, **46**, 6114.

15. K. W. Stender, N. Wolki and G. Klar, *Phosphorus, Sulfur, and Silicon Relat. Elem.*, 1989, **42**, 111.

16. **(a)** E. J. Wharton and J. A. McCleverty, *J. Chem. Soc. A*, 1969, 2258; **(b)** A search of the CSD (2013) revealed 639 structures containing a benzo-dithiolate core. 68% of these complexes comprised either benzene dithiolate or toluene dithiolate at 53% and 15% respectively.

17. J. D. Wrixon, J. J. Hayward, O. Raza and J. M. Rawson, *Dalton Trans.*, 2014, **43**, 2134.

18. *Microwave-Assisted Organic Synthesis*, J.P. Tierney and P. Lidstrom Eds., Blackwell: Oxford, UK, 2005.

19. For examples see; **(a)** F. K. Keter, I. A. Guzei and J. Darkwa, *Inorg. Chem. Commun*., 2013, **27**, 60; **(b)** C. Mugge, C. Rothenburger, A. Beyer, H. Gorls, C. Gabbiani, A. Casini, E. Michelucci, I. Landini, S. Nobili, E. Mini, L. Messori and W. Weigand, *Dalton Trans*., 2011, **40**, 2006; **(c)** K. Arumugam, M. C. Shaw, P. Chandrasekaran, D. Villagran, T. G. Gray, J. T. Mague and J. P. Donahue, *Inorg Chem*., 2009, **48**, 10591; **(d)** K. A. Van Houten, D. C. Heath, C. A. Barringer, A. L. Rheingold and R. S. Pilato, *Inorg. Chem.*, 1998, **37**, 4647.

20. *Organotransition Metal Chemistry: From Bonding to Catalysis*, ed. J. F. Hartwig, University Science Books: Sausalito, California, 2010.

21. DFT calculations for complexes **1-3** were performed by Dr. John Hayward.

22. P. J. Hay and W. R. Wadt, *J. Chem Phys*., 1985, **82**, 299.

23. N. Fey, B. M. Ridgway, J. Jover, C. L. McMullin and J. N. Harvey, *Dalton Trans*., 2011, **40**, 11184

24. **(a)** A. Davidson, N. Edelstein, R. H. Holm and A. H. Maki, *Inorg. Chem*., 1964, **3**, 814; **(b)** G. C. Fortman, T. Kegl and C. D. Hoff, Curr. *Org. Chem*., 2008, **12**, 1279; **(c)** V. G. Albano, M. Monari, I. Orabana, A. Panunzi and F. Ruffo, *J. Am. Chem. Soc*., 2001, **123**, 4352; **(d)** V. P. Ananikov, I. P. Beletskaya, G. G. Alexsandrov and I. L. Eremenk, *Organometallics*, 2003, **22**, 1414; **(e)** S. M. Aucott, H. L. Milton, S. D. Robertson, A. M. Z. Slawin, G. D. Walker and J. D. Woollins, *Chem.–Eur. J*., 2004, **10**, 1666; **(f)** W. Weigand, G. Bosl, von B. Dielingen and K. Gollnick, *Z. Naturforsch., B: Chem. Sci*., 1994, **49**, 513; **(g)** U. Siemeling, F. Bretthauer, C. Bruhn, T. Fellinger, W. Tong and M. C. W. Chan, *Z. Naturforsch., B: Chem. Sci*., 2010, **65**, 1089

25. APEX-II, Bruker AXS Inc., Madison, Wisconsin, USA.

26. Sadabs, Bruker AXS Inc., Madison, Wisconsin, USA.

27. SHELXTL package for crystal structure solution and refinement, Bruker AXS Inc., Madison, Wisconsin, USA.

CHAPTER 3

Phosphine-control of the oxidative addition chemistry of tetrathiocines to Pd(0): Characterization of mono-, di- and hexa-nuclear Pd(II) dithiolate complexes

3.1 Introduction

As mentioned in the previous chapter, metal-dithiolene chemistry has continued to be an active field of study and has been built on a solid foundation of both the synthesis and characterization of these sorts of complexes.[1] It was observed in Chapter 2 that a homologous series of group 10 complexes **2 – 4** containing the $dmobdt^{2-}$ ligand could be prepared in high yield in a one-pot microwave synthesis from the oxidative addition of the corresponding bis(dimethoxybenzo)tetrathiocine (**1**) to zero-valent group 10 metal complexes in the presence of the chelating phosphine ligand dppe.[2] These systems comprise a series of complexes of general formula M(dmobdt)(dppe) (M = Ni, Pd, Pt). In the absence of a phosphine the propensity for the group 10 complexes to form square-planar geometries would be expected to lead to a series of oligomeric complexes $[ML]_n$ where L is a dithiolato ligand. The group 10 metals account for approximately 80% of the homoleptic metal dithiolate complexes that have been structurally observed in the literature.[1] However, of these complexes, the vast majority of these structures obtained are homoleptic bis(dithiolene) complexes, ML_2^{n-}, with very few homoleptic oligomeric mono(dithiolene) complexes, $(ML)_n$, crystallographically determined. During the oligomerisation process the coordination sphere of the central metal atom can be satisfied by the S atoms of the dithiolene ligands which can form additional dative bonds generating a variety of "cluster-like" structures. These clusters have been observed using a variety of different transition metals.[3] A common example of a homoleptic $[ML]_n$ complex can be seen with nickel thiolates in which a series of cyclic clusters $[Ni(SR)_2]_n$ are formed. These nickel complexes range in size, starting from a small tetrameric

$[Ni(SR)_2]_4$ cyclic system[4] through to a much larger dodecanuclear ring $[Ni(SR)_2]_{12}$[5] (**Figure 3.1**). Other examples in the literature contain nickel clusters which also contain a phosphine co-ligand $[Ni(SR)_2]_{\underline{n}}(PR_3)_y$.[6] The addition of the phosphine co-ligand appears to have a limiting effect on the size of the cluster. In this Chapter the role of the phosphine in determining the outcome of the oxidative addition reaction are discussed, playing particular attention to the lability of the phosphine chosen.

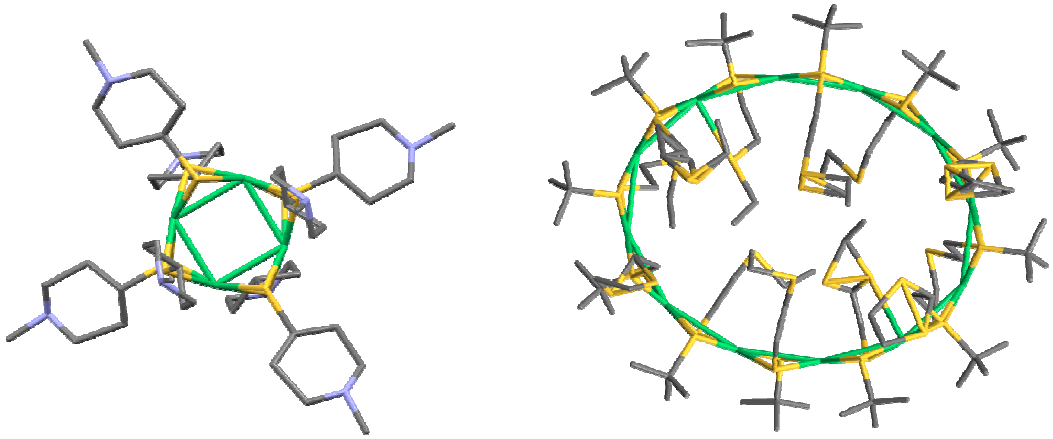

Figure 3.1 Examples of different size homoleptic Nickel clusters: $[Ni(SR)_2]_4$ (left) and $[Ni(SR)_2]_{12}$ (right).

3.1.1 Phosphine Ligands

Phosphine ligands are very commonly used in transition metal chemistry as they exhibit good solubility in organic solvents, have been observed to bind strongly to metals in low oxidation states,[7] and more importantly due to their ability to fine-tune the donor/acceptor properties of the metal centre to facilitate catalytic reactions.[8]

Phosphines are neutral $2e^-$ donors, analogous to amines. However unlike amines which are considered as pure σ-donors, phosphines are considered as π-acceptors and give rise to stronger ligand fields, reflected in a significantly higher position in the Spectrochemical Series. The origin of the π-acceptor character of phosphines has been debated at length with original arguments based on *d*-orbital participation from P. However current consensus is that the bonding within main group materials does not

utilise *d*-orbitals but rather a combination of low-lying σ* orbitals.[9] In the case of phosphines these are P-C σ* orbitals. Phosphines are considered as soft bases based on Pearson's Hard-Soft Acid Base theory and therefore favourable ligands for heavier transition metals in lower oxidation states.[10] The ability to tune both the electronic and steric properties of phosphines, PR_3, through careful tailoring of the R group has made phosphines a particularly important ligand in coordination and organometallic chemistry. In addition the high natural abundance of ^{31}P ($I = ½$) and large chemical shift range make it a particularly amenable reporter group for monitoring and characterising chemical reactions. These aspects of phosphines are discussed in sections ***3.1.1.a – 3.1.1.c*** below.

3.1.1.a Monodentate and Bidentate Tertiary Phosphines. Tertiary phosphines, PR_3, are among the most recognized ligands utilized in the formation of transition metal complexes, specifically among the late transition metals. The soft donor ability of phosphorus is very well suited for the soft low-valent metals and the ability to modify the substituents on the phosphorus heteroatom has a large effect on the properties and reactivity of the metal center.[12] These ligands are most commonly used in both inorganic and organometallic chemistry and are classified by their denticity,[11] whilst their reactivity is greatly influenced by a wide range of electronic and steric effects.[12,13] Multi-dentate phosphorus ligands comprise multiple P-donor atoms tethered to one another in order to create a ligand that can bind to a metal center through more than one bond.[8] Such poly-dentate complexes lead to enhanced stability through the chelate effect in which the complex is entropically stabilised. The most commonly utilized derivatives of these ligands are the bidentate phosphines, such as bis(diphenylphosphino)methane (dppm) and bis(diphenylphosphino)ethane (dppe), which contain two phosphorus heteroatoms tethered together by a carbon backbone.[13] In the context of this thesis, both dppm and dppe are examined as potential chelate ligands as well as redox-active dppf (**Figure 3.2**).

3.1.1.b Steric Effects. During the 1970s, Tolman described the steric effect in molecules as a result of non-bonding forces that are felt between neighbouring parts of a molecule.[12] From this definition, Tolman developed the ligand cone angle parameter (**θ**) which is defined as the angle at the peak of the "cone" that can be imagined to surround the phosphine ligand coordinated to a metal (**Figure 3.3**). It became clear to Tolman that the

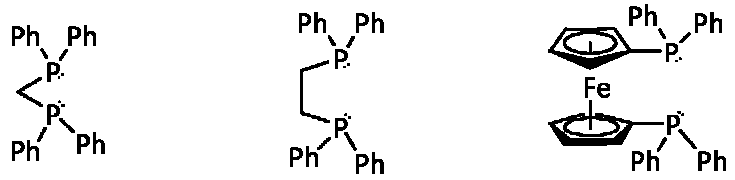

dppm ***dppe*** ***dppf***

Figure 3.2 Bidentate tertiary phosphate ligands explored in this chapter.

ability for phosphine ligands to compete for coordination positions on a metal could not be explained electronically, but rather due to the size of the ligand. Initial studies using a variety of phosphine ligands such as PMe_3, $P(OPh)_3$, PPh_3, PCy_3, and $P(^tBu)_3$ indicated that there was a decreasing affinity for coordination to a metal in the respective order. As this work was done before the time of computer modelling, molecular modelling kits were initially used to determine the relative overcrowding that would occur around the bonding face of the phosphorus atom. It was determined that as the size of the cone angle increased, the affinity of the phosphine ligand to bind to a metal decreased due to the steric effect of the ligand. Crystallographic studies of $W(CO)_5PMe_3$ and $W(CO)_5P(^tBu)_3$ provided proof of this phenomenon through the measurement of M-P bond length.[14] With a ~ 0.17 Å difference between the W-P bond lengths of $W(CO)_5PMe_3$ (2.516(2) Å) and $W(CO)_5P(^tBu)_3$ (2.686(4) Å) it can be concluded that the increased steric effect of the bulkier phosphine ligand influences the overall strength of the M-P bond. In this thesis PPh_3 (θ = 145°) and P^tBu_3 (θ = 182°) are considered as more sterically demanding and labile ligands alongside the chelate ligands previously mentioned.

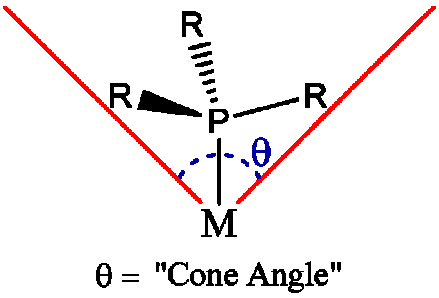

Figure 3.3 Diagram representation of the Tolman cone angle. *Figure adapted from reference 12.*

Table 3.1 Selected Tolman cone angles for common tertiary phosphine ligands. *Table reproduced from data found in reference 12.*

Phosphorus Ligand	Cone Angle (°)
PH_3	87
PF_3	104
$P(OMe)_3$	107
PMe_3	118
PMe_2Ph	122
$P(OPh)_3$	128
PEt_3	132
PPh_3	145
PCy_3	170
$P(tBu)_3$	182
$P(o\text{-tol})_3$	194

3.1.1.c ^{31}P NMR. In terms of practicality, the large range (approximately -250 ppm to 250 ppm) and characteristic chemical shifts present in ^{31}P NMR makes it is easy to determine the purity and examine the completeness of chemical reactions of phosphorus-containing compounds.[15] The ^{31}P NMR chemical shifts of a large number of commercial phosphine ligands are well established permitting reactivity to be readily monitored by NMR spectroscopy. Furthermore, phosphines make interesting ligands in transition metal chemistry as they are one of a select few classes of ligands that have tuneable electronic and steric properties by changing the substituent R groups.[7] A change in R substituent groups or Tolman angle have been observed to have a variety of influences on the phosphorus chemical shifts to which these complexes exhibit (see **Table 3.2**).[12] The phosphorus chemical shifts of phosphines are highly dependent on the number of hydrogen substituents present. Tertiary phosphines (PR_3) generally range between -70 and 70 ppm, whereas primary (RPH_2) and secondary (R_2PH) phosphines range between -170 to -70 and -100 to 20 ppm respectively. It has been observed in the literature that substituting hydrogen atoms for more electronegative carbon atoms leads to a downfield shift. Furthermore, increasing alkyl substitution of a tertiary phosphine also leads to a further downfield shift in the phosphorus resonance. Alternatively, the addition of phenyl substituents has been observed to shift the phosphorus chemical shift upfield. The

coordination of phosphines to transition metals results in a downfield shift. Metal coordination typically leads to a deshielding effect (downfield shift).

Table 3.2 Effect of Substituents and Tolman cone angle on ^{31}P chemical shifts of phosphorus. *Table reproduced from data found in reference 12.*

Phosphorus Ligand	δ_P (ppm)
PH_3	-239
$PMeH_2$	-163.5
PMe_2H	-99
PMe_3	-62.2
P^tBuCl_2	198.6
P^tBu_2Cl	145
P^tBu_3	63
$PPhCl_2$	165
PPh_2Cl	81.5
PPh_3	-6

3.1.2 Project Objectives

In this section the influence of the phosphine on the oxidative addition of bis(dimethoxybenzo)tetrathiocine to Pd(0) is described, implementing a range of monodentate and bidentate phosphine ligands. In addition preliminary studies of the reactivity with the related Pt(0) complexes are considered and compared with the corresponding palladium chemistry.

3.2 Results and Discussion

3.2.1 Synthesis and Structural Studies of Mononuclear Complexes

In the previous chapter, oxidative addition of tetrathiocines to Pd(0) in the presence of the bidentate chelating phosphine dppe was shown to result in the formation of a mononuclear dithiolate complex, Pd(dmobdt)(dppe). Replacement of dppe by the more strained dppm or redox-active dppf under microwave irradiation (**Scheme 3.1**) resulted in the formation of a dark red (**5**) and brown (**6**) solution respectively.

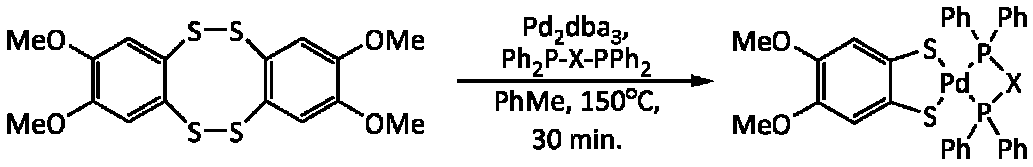

Scheme 3.1 Formation of Pd(II) dithiolate complexes containing bidentate phosphine co-ligands (X = CH_2 , CH_2CH_2 or $C_5H_4FeC_5H_4$).

The solvent was removed in *vacuo* for both samples and recrystalization from a saturated CH_2Cl_2 solution by layering with hexanes afforded crystals of (dmobdt)Pd(dppm) (**5**), whereas slow diffusion of Et_2O into a saturated CH_2Cl_2 solution afforded large crystals of (dmobdt)Pd(dppf) (**6**) suitable for X-ray diffraction (see **Figure 3.4**).

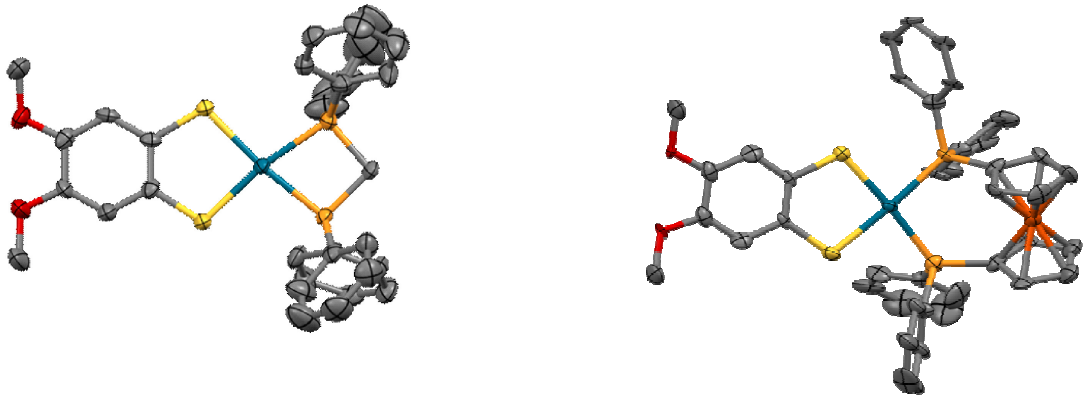

Figure 3.4 Crystal structure of complex **5** (left) and **6** (right) with thermal ellipsoids drawn at 75% probability. *Note that all hydrogen atoms and solvate molecules have been removed for clarity.*

Complex **5** crystallises in the monoclinic space group $P2_1/c$ with two molecules in the asymmetric unit, whereas **6** crystallised in the triclinic space group P-1 with three

molecules in the asymmetric unit. Representative molecules from each of these two structures are presented in **Figure 3.4**. The Pd-S bond lengths in **5** and **6** are similar to the previously reported (dmobdt)Pd(dppe) complex (2.2977(6) Å) described in Chapter 2, spanning the range 2.276(3) – 2.304(4) Å. The SPdS chelate angles in all three complexes are also similar (85.5(1) – 89.74(5)^{o}). While the palladium-dithiolate component appears somewhat invariant, more pronounced differences are observed in the palladium-phosphine component. Although the Pd-P distances (2.270(2) – 2.284(2) Å) in **5** are similar to those in (dmobdt)Pd(dppe) (2.2740(6) Å), the smaller 'bite' of the dppm ligand leads to some strain with a smaller P-Pd-P chelate angle (73.29(4) – 73.50(4)^{o}) *cf* (dmobdt)Pd(dppe) at 84.98(3)^{o}. Conversely the larger bite of the dppf ligand is accommodated by larger Pd-P distances (2.280(3) – 2.321(3) Å) and larger P-Pd-P angles (96.7(1) – 97.4(1)^{o}). Nevertheless, despite these geometric changes, the Pd centre in all these complexes is close to planarity, with the sum of the internal angles at Pd in the range 357.3 – 360.0^{o}.

In order to confirm the purity of complexes **5** and **6**, high resolution mass spectrometry measurements were obtained by positive ion ESI-TOF indicating the presence of the expected $[M + H]^+$ ion peaks with three replicate acquisitions completed with better than 0.5 ppm mass accuracy. Elemental analysis confirmed the composition as **5**·½CH_2Cl_2 and **6**. The presence of residual dichloromethane in **5** was consistent with the X-ray structure and ^{1}H NMR. The ^{31}P NMR of complex **5** indicated the presence of a single peak (35.36 ppm) shifted downfield with respect to free dppm ligand (-23.6 ppm)[10] similar to other Pd^{II}-dppm complexes.[16] Complex **6** also exhibited a single peak (26.6 ppm) similar to other Pd^{II}-dppf complexes with PdP_2S_2 coordination geometries, such as (dppf)Pd(bdt) (+25.08 ppm),[17] again shifted with respect to the free dppf ligand (-17.2 ppm).[18]

3.2.2 Synthesis and Structural Studies of Dinuclear Complexes

In order to further investigate the effect of the phosphine on the outcome of these oxidative addition reactions, the more labile monodentate PPh_3 co-ligand was used which offers a large Tolman cone angle (145°). Treatment of Pd_2dba_3 with tetrathiocine, **1**, in the presence of the monodentate phosphine under identical microwave conditions to the formation of **5** and **6** above, led to the formation of a dark green solution of **7** (**Scheme 3.2**). Recrystallization from hexanes layered onto a saturated CH_2Cl_2 solution resulted in green crystals (see **Figure 3.5**) which were suitable for X-ray diffraction, albeit in low yield (< 5%). Subsequent crystallographic studies revealed these to be the dimeric complex, $Pd_2(dmobdt)_2(PPh_3)_2$ (**7**) in which one of the two dithiolate S atoms adopts a μ_2-bridging mode.

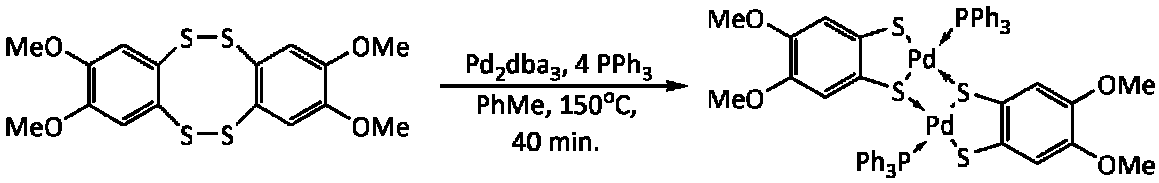

Scheme 3.2 Synthesis of the dinuclear complex **7**.

Complex **7** crystallized in the orthorhombic space group $P2_12_12$ as a CH_2Cl_2 solvate with the dimer located about a crystallographic 2-fold axis (**Figure 3.5**). The Pd-S2 bond length (2.2795(5) Å) is at the shorter end of those seen in other Pd(dmobdt) complexes (2.276(3) – 2.304(4) Å) but the Pd-S1 distance (2.3246(5) Å) is longer, in agreement with its μ_2-coordination mode. The sum of the internal angles at Pd (359.74°) is again consistent with a planar geometry. While the S(1)-Pd-S(2) angle of 89.31(2)° is similar to that observed in other (dmobdt)Pd complexes (85.5(1) – 89.74(5)°), there are significant distortions from idealized square planar geometry. In particular the bridging S1-Pd-S1 angle (79.57(2)°) is rather acute and the P-Pd-S1 angle (99.70(2)°) is somewhar larger leading to a trans S1-Pd-S2 angle of 166.09(2)° to accommodate the bulk of the Ph_3P group. A search of the CSD reveals two similar dimetallic Pd complexes of this type; $[Pd(S_2C_2H_2)(PPh_3)]_2$ and $[Pd(S_2C_2H_4)(PPh_3)]_2$.[19]

Table 3.3 Bond lengths and bond angles for complex **7**.

Bond Lengths (Å)		Bond Angles (°)	
Pd – S2	2.2795(5)	S2-Pd-S1	89.31(2)
Pd – P1	2.2742(5)	S2-Pd-P1	91.16(2)
Pd – S1	2.3246(5)	P1-Pd-S1′	99.70(2)
Pd – S1′	2.3660(5)	S1-Pd-S1′	79.57(2)
		Pd-S1-Pd′	76.83(2)

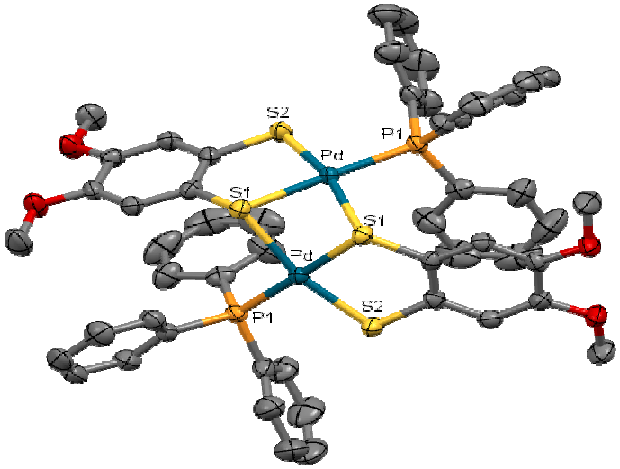

Figure 3.5 Crystal structure of complex **7** with thermal ellipsoids drawn at 75% probability. *Note that all hydrogen atoms and solvate molecules have been removed for clarity.*

In order to improve the yield of **7**, purification by column chromatography was employed to remove any remaining impurities such as unreacted PPh_3. A dark green solution was eluted from the column and the solvent (50% acetone / 50% hexanes) was removed affording bright green oil. The oil was recrystallized by slow diffusion of Et_2O into a saturated CH_2Cl_2 solution resulting in large green crystals with an increased yield of ~ 25%.

Sample purity was reflected in microanalytical data in very good agreement with the formulation **7**·CH_2Cl_2. Characterization of **7** by FAB+ mass spectrometry indicated a distribution of isotopomers around *m/z* = 1138 consistent with the molecular ion $\mathbf{7}^+$ (*m/z* = 1137.96). A second set of ions were observed around *m/z* = 876 consistent with the

fragment ion $[\mathbf{M} - PPh_3]^+$ (*m/z* = 875.67). A third peak at *m/z* = 263 is consistent with free PPh_3 (*m/z* = 262.29).

In order to determine whether the dimeric structure of **7** was retained in solution, rather than dissociate into monomeric Pd(dmpbdt)(PPh_3), complex **7** was further characterized by NMR spectroscopy. The ^{31}P NMR of **7** exhibits a singlet at 34.63 ppm. This chemical shift appears markedly different to the bidentate phosphine complex Pd(dmobdt)(dppe) (51.94 ppm). However chelate effects can exhibit a significant effect on the ^{31}P NMR chemical shift[18] so the position of the ^{31}P NMR resonance of **7** is, in itself, not diagnostic of a different chemical environment. Indeed the more strained chelate Pd(dmobdt)(dppm) (**5**) appears at 35.36 ppm reflecting the substantial effect of chelation on ^{31}P chemical shift. Conversely the ^1H NMR of **7** was diagnostic of retention of the dimer in solution. The ^1H NMR spectrum clearly indicated a separation in the chemical shifts for both the methoxy protons and aromatic protons from the respective bridging dithiolate ligands (**Figure 3.6**). The presence of chemically distinct methoxy and aryl ^1H environments is consistent with retention of the dimeric structure in solution in which the aryl and methoxy groups are in chemically inequivalent positions whereas monomeric Pd(dmobdt)(PPh_3) with a trigonal planar coordination environment at Pd would be anticipated to generate chemically equivalent ^1H environments.

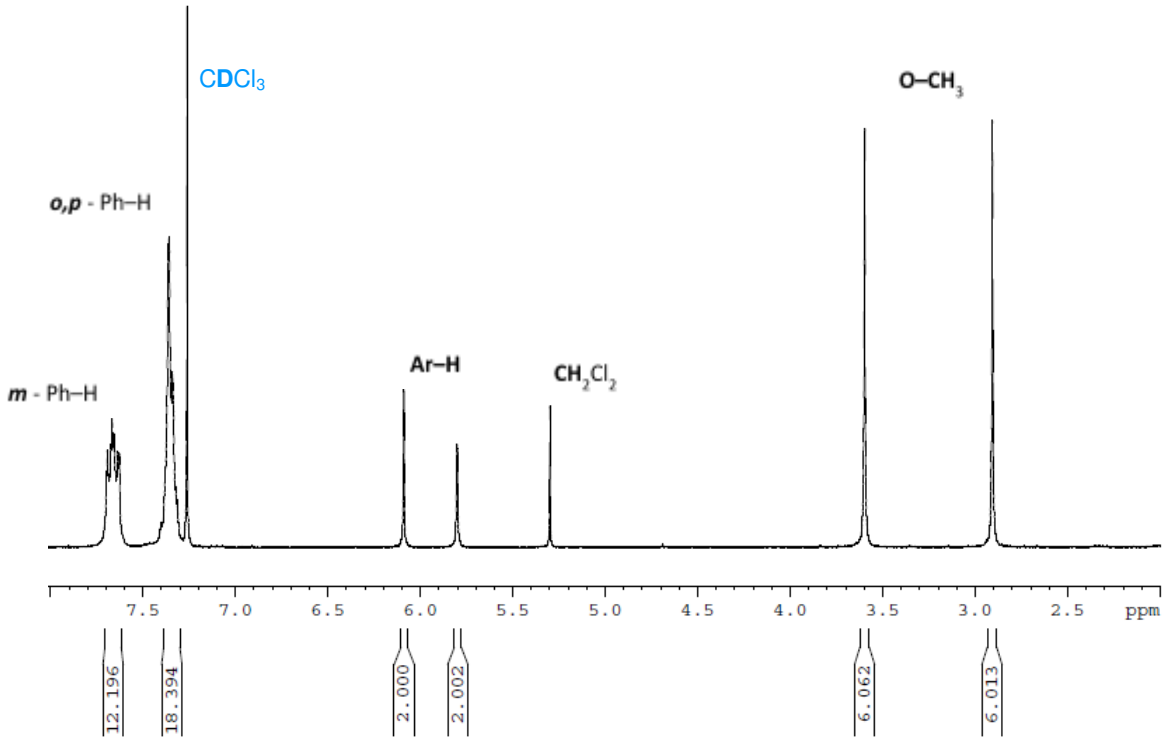

Figure 3.6 ^{1}H NMR spectra of complex **7** in $CDCl_3$ revealing the two chemically distinct aryl-H and methoxy H resonances.

Reaction of $Pt(PPh_3)_4$ in place of Pd_2dba_3 under otherwise identical conditions proved insightful into the reaction mechanism. The kinetics of Pt chemistry is typically somewhat slower than their Pd analogues[21] and this permitted us to identify a key intermediate in this reaction.

Preliminary results found that treatment of $Pt(PPh_3)_4$ with **1** led to the formation of a bright orange solution with more complex ^{31}P and ^{1}H NMR spectra than **7** (see **Figures 3.7** and **3.8**). Unlike complex **7**, purification by column chromatography (50% ethyl acetate / 50% hexanes) afforded two coloured products; A yellow solution was eluted from the column first followed by a red solution and the solvent removed to afford both yellow and red residues respectively. Both these materials were recrystallized by slow diffusion of Et_2O into a saturated CH_2Cl_2 solution to afford large orange blocks of $Pt(dmobdt)(PPh_3)_2$ (**9**) (**Figure 3.9**) and red needle crystals of $Pt_2(dmobdt)_2(PPh_3)_2$ (**8**) respectively (**Figure 3.10**).

Both the ^{31}P and ^{1}H NMR spectra of the reaction mixture therefore comprise components from both monometallic (dmobdt)$Pt(PPh_3)_2$ (**9**) and the dimeric product $[Pd(dmobdt)(PPh_3)]_2$ (**8**) which are readily assigned based on the ^{31}P and ^{1}H NMR spectra of pure **8** and **9**.

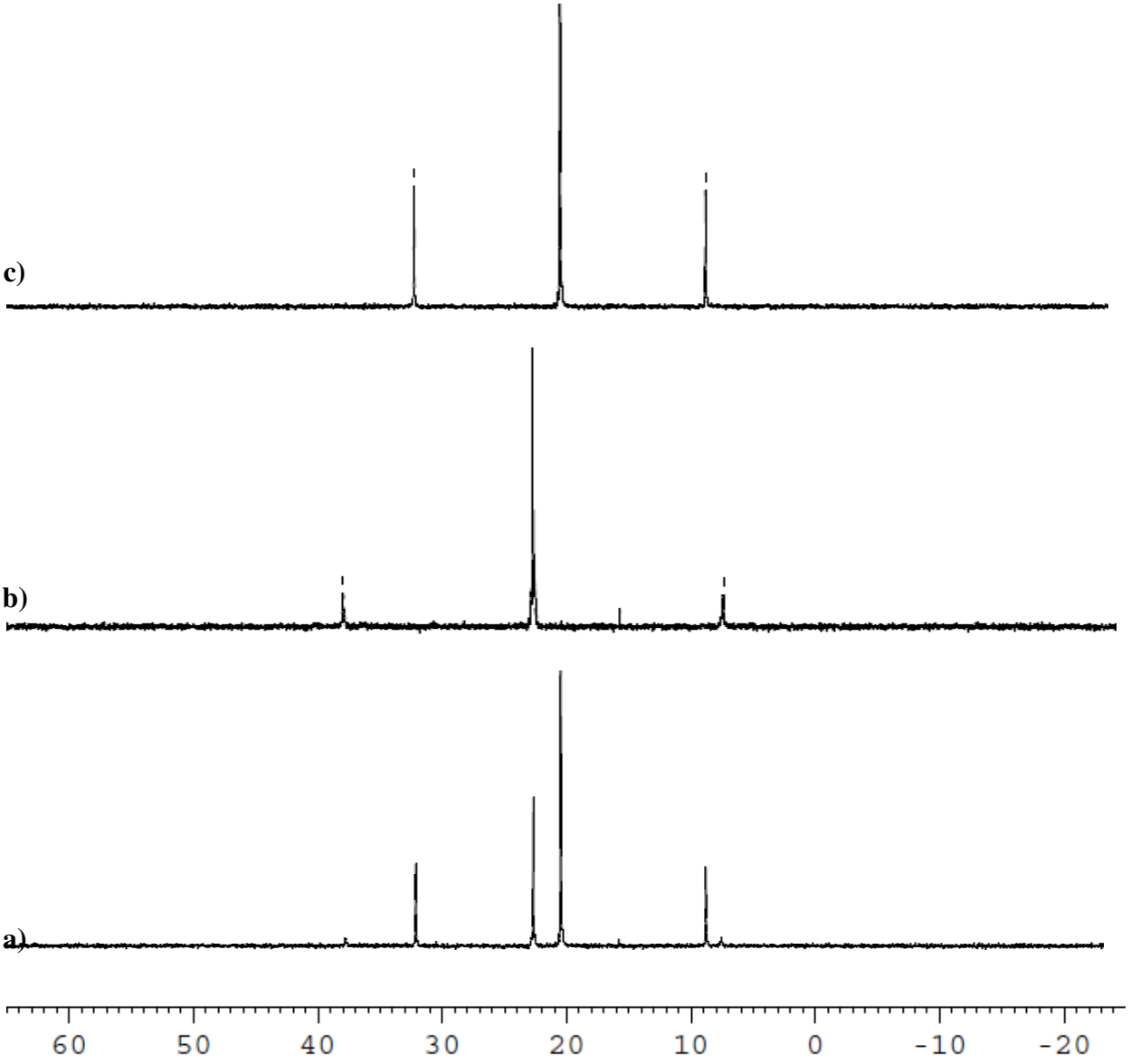

Figure 3.7 ^{31}P NMR spectra of: **a)** reaction mixture of **1** with $Pt(PPh_3)_4$; **b)** complex **8**; and **c)** complex **9**.

The ^{31}P NMR chemical shift of **8** (+21.24 ppm) is comparable with that observed for the dimeric Pd complex **7**, (+34.6 ppm) consistent with formation of dimeric $Pt_2(dmobdt)_2(PPh_3)_2$ and also revealed two similar sets of ^{1}H NMR resonances for the $dmobdt^{2-}$ reflecting the two distinct aryl C-H and methoxy C-H chemical environments. Conversely complex **9** revealed chemically equivalent methoxy and aryl ^{1}H environments consistent with the symmetry equivalent square planar mononuclear geometry of **9**. Extending the reaction times afforded selectively (^{31}P NMR) the dimetallic complex **8**, suggesting **9** is an intermediate *en route* to **8**.

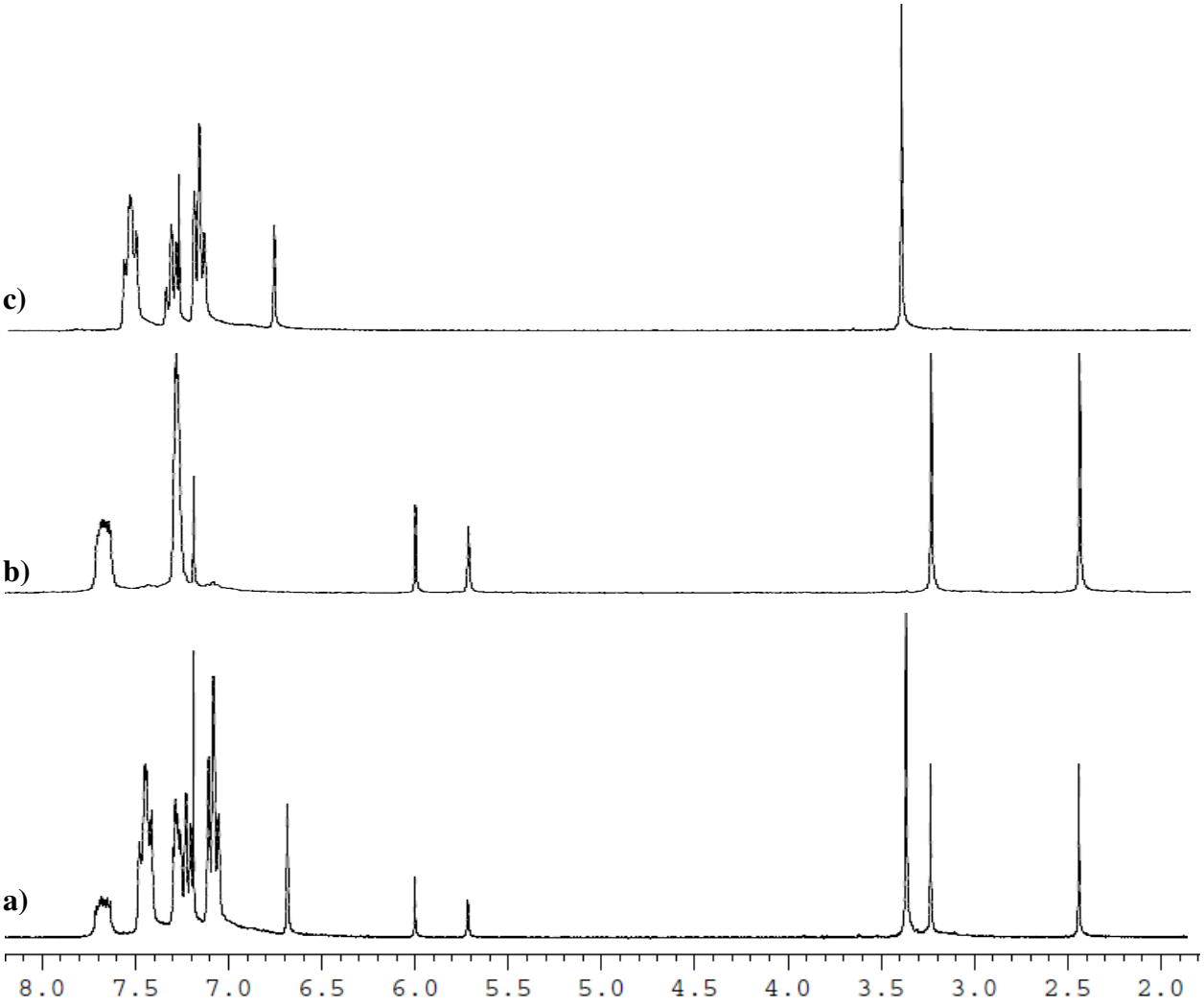

Figure 3.8 ^{1}H NMR spectra of: **a)** reaction mixture of **1** with $Pt(PPh_3)_4$; **b)** complex **8**; and **c)** complex **9** in $CDCl_3$.

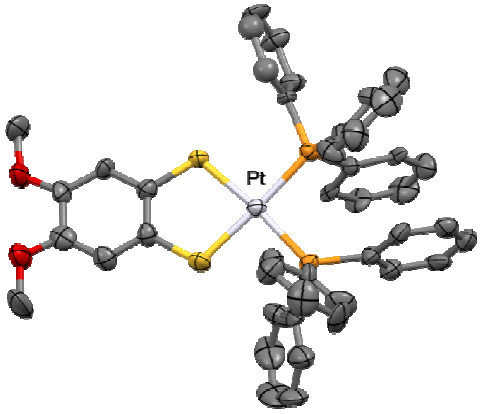

Figure 3.9 Crystal structure of complex **9** with thermal ellipsoids drawn at 75% probability. *Note that all hydrogen atoms and solvate molecules have been removed for clarity.*

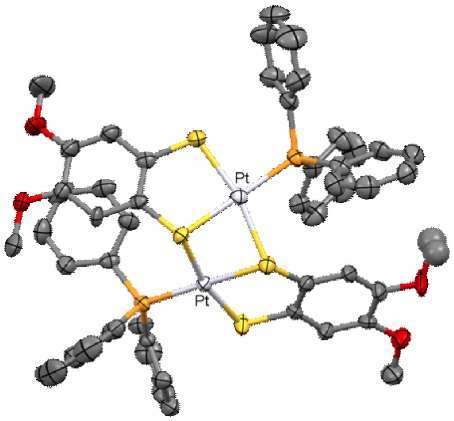

Figure 3.10 Crystal structure of complex **8** with thermal ellipsoids drawn at 75% probability. *Note that all hydrogen atoms and solvate molecules have been removed for clarity.*

3.2.3 Synthesis and Structural Studies of a Hexanuclear Complex, [Pd(dmobdt)]$_6$

To further investigate the effect of the phosphine ligand on reactivity, the effect of increasing the steric demand of the phosphine was explored by replacing PPh_3 (Tolman cone angle of 145º) with P^tBu_3 (cone angle of 182º).[22] Treatment of Pd_2dba_3 with tetrathiocine **1** in the presence of P^tBu_3 under microwave irradiation (see **Scheme 3.3**) led to the formation of a dark brown solution. Recrystallization from layering hexanes onto a saturated solution of CH_2Cl_2 afforded a small number of dark brown crystals suitable for

X-ray diffraction. Structural studies revealed formation of the hexanuclear complex, **10** (see **Figure 3.11**).

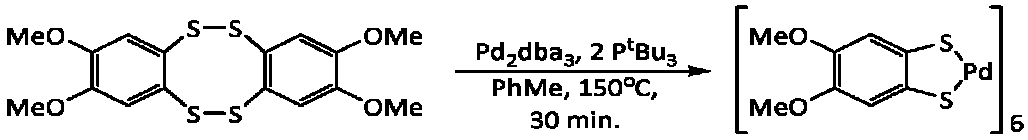

Scheme 3.3 Synthesis of hexanuclear complex **10**.

In order to remove any remaining impurities and improve the initial yield (ca. 2%), preparative TLC was used to purify complex **10** and the resulting brown band was removed from the silica with a mixture of CH_2Cl_2 and CH_3CN resulting in a dark clear brown solution. The solvent was removed to afford a brown oil which was recrystallized by slow diffusion of Et_2O into a saturated CH_2Cl_2 solution affording large dark crystals with an increased yield of 12%.

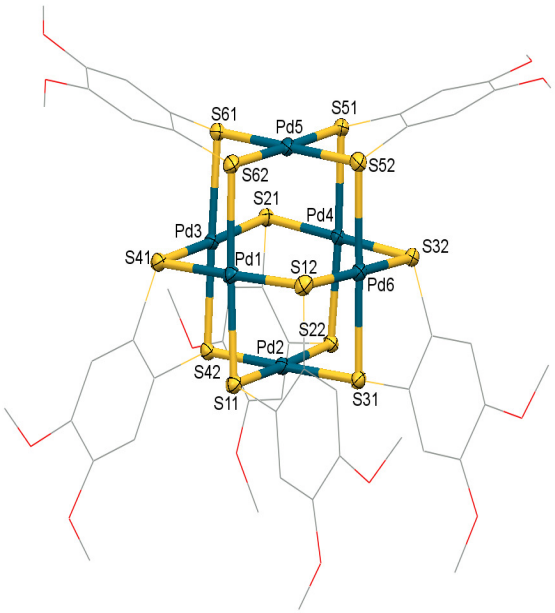

Figure 3.11 Crystal structure of complex **10** with thermal ellipsoids drawn at the 50% probability level for Pd and S. *Note that all hydrogen atoms and solvate molecules have been removed for clarity.*

The structure of **10** comprises an octahedron of Pd ions with each S atom of a dithiolate anion adopting a μ_2-bridging mode. Four $dmobdt^{2-}$ anions bridge from the basal Pd(2) to

the four 'equatorial' Pd centres (Pd1, Pd3, Pd4 and Pd6) whereas two dmobdt^{2-} ligands bridge from the apical Pd5 to the four equatorial Pd centres. The Pd-S distances fall in the range 2.294(2) – 2.361(2) Å. It is noteworthy, within the context of the ^{1}H NMR (*vide infra*) that there is a non-crystallographic 2-fold rotation axis passing through Pd2 and Pd5 such that the six dmobdt^{2-} ligands comprise three distinct coordination geometries. Although a range of homoleptic Pd^{II} dithiolate complexes of formula $[Pd(SR)_2]_6$ are known, these are almost invariably based upon cyclic structures.[23] Just one previous example of a hexanuclear dithiolate of this type has been reported previously;[24] $[PdS_2C_2(COOMe)_2]_6$ was prepared by transmetallation of $(tmeda)ZnS_2C_2(COOMe)_2$ with $Pd(MeCN)_2Cl_2$ with the zinc precursor formed in a multi-step reaction sequence.[25]

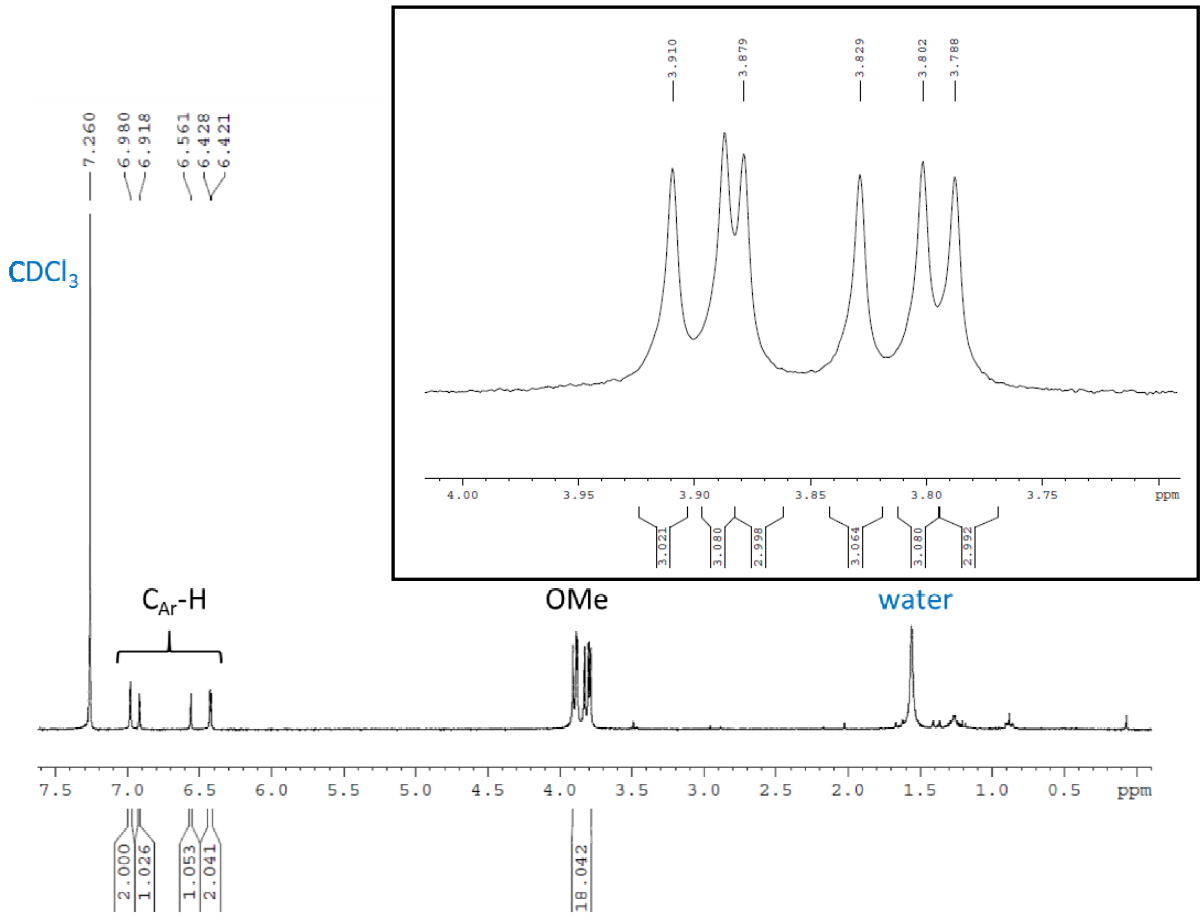

Figure 3.12 ^{1}H NMR (300 MHz, $CDCl_3$) of **10** with expansion of the methoxy region (inset).

Characterization of **10** by FAB+ mass spectrometry indicated a distribution of isotopomers around *m/z* = 1839 consistent with the mass of **10** (*m/z* = 1839.4). Elemental analysis confirmed the sample composition as **10**·½Et_2O. Complex **10** was further characterized using ^{1}H NMR which revealed the presence of three chemically distinct $dmobdt^{2-}$ ligand environments (each providing two metoxy and aryl C-H environments) consistent with the structure determined by X-ray diffraction, suggesting retention of the hexanuclear structure in solution (**Figure 3.12**).

3.2.4 Cyclic Voltammetry Studies on 7 and 10

Cyclic voltammetry studies (**Figure 3.13**) were made on solutions of **7** and **10** in CH_2Cl_2 using 0.01 M and $3.5x10^{-3}$ M [^{n}Bu_4N][PF_6] respectively as the supporting electrolyte, in order to compare and contrast the effects of increasing the number of metal centers on the redox properties of the complexes. Complex **7** containing two Pd metal centers was found to exhibit a reversible one-electron oxidation at 0.71 V with a peak-to-peak potential of 0.16 V.

The voltammagram of the hexanuclear complex **10** exhibits two reversible 1e^- reductions with $E_{1/2}$ = -0.91 and -1.34V (with respect to the Ag/Ag^+ reference electrode) and one clear reversible one-electron oxidation ($E_{1/2}$ = +1.25 V) coupled with a second oxidation around +1.52 V, close to the boundary of the electrochemical window. Attempts to use alternative solvents with different potential windows have so far proved unsuccessful due to lower solubility. The behaviour of **10** is markedly different from the previously reported complex $[PdS_2C_2(CO_2Me)_2]_6$ which displays four quasi-reversible one-electron reductions with peak-to-peak potentials of -0.186 V, -0.484 V, -1.174 V and -1.524 V respectively at a scan rate of 30 mV/s.[24]

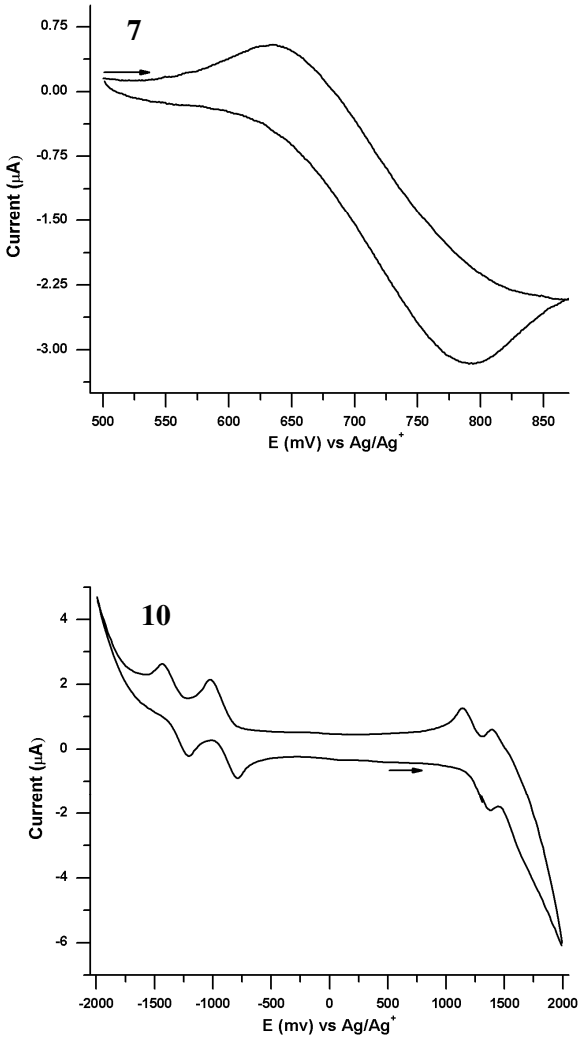

Figure 3.13 Cyclic voltammograms of complex **7** (top) and complex **10** (bottom) using 0.01 M and $3.5x10^{-3}$ M [$^{n}Bu_4N$][PF_6] supporting electrolyte in CH_2Cl_2 (scan rates 20 mV/s and 100 mV/s respectively).

3.3 Conclusion

In this chapter, the outcome of oxidative addition of tetrathiocines to low valent transition metal centres appears extremely sensitive to the steric and potentially electronic effects of the phosphine co-ligand. It was observed that the chelate effect of bidentate phosphines appears to favour the formation of mononuclear dithiolates **3**, **5**, and **6** whereas more labile monodentate phosphines lead to aggregation; PPh_3 afforded the di-nuclear dithiolate **7** whereas P^tBu_3 generated the phosphine-free hexanuclear complex **10**. Preliminary studies of the oxidative addition of **1** to $Pt(PPh_3)_4$ resulted in the formation of a mixture of both the monmeric (**9**) and dimeric (**8**) species. In addition longer reaction times afforded pure dimetallic complex suggesting that the mono-metallic $(dmobdt)Pt(PPh_3)_2$ is an intermediate generated *en route* to dimetallic $Pt_2(dmobdt)_2(PPh_3)_2$. A combination of mass spectroscopy, multinuclear NMR and electrochemistry suggest retention of the dinuclear and hexanuclear structures in solution.

In order to further probe the reactivity of these complexes, further studies on the co-ligand control of the oxidative addition of tetrathiocines to other low valent transition metals should be undertaken using other P-, N-, and O-donor co-ligands. In the next chapter, the effect of altering the dithiolate co-ligand on the structure and properties of these complexes is investigated.

3.4 Experimental

3.4.1 Electrochemistry

Cyclic voltammetry measurements were made on solutions of **7** and **10** in CH_2Cl_2 using 0.01 M and $3.5x10^{-3}$ M $[^nBu_4N][PF_6]$ respectively as the supporting electrolyte (electrochemical grade, Fluka) using a BAS 100B Electrochemical Analyzer with BAS 100W software using a sweep rate of 20 mV/s and 100 mV/swith glassy carbon working electrode, Pt wire auxiliary electrode and a Ag/AgCl reference electrode against which the Fc/Fc^+ couple appeared at +0.73 V.

3.4.2 Crystallographic Studies

Crystals were mounted on a cryoloop with paratone oil and examined on a Bruker SMART or Bruker APEX-II diffractometer equipped with a CCD area detector and an Oxford Cryostream cooler. Data were measured at 150(2) K using graphite-monochromated Mo-Kα radiation (λ = 0.71073 Å) using the APEX-II software.[26] Final cell constants were determined from full least squares refinement of all observed reflections. The data were corrected for absorption (sadabs)[27] and the structures solved by direct methods to reveal most non-H atoms. Remaining heavy atom positions were located in subsequence difference maps and the structure refined with full least squares refinement on F^2 within the SHELXTL suite.[28] Hydrogen atoms were placed at calculated positions and refined isotropically with a riding model. In some cases (**7**) lattice solvent was sufficiently well located to permit refinement but in others (**6**, **8** and **10**) lattice solvent was poorly located and treated with SQUEEZE within PLATON.[29]

For complex **6**, the large number of atoms and correlations coupled with modified hkl intensities due to SQUEEZE, a small number of light atoms (C) provided rather poor refinements and were refined with common thermal parameters (EADP) in the latter stages of refinement. This did not affect the R_1 and wR_2 values significantly but provided more sensible U_{ij} values. For complex **10** a TWIN command was additionally included due to a small but non-zero Flack parameter and refined as a 2-component inversion twin (96:4).

For complex **9**, refinement stalled at R1 = 15% with residual diffuse electron density consistent with poorly located lattice solvent. This was treated with SQUEEZE within PLATON which led to a modest improvement in residuals but R1 still stalled at 11%. A small number of highly disagreeable reflections were omitted (I > 7sigma) but failed to provide a large improvement in R1. Nevertheless the connectivity appears correct.

3.4.3 General Experimental Procedures

NMR spectra were recorded on a Bruker DPX300 UltraShield 300 MHz spectrometer with a Broadband AX Probe using $CDCl_3$ (^1H δ = 7.26 ppm, s) as an internal reference point relative to Me_4Si (δ = 0 ppm). ^{31}P NMR spectra were referenced to 85% H_3PO_4 (δ = 0 ppm). IR spectra were obtained using a Bruker Alpha FT-IR spectrometer equipped with a Platinum single reflection diamond ATR module. Elemental compositions were determined on a PerkinElmer 2400 Series II Elemental Analyzer. Mass spectra were recorded on a Waters Micromass LCT Classic Electrospray Ionization Time of Flight (ESI-TOF) mass spectrometer operated in positive mode while FAB+ spectra were recorded on a MSI/Kratos Concept 1S High Resolution Mass Spectrometer (Brock University).

3.4.4 Preparation of (dmobdt)Pd(dppm), (5).

Pd_2dba_3 (0.100 g, 0.109 mmol), dppm (0.084 g, 0.218 mmol) and tetrathiocine **1** (0.044 g, 0.109 mmol) were placed in an oven dried microwave vial under an inert nitrogen atmosphere. Dry toluene (5 mL) was added to the vial and the suspension was placed in the microwave for 20 mins at 150 °C to afford a red-brown solution over a small quantity of a dark precipitate. The solution was filtered off and evaporated *in vacuo* (0.098 g, 65% yield). The solid was recrystallized by slow diffusion of Et_2O into a saturated CH_2Cl_2 solution affording dark red-brown crystals suitable for X-ray diffraction.

NMR (ppm) ($CDCl_3$)**:** δ_H = 7.85 (8H, 7.87-7.83, m, *m*-H), 7.40 (12H, 7.46–7.38, m, *o,p*-H), 7.05 (2H, s, benzo C–H), 4.34 (2H, t, J = 9.6 Hz, PCH_2), 4.34 (6H, s, CH_3); $\delta_P\{^1H\}$ = -35.36.

HRMS (ESI-TOF) ***m/z***: $[M + H]^+$ calc. for $C_{33}H_{31}O_2P_2S_2Pd^+$ 691.0270; found 691.0311.

Elemental Analysis calc. for $C_{33}H_{30}O_2P_2S_2Pd \cdot ½CH_2Cl_2$: C 54.85; H 4.26%; found: C 55.07; H 4.25%.

IR ν_{max} (cm^{-1}): 3048(w), 2989(w), 2933(w), 2902(w), 2830(w), 1584(w), 1482(m), 1463(m), 1433(vs), 1339(m), 1239(s), 1198(m), 1173(m), 1097(s), 1036(s), 997(m), 845(m), 728(s), 689(vs), 536(m), 503(s).

3.4.5 Preparation of (dmobdt)Pd(dppf), (6).

Pd_2dba_3 (0.100 g, 0.109 mmol), dppf (0.121 g, 0.218 mmol) and tetrathiocine **1** (0.044 g, 0.109 mmol) were placed in an oven dried microwave vial under an inert nitrogen atmosphere. Dry toluene (5 mL) was added to the vial and the suspension was placed in the microwave for 20 mins at 150 °C. The resultant dark solution was filtered off leaving behind a small amount of dark solid. The filtrate was evaporate *in vacuo* to afford a brown solid (0.093 g, 50% yield). The solid was recrystallized from a saturated CH_2Cl_2 solution layered with hexanes to produce dark orange-brown crystals suitable for X-ray diffraction.

NMR (ppm) ($CDCl_3$)**:** δ_H = 7.79 (8H, 7.80-7.77, m, *m*-H), 7.47 (12H, 7.49–7.44, m, *o,p*-H), 7.35 (H, 7.37-7.33, m, o,p-H), 6.63 (2H, s, benzo C–H), 4.35 (4H, s, ferrocene C-H), 4.32 (4H, s, ferrocene C-H), 3.70 (6H, s, CH_3); $\delta_P\{^1H\}$ = 26.55.

HRMS (ESI-TOF) ***m/z***: $[M + H]^+$ calc. for $C_{42}H_{37}O_2P_2S_2PdFe^+$ 861.0089; found 861.0114.

Elemental Analysis calc. for $C_{42}H_{36}O_2P_2S_2PdFe$: C 58.60; H 4.22%; found: C 59.17; H 4.50%.

IR ν_{max} (cm^{-1}): 3047(w), 2988(w), 2931(w), 2901(w), 2830(w), 1584(w), 1480(s), 1433(vs), 1340(m), 1305(m), 1238(s), 1198(s), 1164(s), 1092(s), 1038(s), 998(m), 844(m), 822(m), 781(m), 730(vs), 690(vs), 632(s), 544(vs), 511(vs), 488(vs), 463(vs), 429(s).

3.4.6 Preparation of [(dmobdt)Pd(PPh$_3$)]$_2$, (7).

Pd_2dba_3 (0.100 g, 0.109 mmol), PPh_3 (0.115 g, 0.438 mmol) and tetrathiocine **1** (0.044 g, 0.109 mmol) were combined in an oven dried 5 mL microwave vial under an inert nitrogen environment. Dry toluene (5 mL) was added to the vial and the suspension was heated in the microwave for 40 min at 150 °C. The resultant dark green solution was isolated from a small amount of dark solid by filtration. The solution was concentrated by evaporation of solvent and purified by column chromatography. A bright green band was eluted from the column and the solvent removed by evaporation to afford a dark green oil. The oil was recrystallized from the slow diffusion of diethyl ether into a concentrated CH_2Cl_2 solution to produce dark green crystals suitable for X-ray diffraction. The crystals of **7** were washed with Et_2O and hexanes and dried in air (0.037 g, 30% yield).

NMR (ppm) ($CDCl_3$)**:** δ_H = 7.66 (12H, 7.69-7.63, m, *m*-H), 7.35 (18H, 7.36–7.34, m, *o,p*-H), 6.09 (2H, s, benzo C-H), 5.80 (2H, s, benzo C–H), 3.60 (6H, s, CH_3), 2.91 (6H, s, CH_3); $\delta_P\{^1H\}$ = 34.63.

m/*z* *(FAB$^+$ 3-NOBA Matrix, Unit Mass)*: calc. for $C_{52}H_{46}O_4P_2S_4Pd_2$ 1137.96; found 1138.

Elemental Analysis calc. for $C_{52}H_{46}O_4P_2S_4Pd_2 \cdot 3CH_2Cl_2$: C 47.43; H 3.76%; found: C 47.77; H 3.82%.

IR ν_{max} (cm^{-1}): 3051(w), 2993(w), 2934(w), 2901(w), 2832(w), 1586(m), 1555(w) 1477(s), 1434(vs), 1345(m), 1241(vs), 1202(s), 1176(s), 1095(s), 1037(s), 998(m), 922(w), 845(m), 784(m), 742(s), 691(vs), 525(vs), 511(s).

3.4.7 Preparation of [(dmobdt)Pt(PPh$_3$)]$_2$ (8) and (dmobdt)Pt(PPh$_3$)$_2$ (9).

$Pt(PPh_3)_4$ (0.500 g, 0.402 mmol) and tetrathiocine **1** (0.080 g, 0.200 mmol) were combined in an oven dried 5 mL microwave vial in an inert nitrogen environment. Dry toluene (5 mL) was added to the vial and the bright yellow suspension was heated in the microwave for 30 min at 150 °C. The resultant bright red solution was concentrated by evaporation of solvent and purified by column chromatography. A bright red-orange band was eluted from the column and the solvent removed by evaporation to afford a red

residue. The residue was recrystallized from the slow diffusion of diethyl ether into a saturated CH_2Cl_2 solution to produce both red (**8**) and orange (**9**) crystals suitable for X-ray diffraction. The crystals were washed with Et_2O and hexanes, dried in air and carefully separated by hand under a microscope (0.046 g of **8**, 27 % of mixture; 0.123 g of **9**, 73 % of mixture).

Complex 8:

NMR (ppm) ($CDCl_3$)**:** δ_H = 7.69 (12H, 7.71-7.68, m, *m*-H), 7.34 (18H, 7.36–7.33, m, *o,p*-H), 6.16 (2H, s, benzo C-H), 5.89 (2H, s, benzo C–H), 3.59 (6H, s, CH_3), 2.86 (6H, s, CH_3); $\delta_P\{^1H\}$ = 21.24 ($^1J_{Pt-P}$ = 4641 Hz).

HRMS (MALDI-TOF+) ***m/z***: $[M]^+$ calc. for $C_{52}H_{46}O_4P_2S_4Pt_2^+$ 1314.1042; found 1314.1042.

Elemental Analysis calc. for $C_{52}H_{46}O_4P_2S_4Pt_2 \cdot CH_2Cl_2$: C 45.46; H 3.46%; found: C 45.84; H 3.53%.

IR ν_{max} (cm^{-1}): 3053(w), 2992(w), 2934(w), 2902(w), 2833(w), 1589(w), 1488(s), 1435(vs), 1347(w), 1244(vs), 1203(m), 1177(w), 1097(s), 1038(m), 845(w), 785(m), 744(m), 692(s), 534(vs), 516(m), 499(m).

Complex 9:

NMR (ppm) ($CDCl_3$)**:** δ_H = 7.48 (12H, 7.50-7.47, m, *m*-H), 7.30 (6H, 7.32–7.28, m, *p*-H), 7.16 (12H, 7.19-7.14, m, *o*-H), 6.79 (2H, s, benzo C-H), 3.72 (6H, s, CH_3); $\delta_P\{^1H\}$ = 19.73 ($^1J_{Pt-P}$ = 3573 Hz).

MS (MALDI-TOF+) ***m/z***: 919 $[M]^+$, 719 [M^+ - dmobdt], 657 [M^+ - PPh_3].

Elemental Analysis calc. for $C_{44}H_{38}O_2P_2S_2Pt$: C 57.54; H 4.16%; found: C 57.20; H 4.30%.

IR ν_{max} (cm^{-1}): 3052(w), 2991(w), 2951(w), 2831(w), 1586(w), 1481(s), 1434(vs), 1342(m), 1242(s), 1201(w), 1093(s), 845(w), 743(m), 692(s), 541(s), 525(vs), 515(s).

3.4.8 Preparation of [Pd(dmobdt)]$_6$, (10).

Pd_2bda_3 (0.100 g, 0.109 mmol), P^tBu_3 (0.044 g, 0.218 mmol) and tetrathiocine **1** (0.044 g, 0.109 mmol) were combined in an oven dried 5 mL microwave vial in an inert nitrogen environment. Dry toluene (5 mL) was added to the vial and the suspension was heated in the microwave for 30 min at 150 °C. The resultant dark brown solution was isolated from a small amount of black solid by filtration. The solution was concentrated by evaporation of solvent and purified by preparative TLC (1:1 mixture of acetone and hexanes). The brown-yellow band was scratched from the silica plate and dissolved in a mixture of CH_2Cl_2 and MeCN. Evaporation of the solvent resulted in a brown oil and recrystallized from the slow diffusion of diethyl ether into a saturated CH_2Cl_2 solution to produce dark brown-yellow crystals suitable for X-ray diffraction. The crystals were washed with hexanes and dried in air (0.008 g, 12% yield).

NMR (ppm) ($CDCl_3$)**:** δ_H = 6.98 (4H, d, benzo C-H), 6.91 (2H, d, benzo C-H), 6.56 (2H, s, benzo C–H), 6.42 (4H, d, benzo C-H), 3.91 (6H, s, CH_3), 3.88 (12H, d, CH_3), 3.83 (6H, s, CH_3), 3.79 (12H, d, CH_3).

***m/z (FAB$^+$ NBA Matrix, Unit Mass)*:** calc. for $C_{48}H_{48}O_{12}S_{12}Pd_6^+$ 1839.4; found 1839.

Elemental Analysis calc. for $C_{48}H_{48}O_{12}S_{12}Pd_6 \cdot ½Et_2O$: C 31.99; H 2.85; found: C 32.26; H 2.79 %.

IR ν_{max} (cm^{-1}): 2994(w), 2933(w), 2895(w), 2834(w), 2582(w), 2038(w), 1579(m), 1474(s), 1430(vs), 1350(m), 1327(m), 1244(vs), 1204(vs), 1175(s), 1028(vs), 916(m), 847(m), 785(s), 731(m), 679(m), 575(w), 457(m).

3.5 References

1. *Dithiolene chemistry: Synthesis, properties, and applications,* ed. E. I. Stiefel, Interscience, Hoboken, New Jersey, 2003.

2. J. D. Wrixon, J. J. Hayward, O. Raza and J. M. Rawson, *Dalton Trans.*, 2014, **43**, 2134.

3. For examples see: **(a)** B. E. Bosch, M. Eisenhawer, B. Kersting, K. Kirschbaum, B. Krebs and D. M. Giolando, *Inorg. Chem.*, 1996, **35**, 6599; **(b)** C. C. McLauchlan and J. A. Ibers, *Inorg. Chem.*, 2001, **40**, 1809.

4. W.Gaete, J.Ros, X.Solans, M.Font-Altaba and J.L.Brianso, *Inorg. Chem.*, 1984, **23**, 39.

5. C. Zhang, T. Matsumoto, M. Samoc, S. Petrie, S. Meng, T.C. Corkery, R. Stranger, J. Zhang, M.G. Humphrey and K.Tatsumi, *Angew. Chem. Int. Ed.*, 2010, **49**, 4209.

6. **(a)** E. Cerrada, A. Moreno and M. Laguna, *Dalton Trans.*, 2009, 6825; **(b)** R. Cao, M. Hong, F. Jiang, X. Xie and H. Liu, *Dalton Trans.*, 1994, 3459.

7. R. J. Puddephatt, *Chem. Soc. Rev*., 1983, **12**, 99.

8. *The Organometallic Chemistry of the Transition Metals,* R. H. Crabtree, John Wiley and Sons: Chichester, 1994.

9. **(a)** A. G. Orpen and N.G. Connelly, *Organometallics*, 1990, **9**, 1206; **(b)** D.G. Gilheany, *Chem. Rev.*, 1994, **94**, 1339; **(c)** N. Fey, A.G. Orpen, and J.N. Harvey, *Coord. Chem. Rev.*, 2009, **253**, 704.

10. **(a)** R.G. Pearson, *J. Chem. Ed.* 1968, **45**, 581; **(b)** R.G. Pearson, *J. Chem. Ed.,* 1968, **45**, 643.

11. T. Appleby and J. D. Woollins, *Coord. Chem. Rev.*, 2002, **235**, 121.

12. C. A. Tolman, *Chem. Rev*., 1977, **77**, 313-348.

13. **(a)** R. Romeo, G. Arena and L. M. Scolaro, *Inorg. Chem.*, 1992, **31**, 4879; **(b)** F. Ozawa, T. Ito and A. Yamamoto, *J. Am. Chem. Soc*., 1980, **102**, 6457.

14. K. J. Lee and T. L. Brown, *Inorg. Chem.*, 1992, **31**, 294.

15. O. Kuhl, Phosphorus-31 NMR Spectrscopy, Springer-Verlag, Berlin, Heidelberg, 2008.

16. **(a)** A. J. Blake, Y. V. Roberts and M. Schroder, *J. Chem. Soc., Dalton Trans*., 1996, **9**, 1885; **(b)** Z. Qin, M. C. Jennings and R. J. Puddephatt, *Inorg. Chem*., 2001, **40**, 6220.

17. **(a)** Y. C. Neo, J.J. Vittal and T. S. A. Hor, *J. Organomet. Chem.*, 2001, **637**, 757; **(b)** M. J. D. Champion, R. Solanki, L. Delaude, A. J. P. White and J. D. E. T. Wilton-Ely, *Dalton Trans*., 2012, **41**, 2386; **(c)** S. A. Al-Jibori, T. F. Khaleel, S. A. O. Ahmed, L. J. Al-Hayaly, K. Merzweiler, C.Wagner and G. Hogarth, *Polyhedron*, 2012, **41**, 20; **(d)** C. Herrera-Alvarez, V. Gomez-Benitez, R. Redon, J. J. Garcia, S. Hernandez-Ortega, R. A. Toscano and D. Morales-Morales, *J. Organomet. Chem.*, 2004, **689**, 2464; **(e)** T. F. Baumann, J. W. Sibert, M. M. Olmstead, A. G. M. Barrett and B. M. Hoffman, *J. Am. Chem. Soc*., 1994, **116**, 2639; **(f)** L. L. Maisela, A. M. Crouch, J. Darkwa and I. A. Guzei, *Polyhedron*, 2001, **20**, 3189.

18. L. Xiulian, Ph.D. Dissertation, National University of Singapore, 2003.

19. **(a)** F. Pop, D. G. Branzea, T. Cauchy and N. Avarvari, *Compt. Rend*, 2012, **15**, 904; **(b)** R. Cao, M. Hong, F. Jiang and H. Liu, *Acta Cryst*., 1995, **C51**, 1280.

20. P. E. Garrou, *Chem. Rev*., 1981, **81**, 229-266.

21. *Chemical Kinetics and Inorganic Reaction Mechanisms,* 2nd ed., S. Asperger, Springer Science and Business Media: New York, 2003.

22. *Inorganic Chemistry*, 3rd ed., C. E. Housecroft and A.G. Sharpe, Prentice-Hall, Harlow, England, 2008.

23. **(a)** V.P. Ananikov, N.V. Orlov, S.S. Zalesskiy, I.P. Beletskaya, V.N. Khrustalev, K. Morokuma and D.G. Musaev, *J. Am. Chem. Soc.*, 2012, **134**, 6637; **(b)** Z. Yang, A.B. Smetana, C.M. Sorenson and K.J. Klabunde, *Inorg. Chem.* 2007, **46**, 2427.

24. C. L. Beswick, R. Terroba, M. A. Greaney and E. I. Stiefel, *J. Am. Chem. Soc*., 2002, **124**, 9664.

25. A. K. Verma, T. B. Rauchfuss and S. R. Wilson, *Inorg. Chem.*, 1995, **34**, 3072.

26. APEX-II, Bruker AXS Inc., Madison, Wisconsin, USA.

27. Sadabs, Bruker AXS Inc., Madison, Wisconsin, USA.

28. SHELXTL package for crystal structure solution and refinement, Bruker AXS Inc., Madison, Wisconsin, USA.

29. **(a)** A.L. Spek, *Acta. Cryst.*, 2015, **C71**, 9; **(b)** A.L. Spek, *Acta. Cryst.*, 2009, **D65**, 148.

CHAPTER 4

Synthesis and Structural Characterization of Mononuclear Palladium (II) Complexes of bis(alkoxy) benzene dithiolates

4.1 Introduction

In the second chapter, the high yield synthesis and characterisation of a series of group 10 complexes **2-4** containing the dmobdt^{2-} ligand was described *via* the one-pot microwave-assisted oxidative addition of bis(dimethoxybenzo)tetrathiocine (**1**) to zero-valent group 10 metal complexes in the presence of the chelating phosphine ligand dppe. In the subsequent chapter, the influence of the phosphine on the oxidative addition of bis(dimethoxybenzo)tetrathiocine to Pd(0) was studied yielding a variety of structures containing mono-, di-, and multi-metallic complexes. In this chapter, the oxidative addition of a variety of benzotetrathiocines to Pd(0) in the presence of dppe was studied in order to probe the effect of tetrathiocine functionalization.

4.1.1 Dialkoxy-benzene Tetrathiocines

In 1989, Stender *et al.* developed a methodology for the ready access of a range of alkoxy-functionalized tetrathiocines in multi-gram quantities in a one-pot reaction.[1] Recent studies within the Rawson group have pursued this reactivity and replicated the syntheses of **1**, as well as **11**–**12** (**Figure 4.1**) as precursors to benzo-fused 1,3,2-dithiazoles (Chapter 5).[2] In this Chapter the syntheses of additional tetrathiocines **13** – **16** (**Figure 4.1**) are described and their oxidative addition to Pd(0) examined. In particular the novel tetrathiocine bearing a benzene-15-crown-5 substituent (**16**, **Figure 4.1**) offers the potential to construct novel multi-heterometallic complexes through selective coordination of hard metals at the crown and soft metal binding at the dithiolate and the potential to encompass the wide applications associated with both crown ethers and transition metal dithiolate complexes. The synthesis and properties of crown ethers were first discovered by Charles Pederson in 1967 while attempting to prepare a complexing agent for divalent cations.[3] His discovery, which led to his 1987 Nobel Prize in

Chemistry, has been extensively pursued in coordination chemistry with a broad range of applications, particularly based on the metal-selective coordination of different crown-ethers dependent upon donor atoms and ring size.[4]

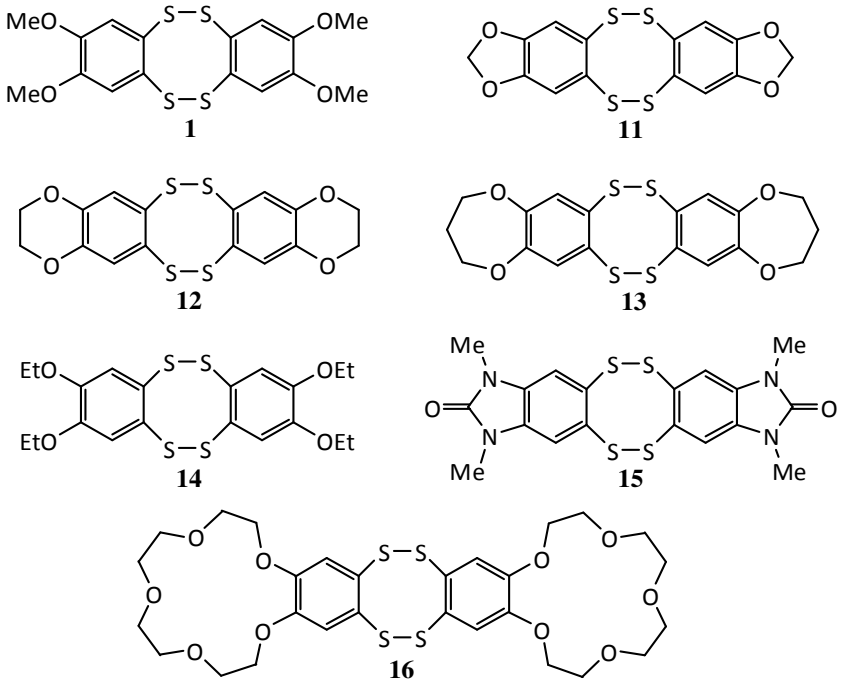

Figure 4.1 The library of di-benzo-functionalised tetrathiocine derivatives prepared and implemented in this Chapter.

4.2 Results and Discussion

4.2.1 Synthesis of Various Tetrathiocine Ligands, (11 – 16).

The preparation of tetrathiocines occurs *via* an electrophilic aromatic substitution reaction (**Scheme 1.4**) in which the strongly ionizing glacial acetic acid solvent appears to assist generation of ClS_2^+ from S_2Cl_2. The alkoxy groups are strongly *para*-directing with respect to electrophilic substitution and it is this feature which was exploited by Stender who described the synthesis of **1** and **14**. Tetrathiocines **1, 11–12** were previously prepared in the Rawson group by Efren Navarro-Moratalla[2,5] and **14** by T. Wilson.[6] Samples of **1, 11 – 14** were prepared according to this general methodology (**Scheme 1.4**). In order to further extend this methodology we targeted:

(a) the 2′,3′,8′,9′ -bisdioxepinyldibenzo-1,2,5,6-tetrathiocine (**13**)

(b) the *N,N′*-dimethylbenzimidazole-1,2,5,6-tetrathiocine (**15)** which possesses strongly activating π-donor N groups as an alternative to the alkoxy functional group;

(c) the bis-15-crown-5-dibenzo-1,2,5,6-tetrathiocine (**16)** as a model for other benzo-crown chemistry.

With the exception of the *N,N′*-dimethylbenzimidazole which was kindly prepared and provided by Dr. J.J. Hayward, all starting materials were commercially available. Treatment of the substrate in glacial acetic acid with S_2Cl_2 at room temperature afforded the tetrathiocine as a yellow-blue precipitate. The blue colouration, tentatively assigned to poly-sulfur cations, could be decolourised with a few drops of a saturated methanolic solution of tin(II) chloride. The reaction times and recovered yield for each tetrathiocine are summarised in **Table 4.1**. The tetrathiocines typically exhibited limited solubility across a range of organic solvents, hampering full characterisation by multinuclear NMR. However all tetrathiocines provided satisfactory elemental analysis, assuming small quantities of occluded $CHCl_3$.

Table 4.1 Reaction times and respective yields for ligands **1, 11–16**.

Tetrathiocine	Reaction Time (hours)	Recovered Yield (%)
1	18	41
11	48	72
12	120	88
13	168	78
14	60	53
15	72	71
16	168	61

4.2.2 Synthesis of Palladium Complexes Containing Benzene Dithiolate Ligands

In the previous two chapters the oxidative addition of 2′,3′,8′,9′-tetramethoxy-dibenzo-1,2,5,6-tetrathiocine (**1**) to low-valent group 10 metals was shown to afford a variety of M^{II} complexes depending upon the nature of the metal and phosphine co-ligand. In this Chapter, the metal center (Pd) and the phosphine co-ligand (dppe) were held constant and the tetrathiocine varied in order to examine the diversity of functional group which could be appended to the benzenediothiolate ligand. Using the same general one-pot methodology used in Chapter 2, six new mononuclear complexes, Pd(L)(dppe), **17** – **22**, were prepared (L = dithiolate ligand) from the tetrathiocines **11-16** (**Scheme 4.1**). Recrystallization from a saturated CH_2Cl_2 solution by layering with hexanes afforded crystals of **17 - 20**, whereas slow diffusion of Et_2O into a saturated CH_2Cl_2 solution afforded crystals of **21** and **22** suitable for X-ray diffraction (see **Figure 4.2**).

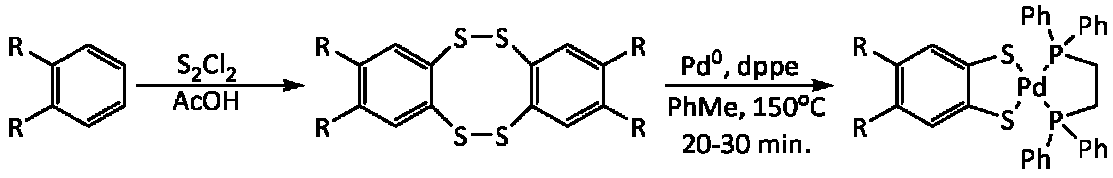

Scheme 4.1 General synthetic methodology to prepare complexes **17-22**.

The crystal structures of **17** – **22** all reveal similar Pd-S bond lengths (**Table 4.2**) which fall in the range 2.283(1) – 2.310(1) Å and Pd-P bond lengths in the range 2.250(1) – 2.303(1) Å. These are comparable with the Pd-S and Pd-P bond lengths in (dmobdt)Pd(dppe) (**3**) described in Chapter 2. The chelate SPdS angles are almost

invariant, falling in the range 88.83(3) – 89.44(3)^o whilst the PPdP angles also show little variation 84.66(3) – 85.93(4)^o (**Table 4.2**). With the exception of **17**, the PdP_2S_2 centres are essentially planar with the sum of the internal angles falling in the range 359.96 – 360.42^o. In this context **17** seems anomalous with the sum of the internal angles equal to 352.83^o with P1 located slightly out of the PdS_2P plane.

To date, only preliminary studies have been undertaken for **21** and further characterization is required in order to confirm purity. The purity of the other five complexes was confirmed by high resolution mass spectrometry (ESI+ TOF) indicating the presence of the expected $[M + H]^+$ ion peaks with three replicate acquisitions completed to better than 0.5 ppm mass accuracy. The structures of **18** and **21** both contained well-defined CH_2Cl_2 lattice solvent and **22** contained a MeCN lattice solvent molecule. Complex **20** exhibited poorly located lattice solvent. However, the propensity of these crystals to lose solvent when removed from the mother liquor is reflected in the microanalytical data which revealed sub-stoichiometric quantities of solvent remaining in the crystal lattice due to desolvation effects (see **Table 4.3**).

Table 4.2 Selected bond lengths and bond angles for complexes **17-22.**

	17	**18**	**19**	**20**	**21**	**22**
Pd-S bond length (Å)	2.301(1)	2.310(1)	2.292(1)	2.2920(7)	2.3005(9)	2.3057(7)
	2.283(1)	2.291(1)	2.3042(8)	2.2984(7)	2.3088(7)	2.293(1)
Pd-P bond length (Å)	2.250(1)	2.269(1)	2.2676(8)	2.2570(7)	2.2737(8)	2.2740(7)
	2.290(1)	2.299(1)	2.2711(9)	2.2807(7)	2.288(1)	2.305(1)
S-Pd-S bond angle (°)	89.23(3)	88.83(3)	89.19(3)	89.41(2)	89.44(3)	89.03(3)
P-Pd-P bond angle (°)	85.33(3)	84.92(3)	85.41(3)	84.69(2)	85.48(3)	85.95(3)

Table 4.3 Microanalytical data and ^{31}P NMR chemical shifts for complexes **17 - 22**. Data for **22** were from a sample recrystallized from CH_2Cl_2.

Complex	Composition	^{31}P NMR (ppm)
17	$C_{33}H_{28}O_2P_2S_2Pd$ calc. C 57.52 H 4.10 found C 57.07 H 3.82	51.52
18	$C_{34}H_{30}O_2P_2S_2Pd \cdot {}^1/_5CH_2Cl_2$ calc. C 57.04 H 4.26 found C 57.07 H 4.13	51.63
19	$C_{35}H_{32}O_2P_2S_2Pd$ calc. C 58.62 H 4.50 found C 57.17 H 4.30	51.96
20	$C_{36}H_{36}O_2P_2S_2Pd$ calc. C 58.98 H 4.95 found C 58.92 H 4.87	51.73
22	$C_{40}H_{42}O_5P_2S_2Pd \cdot ½CH_2Cl_2$ calc. C 55.42 H 4.94 found C 55.36 H 5.14	51.89

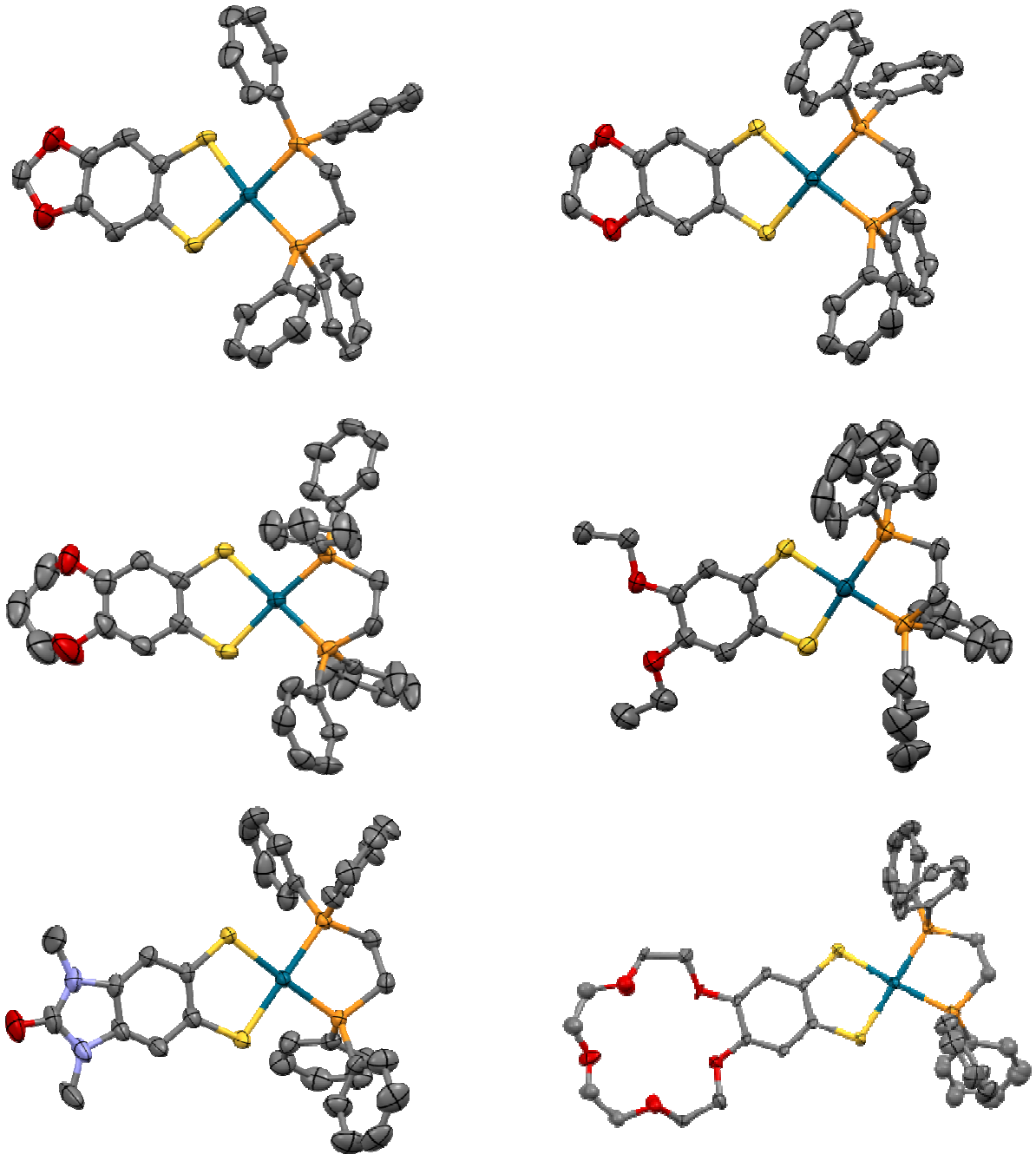

Figure 4.2 Crystal structure of complexes **17, 18** (top); **19** and **20** (middle); **21** and **22** (bottom). Thermal ellipsoids are drawn at 75% probability. *Note that all hydrogen atoms and solvate molecules have been removed for clarity.*

Further analysis by ^{1}H and ^{31}P NMR confirmed the presence of the desired complexes. ^{31}P NMR of complexes **17 – 20**, and **22** indicated the presence of a singlet with chemical shifts ranging from 51.89 – 51.52 ppm (**Table 4.3**) which are very similar to the 51.94 ppm chemical shift for complex **3**. Replacement of the dialkoxy group by the *N,N′*-dimethyl benzimidazole moiety led to an upfield shift for complex **21** (26.55 ppm).

Notably the five oxygen atoms of the macrocycle in **22** are all involved in hydrogen bonding; three of the O atoms form hydrogen-bonds to the acetonitrile solvate. The shortest of these C-H···O14 (1.95 Å) is strongly directional (C-H···O 169°), whereas the other two O atoms form a pair of longer, bifurcated C-H···O contacts; C-H···O12 2.15 Å (C-H···O 144°) and C-H···O11 2.56 Å (C-H···O 138°). The remaining two macrocyclic O atoms form C-H···O contacts to a phenyl ring of the dppe; C-H···O15 2.55 Å (C-H···O 133°) and C-H···O13 2.54 Å (C-H···O 133°) (**Figure 4.3**).

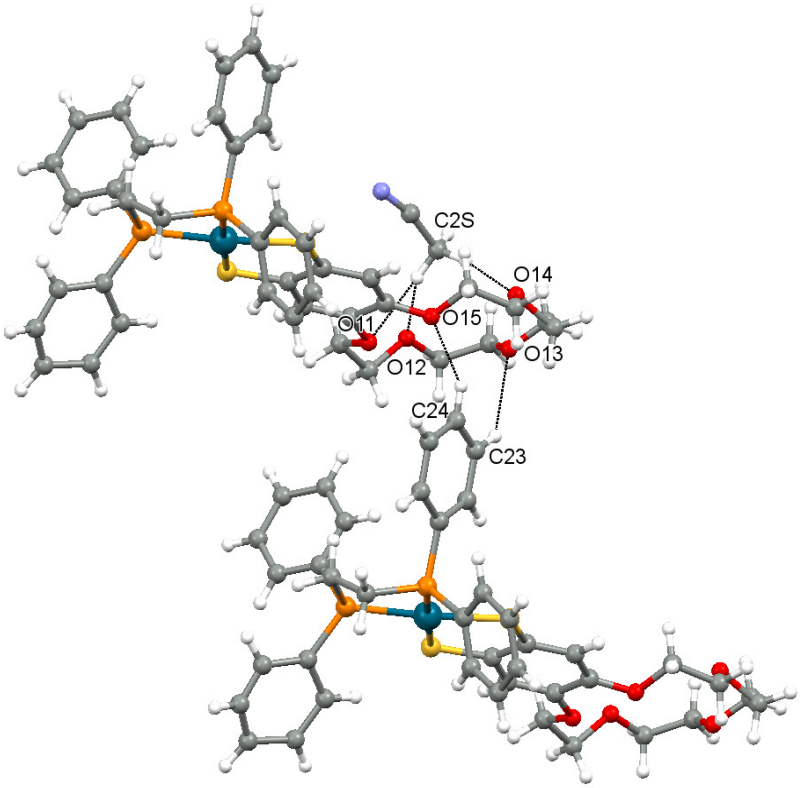

Figure 4.3 Hydrogen bonding between the macrocyclic O atoms of **22** and the acetonitrile solvate molecule and aryl C-H groups.

4.2.3 Crown Complexation of (15-crown-5-bdt)Pd(dppe)

Since their first discovery in 1967 by Pederson,[3] crown ethers have been used extensively as ligands for the complexation of metal ions and various other ionic species. The ability of crown ethers as ligands to select metal cations based on their size and ability to fit within the available open space of the macrocycle, have made them popular in a number of chemical and biochemical reactions and processes.[7] The formation of crown complex **22**, provided the opportunity to conduct preliminary studies on the formation of multi-metallic crown dithiolate complexes. Based on the available space within the pocket of the benzo-15-crown-5 macrocycle, alkali metals are among the most popular metal cations used in complexation reactions, with the crown preferentially binding Na^+ and K^+ ions over smaller ions like Li^+ or larger cations such as Rb^+. Reaction of complex **22** with one equivalent of $Na[BPh_4]$ in a 1:1 mixture of CH_2Cl_2 and MeOH afforded the crown ether complex [**22**·Na][BPh_4] (**23**) which was recrystallized by layering the reaction mixture with hexane.

Complexation of the macrocycle **22** to the Na^+ cation leads to a modest increase in the Pd-S bond lengths from an average of 2.300(1) Å in **22** to 2.315(2) Å in **23**. However other geometric parameters including the C-S bond lengths (average 1.762(4) in **22** and 1.768(3) Å in **23**) remain unchanged within error.

The Na^+ cation is 7-coordinate bound by five O-donors from the benzo-crown-5 macrocycle plus an additional two coordinated methanol molecules with Na-O bond lengths in the range 2.336(3) – 2.559(3) Å. The geometry is highly distorted with ONaO bond angles ranging from 63.53(8) – 164.4(1)^o but approximates to a face-capped trigonal prism (**Figure 4.4**, inset).

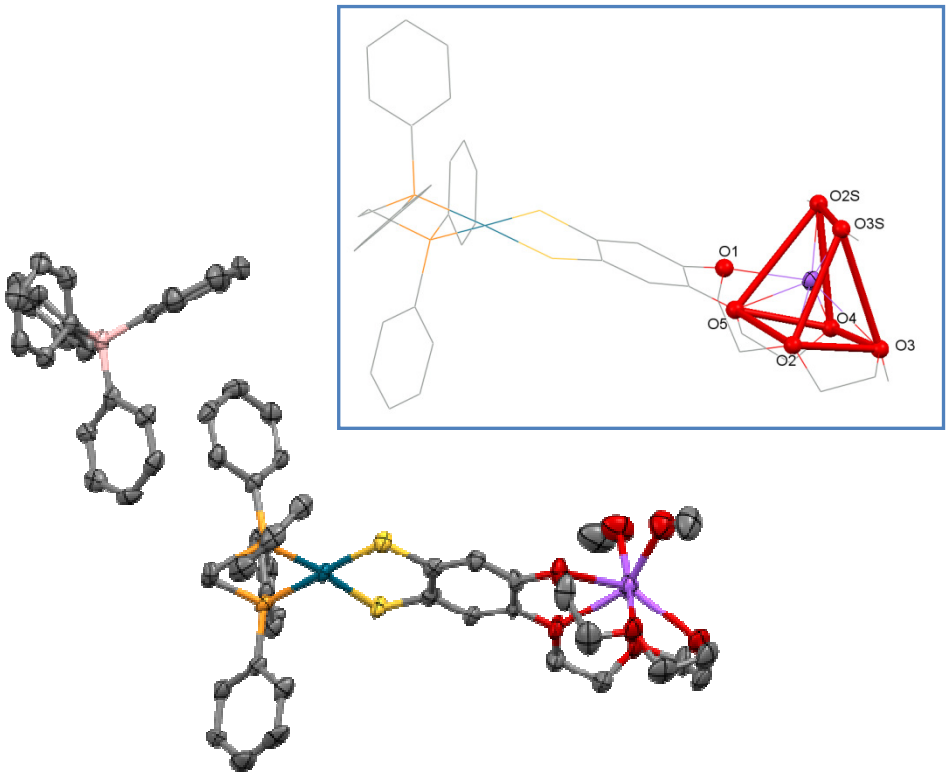

Figure 4.4 Crystal structure of complex **23** with thermal ellipsoids drawn at 75% probability. Inset: the coordination sphere around the Na^+ cation. *Note that all hydrogen atoms and lattice solvent molecules have been removed for clarity.*

Using the same methodology the ferrocene complex **24** could be prepared from **16**, $Pd_2(dba)_3$ and dppf which exhibits a redox-switchable ferrocene unit, a 'push-pull' chromophore and a macrocylic metal-binding cavity. Subsequent treatment with $Na[BPh_4]$ in a 1:1 CH_2Cl_2/MeOH mixture afforded the hetero-trimetallic complex **25** which was recrystallized by layering with hexanes. The structure of **25** contains two crystallographically independent molecules. Each of the two molecules is located about a crystallographic inversion centre such that each of the two crystallographiocally independent units of **25** forms a centrosymmetric dimer in which the Na^+ cation adopts a 6-coordinate NaO_5S geometry, in which one of the dithiolate S atoms adopts a μ_2-bridging mode (**Figure 4.5**).

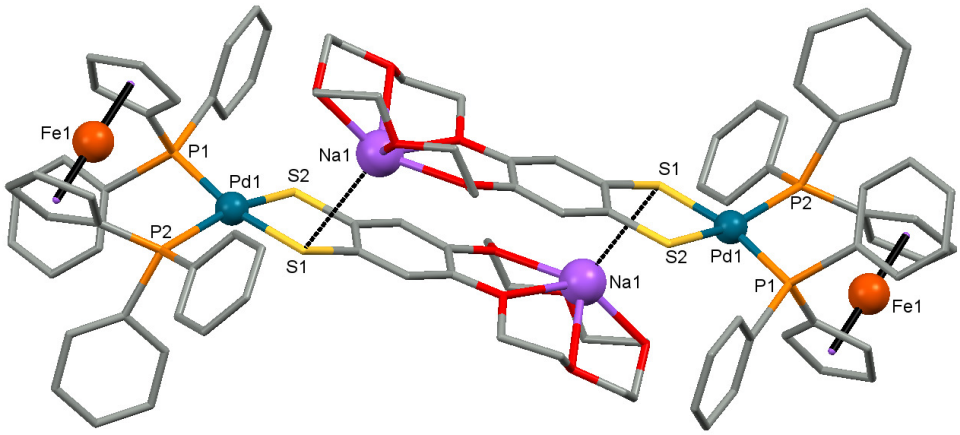

Figure 4.5 One of the two crystallographically independent dimeric cations in the structure of **25**. *The Ph_4B^- and all hydrogen atoms have been removed for clarity.*

The Na-O bond distances to Na1 span the range 2.287(6) – 2.486(5) Å somewhat shorter than the corresponding Na-O bond distances to Na2 (2.355(6) – 2.559(6) Å) in the second crystallographically independent dimer. This variation seems linked to the strength of the Na···S interaction at the sixth coordination site. Here the Na1-S1 distances are somewhat longer at 3.083(4) Å when compared to 2.808(3) Å for Na2-S4, suggesting a move towards a more '5-coordinate' geometry for Na1, favouring shorter Na1-O bonds. Conversely Na2 is closer to a more formal 6-coordinate geometry. The degree of S-coordination to sodium seems to differ between the two crystallographic units and has marked effects on the geometry at the palladium dithiolate part of the molecule. For the first crystallographically independent molecule the bridging S atom (S1) forms a long contact to Na1 (3.083(4) Å) and a short Pd-S bond to Pd1 (2.243(2) Å) which is shorter than Pd1-S2 (2.393(2) Å). Conversely in the second crystallographically independent molecule, the shorter Na2-S4 distance (2.808(3) Å) leads to a longer Pd2-S4 bond (2.539(2) Å) which in turn is now longer than Pd2-S3 (2.274(2) Å). Overall this suggests a synergistic interplay between Na-S and Pd-S bonding within these dimers.

Further work is necessary to fully characterize both **23** and **25** and examine their redox and UV/visible properties in relation to **22** and **24**. Changes in redox behavior or spectroscopic properties could be used to develop sensors which reflect the metal ion

bound in the macrocyclic ‘pocket’ and it will be of interest to compare metal selectivities of **22** and **24** in relation to the parent benzo-crown-5.

4.3 Conclusions

These studies reveal that not only can a wider range of functionalized tetrathiocines be prepared, including those bearing nitrogenous π-donors instead of alkoxy groups, but that these tetrathiocines readily undergo a range of oxidative addition reactions to zero-valent group 10 metals. Preliminary results have shown that benzo-crowns can be functionalized to access benzo-crown-dithiolate complexes in two simple steps leading to materials in which the selective metal-binding capacity of the crown is incorporated into a structure which also offers a redox-active centre (ferrocene) and strong chromophore (metal dithiolate). Such properties offer significant potential to construct a range of sensors and multi-functional materials. Moreover, based on the results obtained in Chapter 3, reaction of the crown-functionalised tetrathiocine with Pd_2dba_3 in the presence of $^tBu_3P$ may afford a hexameric cage decorated with six metal binding pockets, offering a range of potential redox-active polymetallic complexes.

4.4 Experimental

4.4.1 Preparation of 2',3',8',9' -bisdioxolyldibenzo-1,2,5,6-tetrathiocine [$(CH_2O_2)C_6H_2S_2]_2$, (11).[5]

1,3-benzodioxole (3 mL, 29.11 mmol) was added to 30 mL of degassed glacial acetic acid under an inert nitrogen atmosphere. S_2Cl_2 (2.33 mL, 29.11 mmol) was added dropwise to the rapidly stirring solution. The solution was stirred at room temperature for 48 h. A yellow precipitate was isolate *via* vacuum filtration and washed with Et_2O (2 × 15 mL). The solid was redissolved in the minimum amount of $CHCl_3$ (~ 500 mL) and evaporated to half its volume. The dark yellow solution was treated with 300 mL of ice cold MeOH and placed in freezer for 24 h. The yellow solid was isolated *via* vacuum filtration, washed with ice cold methanol (2 × 10 mL) and dried thoroughly *in vacuo* (3.84 g, 72% yield).

Elemental analysis calc. for $C_{14}H_8O_4S_4$: C 45.60; H 2.20%; found: C 43.67; H 2.31%

IR (ν_{max}, cm^{-1}): 2892(w), 1594(w), 1498(m), 1460(vs), 1365(w), 1318(m), 1233(vs), 1133(m), 1071(w), 1033(vs), 938(m), 921(s), 858(s), 828(m), 753(w), 725 (w), 711 (w), 658(w), 640(w), 459(w), 448(w), 434 (w).

4.4.2 Preparation of 2',3',8',9' -bisdioxlyldibenzo-1,2,5,6-tetrathiocine [$(CH_2CH_2O_2)C_6H_2S_2]_2$, (12).

1,4-benzodioxane (2 mL, 16.8 mmol) was added to 30 mL of degassed glacial acetic acid in an inert nitrogen atmosphere. S_2Cl_2 (1.4 mL, 16.8 mmol) was added dropwise to the rapidly stirring solution under a nitrogen environment. After the addition of S_2Cl_2, the bright yellow solution was left to stir. After 18 h, a green precipitate began to form. The reaction was left to stir for 5 days in order to ensure completion. The green-yellow solid was filtered via cannula, washed with Et_2O (2 × 10 mL) and dried thoroughly in *vacuo*. The dried powder was suspended in 60 mL of MeOH and treated with $SnCl_2$ (0.5 g) and left to stir for 48 h at room temperature to afford a pale yellow homogenous solid. The pale yellow solid was isolated via cannula filtration, washed with MeOH (2 × 60 mL), and dried in *vacuo* to afford a powder (2.93 g, 88% yield).

Elemental analysis calc. for $C_{16}H_{12}O_4S_4 \cdot {}^1/_{10}\,CHCl_3$: C 47.34; H 2.99%; found: C 47.48; H 3.26%

IR (ν_{max}, cm^{-1}): 2980(w), 2931(w), 2875(w), 1561(s), 1467(s), 1295(vs), 1276(s), 1251(vs), 1176(m), 1062(vs), 908(s), 894(s), 699(m), 502(w), 461(m).

4.4.3 Preparation of 2',3',8',9'-bisdioxepinyldibenzo-1,2,5,6-tetrathiocine [$(CH_2CH_2CH_2O_2)C_6H_2S_2]_2$, (13).

3,4-dihydro-2H-1,5-benzodioxepin (1.9 mL, 14.3 mmol) was added to 30 mL of degassed glacial acetic acid in an inert nitrogen atmosphere. S_2Cl_2 (1.15 mL, 14.3 mmol) was added dropwise to the rapidly stirring solution under a nitrogen environment. With each addition of S_2Cl_2 the solution turned brighter yellow. The solution was left to stir for 7 days; after 18 h the solution turned orange-red with no precipitate present; after stirring for 5 days, the solution turned dark yellow and a yellow precipitate had started to form along with a brown solid at the bottom of the flask; after 7 days of stirring at room temperature, the yellow solid and brown material were isolated by filtration via cannula, washed with Et_2O (2 × 10 mL), and dried in *vacuo*. Once thoroughly dried, the solid was suspended in 60 mL of MeOH and treated with $SnCl_2$ (0.5 g) and left to stir for 7 days to afford a homogenous yellow solid with no trace of brown material. The solid was isolated by filtration using a cannula and washed with MeOH (2 × 60 mL) before being dried *in vacuo* to afford a yellow powder (2.83 g, 78% yield).

Elemental analysis calc. for $C_{18}H_{16}O_4S_4 \cdot {}^1/_6\,CHCl_3$: C 49.09; H 3.67%; found: C 49.18; H 3.76%

IR (ν_{max}, cm^{-1}): 2955(w), 1541(m), 1448(s), 1383(m), 1299(s), 1247(vs), 1156(m), 1040(s), 981(s), 881(m), 839(m), 674(m), 447(w).

4.4.4 Preparation of 2',3',8',9'-tetraethoxydibenzo-1,2,5,6-tetrathiocine [(EtO)$_2$C$_6$H$_2$S$_2$]$_2$, (14).[6]

1,2-diethoxybenzene (2.49 g, 15.0 mmol) was added to 35 mL of degassed glacial acetic acid. S_2Cl_2 (1.2 mL, 15.0 mmol) was added dropwise to a clear rapidly stirred solution. Upon complete addition, the solution became dark green. After 60 h, a teal colour solid had formed. The solid was filtered *via* cannuala and washed with Et_2O (2 x 15 mL), then dried in *vacuo*. The dried solid was suspended in 200 mL of $CHCl_3$, and treated with a few drops of a methanolic tin solution (3 g of $SnCl_2$ in 5 mL of MeOH) until the dark green suspension turned pale yellow under a yellow solution. The $CHCl_3$ was evaporated to half its volume and treated with 200 mL of ice cold MeOH and placed in freezer for 24 h. The yellow solid was isolated *via* vacuum filtration, washed with ice cold methanol (2 × 10 mL) and dried thoroughly in *vacuo* (1.80 g, 53% yield).

Elemental analysis calc. for $C_{20}H_{24}O_4S_4$: C 49.99; H 5.03%; found: C 49.78; H 4.86%

4.4.5 Preparation of 2',3',8',9' bis-N,N'-dimethylbenzimidazolo-1,2,5,6-tetrathiocine [(N(Me)C(O)N(Me))C$_6$H$_2$S$_2$]$_2$, (15).

N,N'-dimethylbenzimidazole (0.500 g, 3.08 mmol) was added to 15 mL of degassed glacial acetic acid. S_2Cl_2 (0.25 mL, 3.08 mmol) was added dropwise to a clear rapidly stirred solution. Upon complete addition, the solution became bright yellow. After 24 h, a bright yellow solid began to form and the mixture left to stir at room temperature for a further 2 days. The yellow solid was filtered *via* cannula and washed with Et_2O (2 × 10 mL), then dried in *vacuo* (0.497 g, 71% yield).

Elemental analysis calc. for $C_{18}H_{16}O_2N_4S_4$: C 44.97; H 3.35, N 11.45%; found: C 44.54; H 3.63, N 10.29%.

IR ν_{max} (cm^{-1}): 3051(w), 2933(w), 1703(vs), 1699(vs), 1651(m), 1486(s), 1399(m), 1353(w), 1262(m), 1242(m), 1135(m), 1092(m), 873(m), 862(m), 743(s), 618(s), 580(s), 457(s).

4.4.6 Preparation of bis-15-crown-5-dibenzo-1,2,5,6-tetrathiocine, (16).

Benzo-15-crown-5 (1 g, 3.73 mmol) was added to 15 mL of degassed glacial acetic acid. S_2Cl_2 (0.30 mL, 3.73 mmol) was added dropwise to the clear rapidly stirred solution. Upon complete addition, the solution became bright yellow and was left to stir at room temperature for 7 days. After 2 days, a pale blue-green precipitate began to form. After 7 days, the blue-green solid had turned yellow within a yellow solution. The yellow solid was isolated by filtration via cannula and washed with Et_2O (2 × 10 mL), then dried thoroughly in *vacuo* (0.756 g, 61% yield).

Elemental analysis calc. for $C_{28}H_{36}O_{10}S_4 \cdot {}^1/_2\, CHCl_3$: C 47.50; H 5.12%; found: C 46.93; H 4.99%

IR (ν_{max}, cm^{-1}): 2931(w), 2860(w), 1572(m), 1486(s), 1442(s), 1351(m), 1312(m), 1255(vs), 1209(vs), 1123(s), 1082(s), 1057(s), 1044(s), 972(s), 932(s), 872(s), 805(m), 546(w), 471(m), 443(m).

4.4.7 Preparation of Pd(doxlbdt)(dppe), (17).

Pd_2dba_3 (0.100 g, 0.109 mmol), dppe (0.087 g, 0.218 mmol) and **11** (0.040 g 0.109 mmol) were combined in an oven-dried 5 mL microwave vial in the glove box. Dry toluene (5 mL) was added and the suspension was heated in the microwave for 20 min at 150 °C. The resultant dark red solid was isolated from a pale yellow solution by filtration. The precipitate was washed with hexanes and dried in air (0.125 g, 83% yield). The solid was recrystallized from a saturated CH_2Cl_2 solution layered with hexanes to produce red-orange needle-shaped crystals suitable for X-ray diffraction.

NMR (ppm) ($CDCl_3$): δ_H = 7.84 (8H, 7.87–7.81, m, *m*-H), 7.48 (12H, 7.51–7.44, m, *o,p*-H), 6.85 (2H, s, benzo C–H), 5.82 (2H, s, O-CH_2-O), 2.51 (4H, d, $^2J_{PH}$ = 20.7 Hz, PCH_2); $\delta_P\{^1H\}$ = 51.52.

HRMS (ESI-TOF) ***m/z***: $[M + H]^+$ calcd for $C_{33}H_{29}O_2P_2S_2Pd^+$ 689.0131; found 689.0153.

Elemental Analysis calc. for $C_{33}H_{28}O_2P_2S_2Pd \cdot {}^1/_8\, CH_2Cl_2$: C 56.87; H 4.05%; found: C 57.07; H 3.82%.

IR (ν_{max}, cm^{-1}): 3052(w), 2888(w), 1498(w), 1454(vs), 1435(s), 1309(w), 1216(vs), 1102(m), 1036(m), 998(w), 928(m), 819(m), 745(m), 690(s), 662(m), 527(s), 480(m).

4.4.8 Preparation of Pd(doxbdt)(dppe), (18).

Pd_2dba_3 (0.100 g, 0.109 mmol), dppe (0.087 g, 0.218 mmol) and **12** (0.043 g, 0.109 mmol) were combined in an oven-dried 5 mL microwave vial in the glove box. Dry toluene (5 mL) was added and the suspension was heated in the microwave for 20 min at 150 °C. The resultant red-orange solid was isolated from a pale yellow solution by filtration. The precipitate was washed with hexanes and dried in air (0.137 g, 89 % yield). The solid was recrystallized from a saturated CH_2Cl_2 solution layered with hexanes to produce red-orange needle-shaped crystals suitable for X-ray diffraction.

NMR (ppm) ($CDCl_3$)**:** δ_H = 7.84 (8H, 7.87-7.81, m, *m*-H), 7.46 (12H, 7.49–7.43, m, *o,p*-H), 6.89 (2H, s, benzo C–H), 4.13 (4H, O-CH_2-CH_2-O), 2.50 (4H, d, $^2J_{PH}$ = 20.7 Hz, PCH_2); $\delta_P\{^1H\}$ = 51.63.

HRMS (ESI-TOF) ***m/z***: $[M + H]^+$ calcd for $C_{34}H_{31}O_2P_2S_2Pd^+$ 703.0287; found 703.0265.

Elemental Analysis calc. for $C_{34}H_{30}O_2P_2S_2Pd \cdot {}^1/_5\ CH_2Cl_2$: C 57.05; H 4.26%; found: C 57.07; H 4.13%.

IR (ν_{max}, cm^{-1}): 3052(w), 2972(w), 2917(w), 2869(w), 1556(m), 1458(vs), 1435(vs),1289(vs), 1246(vs), 1093(s), 1067(s), 894(m), 749(m), 690(vs), 529(vs), 483(m).

4.4.9 Preparation of Pd(doxebdt)(dppe), (19).

Pd_2dba_3 (0.100 g, 0.109 mmol), dppe (0.087 g, 0.218 mmol) and **13** (0.046 g, 0.109 mmol) were combined in an oven-dried 5 mL microwave vial in the glove box. Dry toluene (5 mL) was added and the suspension was heated in the microwave for 20 min at 150 °C. The resultant dark red-brown solid was isolated from a pale yellow solution by filtration. The precipitate was washed with hexanes and dried in air (0.122 g, 78 % yield). The solid was recrystallized from a saturated CH_2Cl_2 solution layered with hexanes to produce orange needle-shaped crystals suitable for X-ray diffraction.

NMR (ppm) ($CDCl_3$)**:** δ_H = 7.83 (8H, 7.86–7.80, m, *m*-H), 7.48 (12H, 7.50–7.45, m, *o,p*-H), 7.03 (2H, s, benzo C–H), 3.99 (6H, m, O-CH_2-CH_2-CH_2-O) , 2.50 (4H, d, $^2J_{PH}$ = 21.0 Hz, PCH_2); $\delta_P\{^1H\}$ = 51.96.

HRMS (ESI-TOF) m/z: $[M + H]^+$ calcd for $C_{35}H_{33}O_2P_2S_2Pd^+$ 717.0444; found 717.0462.

Elemental Analysis calc. for $C_{35}H_{32}O_2P_2S_2Pd \cdot {}^1/_4CH_2Cl_2$: C 57.34; H 4.44%; found: C 57.17; H 4.30%.

IR (ν_{max}, cm^{-1}): 3072(w), 2953(w), 2865(w), 1467(vs), 1450(vs), 1435(vs), 1382(m), 1296(m), 1264(vs), 1250(s), 1096(s), 1046(s), 874(m), 690(vs), 528(vs), 482(m).

4.4.10 Preparation of Pd(deobdt)(dppe), (20).

Pd_2dba_3 (0.100 g, 0.109 mmol), dppe (0.087 g, 0.218 mmol) and **14** (0.050 g, 0.109 mmol) were combined in an oven-dried 5 mL microwave vial in the glove box. Dry toluene (5 mL) was added and the suspension was heated in the microwave for 20 min at 150 °C. The resultant pink solid was isolated from a pale yellow solution by filtration. The precipitate was washed with hexanes and dried in air (0.133 g, 83 % yield). The solid was recrystallized from a saturated CH_2Cl_2 solution layered with hexanes to produce red needle-shaped crystals suitable for X-ray diffraction.

NMR (ppm) ($CDCl_3$): δ_H = 7.85 (8H, 7.88–7.81, m, *m*-H), 7.47 (12H, 7.51–7.44, m, *o,p*-H), 6.93 (2H, s, benzo C–H), 3.97 (4H, q, CH_2), 2.51 (4H, d, $^2J_{PH}$ = 20.7 Hz, PCH_2), 1.36 (6H, t, CH_3); $\delta_P\{^1H\}$ = 51.73.

HRMS (ESI-TOF) m/z: $[M + H]^+$ calcd for $C_{36}H_{37}O_2P_2S_2Pd^+$ 733.0757; found 733.0767.

Elemental Analysis calc. for $C_{36}H_{36}O_2P_2S_2Pd$: C 58.98; H 4.95%; found: C 58.92; H 4.87%.

IR (ν_{max}, cm^{-1}): 3050(w), 2974(m), 2901(w), 1583(w), 1463(s), 1434(vs), 1389(m), 1337(m), 1235(vs), 1148(s), 1101(s), 1046(s), 998(w), 877(m), 820(m), 745(m), 690(vs), 528(vs), 483(m).

4.4.11 Preparation of (dmbimdt)Pd(dppe), (21).

Pd_2dba_3 (0.100 g, 0.109 mmol), dppe (0.087 g, 0.218 mmol) and **15** (0.049 g, 0.109 mmol) were combined in an oven-dried 5 mL microwave vial in the glove box. Dry toluene (5 mL) was added and the suspension was heated in the microwave for 20 min at 150 °C. The resultant dark purple solid was isolated from a pale solution by filtration.

The precipitate was washed with hexanes and dried in air (0.104 g, 65% yield). The solid was recrystallized from a saturated CH_2Cl_2 solution layered with hexanes to produce red needle-shaped crystals suitable for X-ray diffraction.

NMR (ppm) ($CDCl_3$): $\delta_P\{^1H\}$26.55

IR (ν_{max}, cm^{-1}): 3048(w), 2960(w), 2915(w), 1690(vs), 1580(m), 1496(m), 1483(m), 1435(s), 1398(m), 1378(m), 1319(w), 1261(s), 1187(w), 1101(s), 1081(m), 1027(m), 998(m), 941(w), 876(w), 820(m), 730(s), 691(s), 650(s), 617(m), 582(m), 530(s), 482(m).

4.4.12 Preparation of Pd(b-15-c-5-dt)(dppe), (22).

Pd_2dba_3 (0.100 g, 0.109 mmol), dppe (0.087 g, 0.218 mmol) and **16** (0.073 g 0.109 mmol) were combined in an oven-dried 5 mL microwave vial in the glove box. Dry toluene (5 mL) was added and the suspension was heated in the microwave for 20 min at 150 °C. The resultant pink microcrystalline solid was isolated from a pale yellow solution by filtration. The precipitate was washed with hexanes and dried in air (0.172 g, 94 % yield). The solid was recrystallized from the slow diffusion of Et_2O into a saturated MeCN solution to produce bright red needle-shaped crystals suitable for X-ray diffraction.

NMR (ppm) ($CDCl_3$)**:** δ_H = 7.83 (8H, 7.81–7.87, m, *m*-H), 7.46 (12H, 7.48–7.44, m, *o,p*-H), 6.93 (2H, s, benzo C–H), 2.51 (4H, 2.54–2.48, d, PCH_2); $\delta_P\{^1H\}$ = 51.89.

HRMS (ESI-TOF) ***m/z***: $[M + H]^+$ calcd for $C_{40}H_{42}O_5P_2S_2Pd^+$ 835.1076; found 835.1097.

Elemental Analysis calc. for $C_{40}H_{42}O_5P_2S_2Pd{\cdot}½CH_2Cl_2$: C 55.42; H 4.95 %; found: C 55.36; H 5.14 %.

IR (ν_{max}, cm^{-1}): 2923(m), 2862(m), 1474(s), 1450(s), 1435(vs), 1244(s), 1134(m), 1102(vs), 1064(m), 876(w), 713(m), 703(s), 691(vs), 528(s), 481(m).

4.4.13 Preparation of [Pd(b-15-c-5-Na-dt)(dppe)][BPh_4]·3MeOH·CH_2Cl_2, (23).

Complex **22** (0.018 g, 0.0218 mmol) and $NaBPh_4$ (0.010 g, 0.0218 mmol) were combined in a small 10 mL vial with a 1:1 mixture of CH_2Cl_2 and MeOH and left to stir for 1 hour under ambient conditions. Crystallization occurred by layering hexanes on a concentrated CH_2Cl_2:MeOH mixture to afford yellow-orange crystals suitable for X-ray diffraction.

4.4.14 Preparation of Pd(b-15-c-5-dt)(dppf), (24).

Pd_2dba_3 (0.100 g, 0.109 mmol), dppf (0.121 g, 0.218 mmol) and **16** (0.072 g 0.109 mmol) were combined in an oven-dried 5 mL microwave vial in the glove box. Dry toluene (5 mL) was added and the suspension was heated in the microwave for 20 min at 150 °C. The resultant dark solution was filtered off leaving behind a small amount of dark red solid. The filtrate was evaporated *in vacuo* to afford dark solid (0.062 g, 57% yield). Recrystallization of the solid was attempted, however crystals suitable for X-ray diffraction could not be obtained.

Elemental Analysis calc. for $C_{48}H_{46}O_5P_2S_2PdFe \cdot {}^1/_4CH_2Cl_2$: C 57.24; H 4.64 %; found: C 57.42; H 5.06 %.

IR (ν_{max}, cm^{-1}): 3053(w), 2911(m), 2865(m), 1480(s), 1450(s), 1435(vs), 1306(w), 1247(s), 1133(m), 1096(s), 1063(m), 931(w), 847(w), 824(w), 746(m), 732(m), 695(vs), 635(w), 546(s), 491(s), 466(m).

4.4.15 Preparation of [Pd(b-15-c-5-Na-dt)(dppf)][BPh_4] , (25).

Complex **24** (0.089 g, 0.089 mmol) and $NaBPh_4$ (0.031 g, 0.089 mmol) were combined in a small 10 mL vial with a 1:1 mixture of CH_2Cl_2 and MeOH and left to stir for 1 hour under ambient conditions. Crystallization occurred by layering hexanes on a concentrated CH_2Cl_2:MeOH mixture to afford orange crystals suitable for X-ray diffraction.

4.5 X-ray Crystallography.

Crystals were mounted in a cryoloop using paratone oil and measured on a Bruker APEX or Bruker APEX-II diffractometer equipped with an Oxford Cryostream low temperature device. Data were collection and processing were undertaken using the APEX-II software[8] and SAINT[9] and an absorption correction applied using SADABS.[10] The structure was solved by direct methods and refined using full matrix least squares against F^2 using SHELXTL.[11] H atoms added at calculated positions using a riding model. A summary of crystallographic data is presented in Tables 4.3 and 4.4.

For complex **18**, despite all atoms heavier than C refined anisotropically, wR_2 proved unacceptably high (wR_2 ~ 0.67). Examination of the crystal data within PLATON[12] revealed a twin component (0 0 -1 0 -1 0 -1 0 0) with BASF ~ 0.39. Subsequent refinement with the twin law led to residuals comparable with expectation based on R_{int} = 0.047.

For complex **19**, one of the phenyl rings of the dppe ligand was disordered (50:50) over two sites. These two rings were constrained to planarity (FLAT) with a common refined P-C bond length (DFIX). The Flack parameter[13] indicated the correct absolute structure.

For complex **20**, refinement stalled with poorly located lattice solvent which was treated with SQUEEZE,[14] within PLATON which led to subsequent satisfactory refinements.

For complex **21**, there were two molecules in the asymmetric unit plus two CH_2Cl_2 solvent molecules but no additional symmetry was identified (ADDSYM in PLATON). One of the two CH_2Cl_2 molecules showed some disorder via rotation about one of the two Cl atoms. The sof for each of the C and Cl atoms were constrained to 0.5 and their thermal parameters constrained to be equivalent (EADP for C and SIMU for Cl) with geometric restraints (SAME).

For complex **22**, one of the phenyl rings of the dppe ligand was disordered over two sites and some disorder in the macrocyclic crown was detected which was also modelled over two sites.

For complex **25**, refinement stalled at R_1 ~ 0.20 due to residual electron density associated with poorly resolved lattice solvent. Application of SQUEEZE[14] within PLATON provided a significant improvement in residuals. Two strongly disagreeable low angle reflections were omitted in the latter stages of refinement and P-C bond length restraints applied (SADI).

Table 4.4 Crystallographic data for complexes **17** – **21**.

Compound	17	18	19	20	21
Chemical formula	$C_{33}H_{28}O_2P_2S_2Pd$	$C_{34}H_{30}O_2P_2S_2Pd$, 0.5 CH_2Cl_2	$C_{35}H_{32}O_2P_2S_2Pd$	$C_{36}H_{36}O_2P_2S_2Pd$	$C_{35}H_{32}N_2OP_2S_2Pd$, CH_2Cl_2
Formula weight	689.01	745.50	717.07	733.11	814.01
Temperature (K)	150(2)	150(2)	150(2)	150(2)	173(2)
Crystal System	Monoclinic	Monoclinic	Orthorhombic	Monoclinic	Monoclinic
Space group	$P2_1/n$	$P2_1/n$	$P2_12_12_1$	$P2_1/c$	$P2_1/c$
a (Å)	11.053(5)	17.797(7)	11.4906(12)	12.247(3)	14.1330(5)
b (Å)	12.788(6)	20.004(7)	12.9099(14)	13.509(4)	24.2766(10)
c (Å)	20.727(9)	17.816(7)	21.333(2)	23.332(7)	22.0469(9)
α (deg)	90	90	90	90	90
β (deg)	97.308(6)	92.047(4)	90	91.730(3)	106.2705(15)
γ (deg)	90	90	90	90	90
V (Å^3)	2906(2)	6338(4)	3164.6(6)	3858.5(19)	7261.4(5)
Z	4	8	4	4	8
D_{calc} (g cm^{-3})	1.575	1.562	1.505	1.262	1.489
μ (mm^{-1})	0.923	0.934	0.851	0.699	0.893
Radiation	0.71073	0.71073	0.71073	0.71073	0.71073
range (deg)	1.88 – 27.70	1.02 – 26.71	1.84 – 27.50	1.746 – 27.568	2.931 – 28.312
Reflns collected	32920	70375	36543	43243	135287
Unique reflns	6655	13391	7243	8824	18020
R(int)	0.0718	0.0470	0.0465	0.0280	0.0641
Data/restraints/parameters	6655/0/361	13391/0/764	7243/68/434	8824/0/390	18020/19/845
R_1, wR_2 ($I > 2\sigma(I)$)	0.0439, 0.0921	0.0304, 0.0694	0.0350, 0.0762	0.0289, 0.0796	0.0408, 0.0837
R_1, wR_2 (all data)	0.0621, 0.0997	0.0321, 0.0704	0.0402, 0.0791	0.0324, 0.0840	0.0661, 0.1001
Flack parameter			0.00		
Residual electron density (e^-/Å^3)	+0.646/-0.712	+1.197/-0.447	+1.029/-0.639	+0.645/-0.259	+1.293/-1.505

Table 4.5 Crystallographic data for complexes **22**, **23**, and **25**.

Compound	22	23	25
Chemical formula	$C_{40}H_{42}O_5P_2S_2Pd$, MeCN	$C_{67}H_{74}BNaO_8P_2S_2Pd$, CH_2Cl_2	$C_{144}H_{132}B_2Fe_2Na2_2O_{10}P_4Pd_2S_4$
Formula weight	876.25	1358.45	2666.70
Temperature (K)	150(2)	150(2)	150(2)
Crystal System	Monoclinic	Triclinic	Triclinic
Space group	$P2_1/c$	P-1	P-1
a (Å)	11.8434(12)	9.565(7)	17.450(4)
b (Å)	13.561(3)	17.558(12)	18.650(4)
c (Å)	24.616(7)	20.088(14)	22.080(4)
α (deg)	90	95.318(9)	82.45(3)
β (deg)	101.568(14)	98.525(9)	89.97(3)
γ (deg)	90	100.269(9)	88.92(3)
V (Å^3)	3873.2(14)	3258(4)	7122(3)
Z	4	2	2
D_{calc} (g cm^{-3})	1.503	1.385	1.243
μ (mm^{-1})	0.716	0.541	0.612
Radiation	0.71073	0.71073	0.71073
range (deg)	1.689 – 27.537	2.07 – 27.60	0.930 – 27.499
Reflns collected	24776	36253	78176
Unique reflns	4810	14503	29815
R(int)	0.0228	0.0410	0.0451
Data/restraints/parameters	4810/5/404	14503/3/779	29813/292/1279
R_1, wR_2 ($I > 2\sigma(I)$)	0.0316, 0.0871	0.0489, 0.1115	0.0972, 0.2418
R_1, wR_2 (all data)	0.0341, 0.0953	0.0642, 0.1207	0.1208, 0.2656
Residual electron density (e^-/Å^3)	+1.152/-0.756	+1.316/-0.719	+2.516/-1.999

4.6 References

1. K. W. Stender, N. Wolki, and G. Klar, *Phosphorus, Sulfur, and Silicon Relat. Elem.*, 1989, **42**, 111.

2. J. M. Rawson, A. Alberola, D. Eisler, R. J. Less, and E. Navarro-Moratalla, *Chem. Comm*. 2010, **46**, 6114.

3 **(a)** C. J. Pedersen, *J Am. Chem. Soc*.,1967, **89**, 2495.; **(b)** C. J. Pedersen, *J. Am. Chem. Soc.*, 1967, **89**, 7017.

4. For examples see: **(a)** J. W. Steed, *Coord. Chem. Rev*., 2001, **215**, 171.; **(b)** Alexandratos and C. L. Stine, *Relative and Functional Polymers*, 2004, **60**, 3; **(c)** R. D. Hancock, *J. Chem. Educ*., 1992, **69**, 615.

5. E. Navarro-Moratalla, ERASMUS Report. University of Cambridge. 2007.

6. T. Wilson, undergraduate thesis report, University of Cambridge, 2008.

7. For examples see: **(a)** G. W. Gokel, W. M. Leevy, and M. E. Weber, *Chem. Rev*., 2004, **104**, 2723.; **(b)** M. Kralj, L. Tusek-Bozic, and L. Frkanec, *Chem. Med. Chem.*, 2008, **3**, 1478.; **(c)** G. W. Gokel and I. A. Carasel, *Chem. Soc. Rev.*, 2007, **36**, 378.

8. APEX-II, Bruker AXS, Madison, WI, USA.

9. SAINT, Bruker AXS, Madison, WI, USA

10. SADABS, Bruker AXS, Madison, WI, USA.

11. SHELXTL, Bruker AXS, Madison, WI, USA.

12. A.L. Spek, *Acta. Cryst.*, 2009, **D65**, 148.

13. H. D. Flack, *Acta Cryst.*, 1983, **A39**, 876

14. A.L. Spek, *Acta. Cryst.*, 2015, **C71**, 9

CHAPTER 5

Synthesis and Characterization of 1,3,2-BDTA Radicals

5.1 Introduction

The previous chapters in this thesis focused on the reactivity of tetrathiocines *via* oxidative addition capabilities to low-valent transition metals in the presence of a neutral phosphine co-ligand to form a variety of transition metal dithiolate complexes. In this chapter, the use of tetrathiocines as precursors to 1,3,2-benzodithiazyl (BDTA) radicals is described.

5.1.1 DTA Radicals as Magnetic Materials

Wolmershäuser[1] synthesized the first benzo-fused dithiazolyl radicals, benzo-1,3,2-dithaizolyl (BDTA) and 4-methyl-benzo-1,3,2-dithiazolyl (MBDTA) in 1984 reporting that both structures were paramagnetic (**Figure 5.1**). However subsequent crystallographic and magnetic studies by Passmore[2] revealed that BDTA adopted a diamagnetic dimeric π*-π* structure (**Figure 5.2**). Since then, the magnetic behaviour of the BDTA radical has been further studied by Awaga *et al.*[3] who reported that the diamagnetic dimeric BDTA radical initially melted upon warming but then re-solidified to form a paramagnetic phase. This new paramagnetic material was observed to exhibit antiferromagnetic order below 11 K.

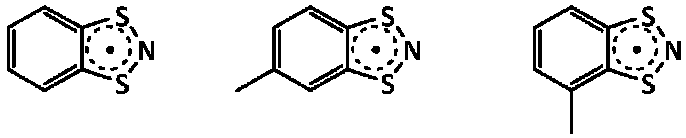

Figure 5.1 The first 1,3,2-dithiazolyl radicals (BDTA) and MBDTA) synthesized by Wolmershäuser[1]; and the M′BDTA derivative characterized by the Rawson group.[4]

Structural and magnetic studies by Rawson revealed that the methyl derivative MBDTA was indeed monomeric and paramagnetic in the solid state. It too exhibited

antiferromagnetic interactions but did not exhibit long range order down to 1.8 K.[5] Notably positioning the methyl group next to the DTA radical afforded a dimeric, diamagnetic structure for 3-methyl-benzo-1,3,2-dithiazolyl (M′BDTA) (see **Figure 5.1** above).[2] This clearly reveals a subtle balance between crystal packing factors and tendency for these DTA radicals to dimerize. Work by Passmore showed that the dimerization energy for the BDTA derivative was approximately 0 kJ/mol in solution[2] confirming a fine balance between entropic and enthalpic factors.

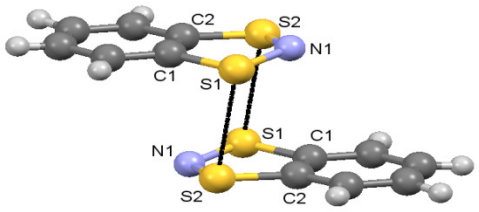

Figure 5.2 Structure of the dimeric π*-π* structure of BDTA reported by Passmore.[2]

Further studies undertaken in the Rawson group using 3′-cyano-BDTA (**Figure 5.3**)[6] revealed it is polymorphic exhibiting both paramagnetic monomer and diamagnetic dimer phases which can interconvert through a solid state phase transition at 250 K, affording a 'spin-switching' material.[7] Several other BDTA analogues prepared in the Rawson and Oakley groups including 4-cyano-BDTA (Fig. 5.3) also exhibit spin-switching.[8] These studies clearly indicate that careful tuning of the substituents on the BDTA radical can therefore be expected to give rise to a range of different structures and properties.

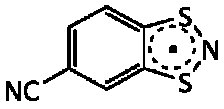

4-cyanobenzo-1,3,2-dithiazolyl

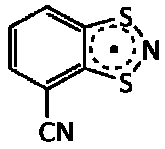

3-cyanobenzo-1,3,2-dithiazolyl

Figure 5.3 Cyano-derivatives studied by the Rawson group.[6,7]

5.1.2 Dialkoxy Substituted Benzo-1,3,2-DTA Radicals

A critical step in DTA radical synthesis is access to suitable versatile synthetic methodologies to prepare 1,2-dimercapto- or 1,2-dithiolate functionalized precursors, since few benzenedithiol derivatives are commercially available. In the past, the synthesis of these 1,3,2-dithiazolyl radicals has required substituent-specific synthetic methods.[9,10] Previous research in the Rawson group has focused on the development of more general and therefore adaptable methodologies. One approach developed in the Rawson group involves the one-pot synthesis of tetrathiocines derived from commercially available dialkoxybenzenes using the method developed by Stender and co-workers[11] and implemented extensively in previous Chapters of this thesis. Oxidation of the tetrathiocine using SO_2Cl_2 or elemental chlorine affords the bis(sulfenyl chloride) which has previously been shown to undergo ring closure with Me_3SiN_3 to afford the dithiazolylium cation as its chloride salt. Subsequent $1e^-$ reduction then leads to the target radical.[12] Previously using this methodology, DMOBDTA and DOXLBDTA radicals (**Figure 5.4**) have been prepared.[12] Like BDTA and MBDTA, these preliminary studies revealed that subtle changes to molecular structure lead to marked changes in solid state structure. Crystallographic studies reveal DMOBDTA is monomeric (**Figure 5.5a**) with a herringbone motif and antiferromagnetic interactions between radicals whereas DOXLBDTA adopts a distorted π-stacked arrangement of π*-π* dimers (**Figure 5.5b**) with the onset of weak paramagnetism observed above 250 K.[12]

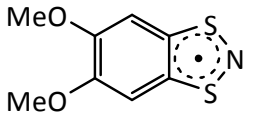

DMOBDTA (**28**)

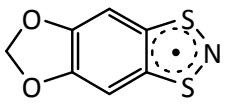

DOXLBDTA (**29**)

Figure 5.4 Dialkoxy-benzo derivatives studied previously in the Rawson group.[11]

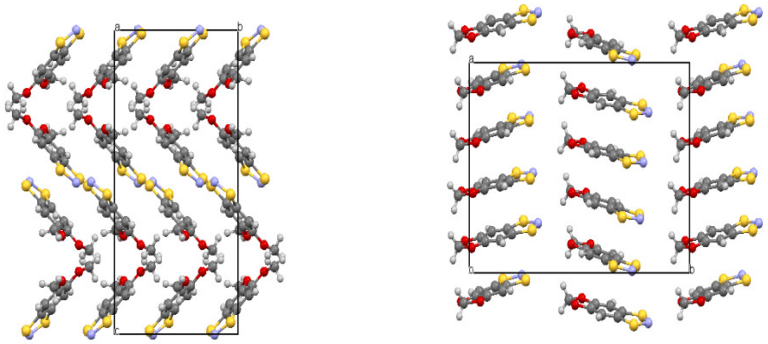

(a) (b)

Figure 5.5 (a) Herringbone motif of DMOBDTA and (b) π-stacked structure of DOXLBDTA dimers.[12]

5.1.3 Project Objectives

These preliminary studies reveal that small changes to the dialkoxy-substituted benzene lead to marked effects on the structure and physical properties of the radical. In order to further study the effect of altering the dialkoxy-substituted benzene on the solid state structure of the radicals, further research on new benzo-derivatives is needed. This Chapter extends this synthetic methodology to two new derivatives (**Figure 5.6**) in order to obtain a more coherent view of the structure-directing interactions and the synthesis and structural characterisation of dioxyl-benzo-1,3,2-dithiazolyl (DOXBDTA) and dioxepinyl-benzo-1,3,2-dithiazolyl (DOXEBDTA) are described. This work was undertaken by myself in conjunction with two undergraduates; Osman Raza and Mohammed Harb who have continued to try and optimise the recovered yields of the radicals reported in this thesis.

Figure 5.6 Molecular structures of target molecules DOXBDTA and DOXEBDTA

5.2 Results and Discussion

5.2.1 Synthesis

Stender *et al.* reported that reaction of several dialkoxy-benzene derivatives with S_2Cl_2, yielded the corresponding tetrathiocines (structure **A**, **Scheme 5.1**).[11] Using their methodology a range of tetrathiocines have been prepared (see Chapter 4). Chlorination of the tetrathiocine with SO_2Cl_2 in refluxing CH_2Cl_2 produces the air-sensitive bis-sulfenyl chloride intermediate as a dark oil (reaction was monitored by the evolution of SO_2) upon removal of solvent. This oil was not purified due to its air-sensitive nature and high boiling point, neither of which facilitated ready distillation. Dissolution of this oil in fresh CH_2Cl_2,[13] followed by dropwise addition of Me_3SiN_3 afforded [DOXBDTA]Cl (**26**) and [DOXEBDTA]Cl (**27**) respectively in 55-80% recovered yield. The rate of dropwise addition of Me_3SiN_3 was monitored by the evolution of gas and each progressive drop was added only after gas evolution ceased. The reaction was then left to warm to room temperature and stirred overnight to ensure completion of the reaction. The brightly coloured (yellow-orange) chloride salts were isolated by filtration, dried *in vacuo* and characterized by elemental analysis and IR spectroscopy, but poor solubility hampered characterization by ^{1}H NMR.

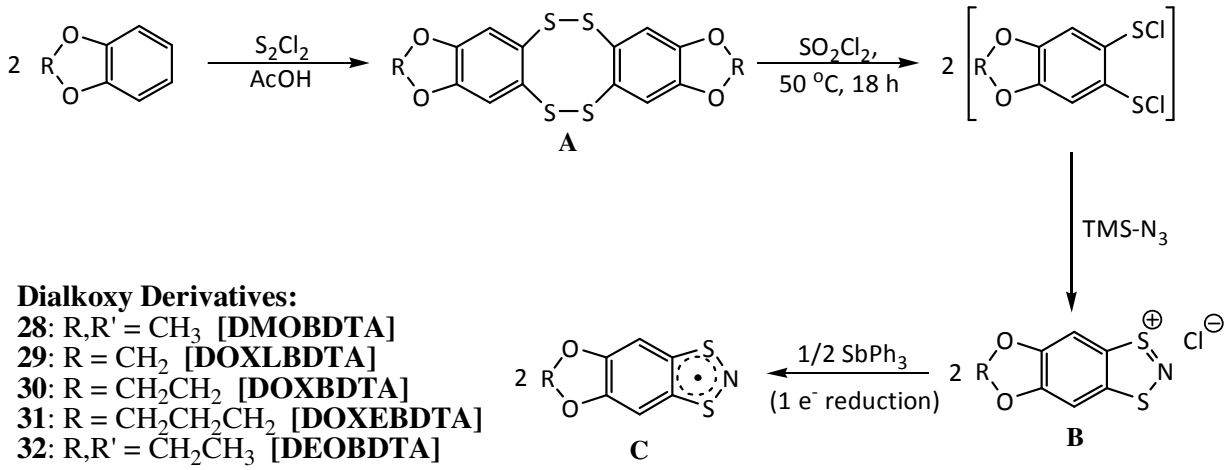

Scheme 5.1 General synthetic method for producing various dialkoxy-benzodithiazolyl derivatives.[5]

Microanalytical data suggest these chloride salts crystallise as CH_2Cl_2 solvates with 0 – 1 residual CH_2Cl_2 solvent molecules per dithiazolylium cation, depending on sample age. Notably other related chloride salts have also found to crystallise as solvates including [BDTA]Cl, which crystallizes as an SO_2 solvate,[14] and its perfluorinated analogue, $[C_6F_4S_2N]Cl$, which crystallizes as both an acetonitrile solvate[15] and as a dihydrate.[16]

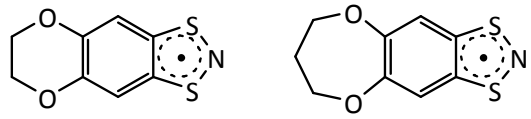

DOXBDTA (**30**) DOXEBDTA (**31**)

Figure 5.7 BDTA derivatives synthesized in this project.

Previous work by Navarro showed that $1e^-$ reduction of the chloride salts using silver powder, zinc-copper couple, or triphenyl antimony and recrystallization by sublimation onto a cold-finger allows for the isolation of the dialkoxy-benzodithiazolyl radicals, DMOBDTA and DOXLBDTA (**Figure 5.4**). Radicals **30** and **31** were prepared by reduction of the corresponding chloride salt with half an equivalent of $SbPh_3$ in CH_2Cl_2 stirring for approximately 3-4 hours, affording dark-colored solutions. Removal of the solvent followed by purification by vacuum gradient sublimation along a glass tube, afforded very small dark crystals of **30** in low yield. Similarly, vacuum sublimation of **31** onto a water-cooled cold finger yielded a small amount of tiny crystals also suitable for X-ray diffraction and a moderate amount of a microcrystalline material.[17]

5.2.2 EPR spectra of 30 and 31

The solution EPR spectra of 1,3,2-dithiazolyls are characterized by a g-value around 2.005 and hyperfine coupling of *ca.* 11 G.[18] Room temperature EPR spectra of **30** and **31** were recorded in CH_3CN and THF respectively. The g-values and hyperfine coupling constants for **30** and **31** are in good agreement with those reported for **28** and **29** as well as other selected DTA radicals (**Table 5.1**).

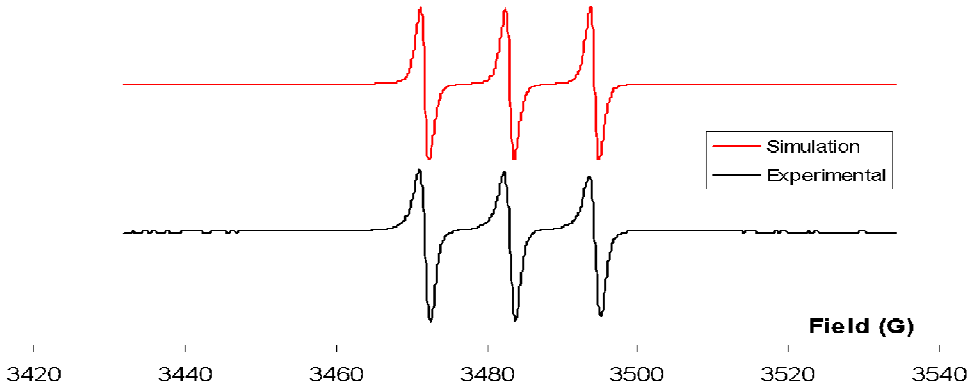

Figure 5.8 Experimental and simulated EPR spectra of **30** in CH_3CN.

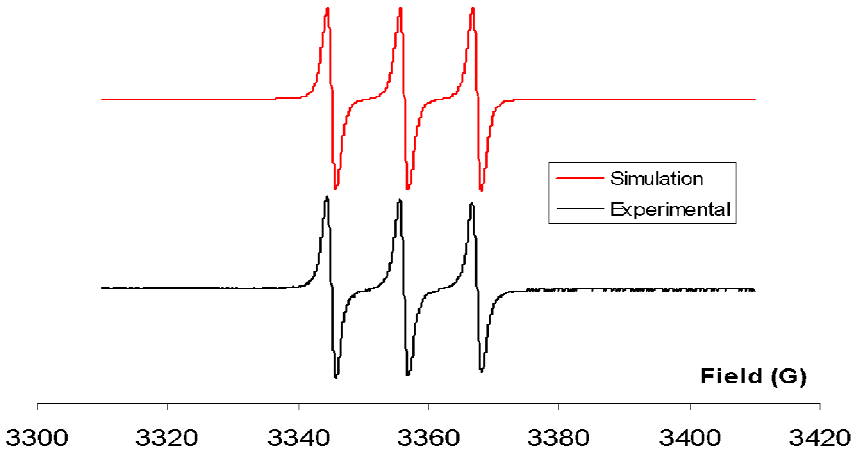

Figure 5.9 Experimental and simulated EPR spectra of **31** in THF.

Table 5.1 Comparison of EPR parameters for **28** – **31** in relation to other closely related DTA radicals.

Compound	g	a_N (G)	Solvent	Ref.
28	2.010	11.15	THF	10
29	2.010	11.15	THF	10
30	2.007	11.15	CH_3CN	This work
31	2.006	11.25	THF	This work
BDTA	2.008	11.01	CCl_3F	14
MBDTA	2.003	11.40	CH_2Cl_2	5
3-NCBDTA	2.006	11.50	PhMe	6
4-NCBDTA	2.008	11.10	PhMe	8

5.2.3 Crystal Structures of Radical Complexes 30 and 31.

Crystals of **30** and **31** were produced by Mohamed Harb and Osman Raza respectively *via* vacuum sublimation proved adequate for structure determination by X-ray diffraction and a summary of the crystallographic data for **30** and **31** is presented in **Table 5.2**. Crystals of **30** were extremely small and did not diffract to high angle but were measured on a micro-focus Cu-source which provided sufficient data to solve and refine the structure, albeit with a slightly low data:parameter ratio. The molecule crystallised in an acentric space group and a merohedral twin law was included in the latter stages of refinement. Crystals of **31** were more strongly diffracting but structure refinement also revealed some evidence for twinning. The heterocyclic parameters are unexceptional and comparable to those previously reported for **28** and **29** (**Table 5.3**).

5.2.3.a Crystal structure of 30. Radical **30** was found to crystallize in the chiral orthorhombic space group $C222_1$ with half a molecule in the asymmetric unit located about a crystallographic 2-fold axis. The fused $O_2C_6S_2N$ unit is essentially planar (max deviation less than 0.02 Å) with the symmetry-equivalent saturated CH_2 units displaced above/below the molecular mean plane by 0.36 Å (**Figure 5.10**).

Table 5.2 Crystallographic data for **30** and **31**.

Compound	30	31
Chemical formula	$C_8H_6NS_2O_2$	$C_9H_8NS_2O_2$
Formula weight	212.26	226.28
Temperature (K)	173(2)	173(2)
Crystal System	Orthorhombic	Orthorhombic
Space group	$C222_1$	Pbca
a (Å)	3.8382(3)	11.5892(4)
b (Å)	19.7534(12)	7.9390(3)
c (Å)	10.7869(7)	20.1201(7)
α (deg)	90	90
β (deg)	90	90
γ (deg)	90	90
V (Å^3)	817.84(10)	1851.18(11)
Z	4	8
D_{calc} (g cm^{-3})	1.724	1.624
μ (mm^{-1})	5.597	0.543
Radiation	Cu-Kα	Mo-Kα
range (deg)	4.10-58.90	3.27-26.42
Reflns collected	2123	21654
Unique reflns	585	1901
R(int)	0.046	0.038
Data/restraints/parameters	585/11/61	1901/0/127
R_1, wR_2 ($I > 2\sigma(I)$)	0.038, 0.100	0.030, 0.072
R_1, wR_2 (all data)	0.040, 0.101	0.037, 0.076
Flack parameter	0.34(6)	--
Residual electron density (e^-/Å^3)	+0.35/-0.26	+0.28/-0.28

Table 5.3 Selected heterocyclic bond lengths and angles for **30** and **31** in realtion to previously reported alkoxy-functionalized BDTA derivatives.

Compound	28	29	30	31	
C-S/Å	1.747(2), 1.745(3)	1.728(7) – 1.747(7)	1.745(4)	1.745(10)	1.738(10)
S-N/Å	1.654(2), 1.656(2)	1.638(6) – 1.669(6)	1.658(3)	1.660(9)	1.655(9)
C-C/Å	1.389(4)	1.40(1) – 1.41(1)	1.397(10)	1.395(14)	
CCS/°	113.4(2), 113.5(2)	111.9(5) – 114.3(5)	113.61(17)	112.8(7)	113.7(7)
CSN/°	99.4(1), 99.5(1)	99.1(3) – 100.3(3)	99.0(2)	100.1(5)	100.0(5)
SNS/°	114.1(1)	113.9(4) – 114.1(4)	114.8(3)	113.4(5)	

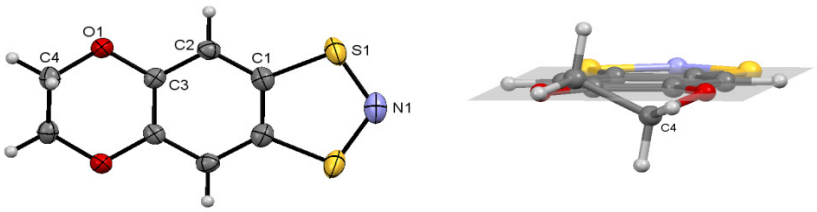

(a) (b)

Figure 5.10 (a) Molecular structure of **30** with atom labelling (molecule lies on a crystallographic 2-fold axis) and thermal elipsoids plotted at the 50% probability level; (b) deviation of the saturated backbone C(4) and C(4)′ from the molecular plane (grey).

The DOXBDTA radical, **30** was observed to adopt a regular π-stacked structure parallel to the *a*-axis (**Figure 5.11**) with the inter-radical separation along the stacking direction corresponding to the crystallographic *a*-axis (3.8382(3) Å, much larger than the S···S distance normally observed with π*-π* dimers (2.9-3.2 Å).[19] These intermolecular contacts indicate that **30** is likely to be paramagnetic in the solid state. Perpendicular to the stacking direction molecules form chains parallel to the crystallographic *b*-axis (**Figure 5.10**), favoured by alignment of molecular dipoles, with N···H-C distance of 3.11 Å. Successive chains align antiparallel to each other and exhibit intermolecular S···S and C-H···O contacts between chains ($d_{S...S}$ = 3.868(2) Å, H···O = 3.09 Å) (**Figure 5.10**).

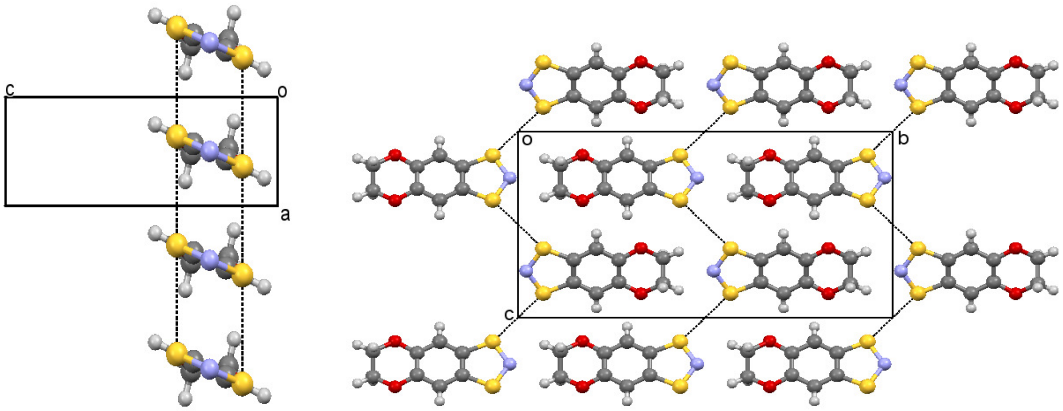

Figure 5.11 (left) π-stacked structure of **30** parallel to the crystallographic *a*-axis; (right) intermolecular S···S contacts in the *bc* plane.

5.2.3.b Crystal structure of 31. The DOXEBDTA radical **31** was found to crystallize in the orthorhombic space group Pbca with one molecule in the asymmetric unit (**Figure 5.12**). The molecular geometry of the **31** radical is unexceptional with S-N bonds of 1.655(9) – 1.660(9) Å, comparable to **28 - 30** (**Table 5.3**). As with **30**, the $O_2C_6H_2S_2N$ plane is essentially planar (max deviation O12 at 0.11 Å) with the saturated $CH_2CH_2CH_2$ component folded out of the plane with the three C atoms displaced out of the $O_2C_6S_2N$ plane (displacements from the mean plane are: C17 0.99 Å, C18 0.75 Å, C19 0.91 Å) .

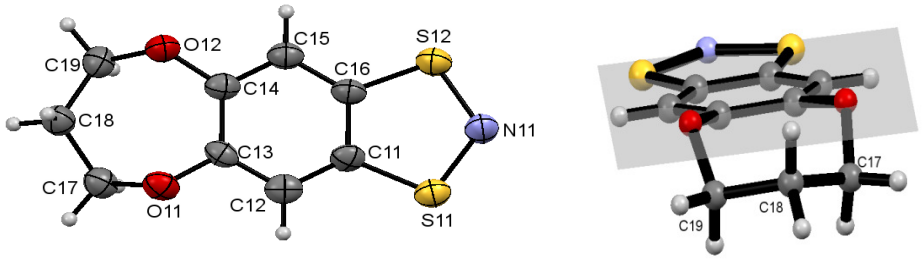

(a) (b)

Figure 5.12 (a) Molecular structure of **31** with atom labelling (molecule lies on a crystallographic 2-fold axis) and thermal ellipsoids plotted at the 50% probability level; (b) deviation of the saturated backbone C(17) – C(19) from the molecular plane (grey).

As with **30**, there are no short S···S contacts reflecting dimerization. The molecular packing of **31** is reflected in a herringbone-like motif in the *ab* plane (**Figure 5.13**) with the closest S···S distances S11···S12 at 3.575(4) and S12···S12′ at 3.973(5) Å. Both the molecular orientation and the S···S distances preclude face-to-face π*-π* dimerisation but potentially form a route for magnetic exchange. In addition to the S···S contacts parallel to the *b*-axis, there are in-plane S···S contacts (**Figure 5.13**) at 3.307(4) Å cross-linking chains of radicals generating a two-dimensional network.

EPR and computational studies on DTA radicals have revealed that the majority of the spin density (>80%) is localized on the SNS fragment of the radical.[7] Thus these S···S contacts are likely to dominate the magnetism of these radicals and the magnetism of **31** will most likely reflect a distorted square-lattice topology. Further synthetic studies by M. Harb within this group aim to prepare sufficient samples of both **30** and **31** for magnetic

characterisation whilst N. Mroz also within this group is examining the magnetic exchange pathway in **30** and **31** through DFT techniques.

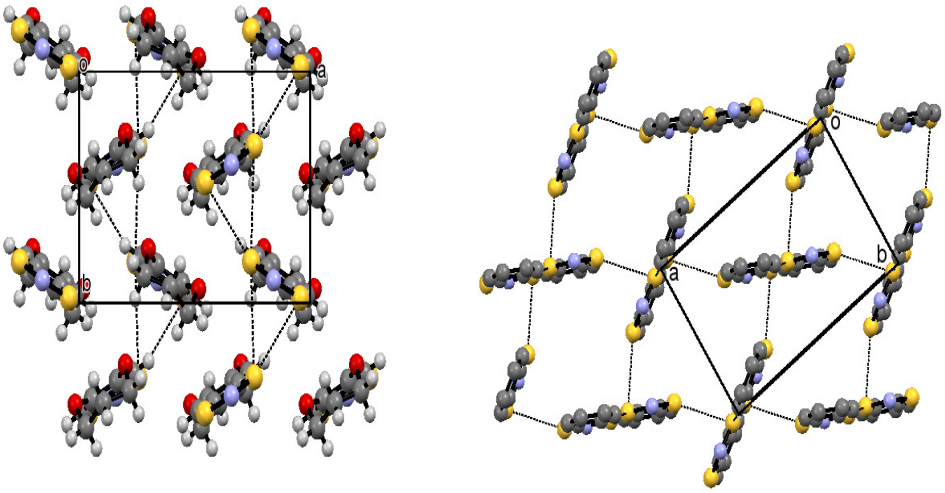

(a) (b)

Figure 5.13 (a) Herringbone motif of **31** highlighting intermolecular contacts parallel to the crystallographic *b*-axis; (b) two-dimensional network of interactions propagating in the *ab* plane (H atoms and $OCH_2CH_2CH_2O$ groups omitted for clarity).

5.3 Conclusions

The methodology previously employed by the Rawson group to generate a variety dialkoxy-benzene substituted 1,3,2-DTA radicals has been successfully applied to generate two new derivatives. The yields of the intermediate chloride salts were adequate (55 – 80 % recovered), but subsequent reduction to generate radicals **30** and **31** proved problematic. Whilst sublimation afforded crystalline material suitable for structural characterization by X-ray crystallography, microanalysis and EPR spectroscopy, the recovered yields were extremely low and this has so far precluded characterization by SQUID magnetometry. The crystal structures reveal both **30** and **31** are monomeric in the solid state thereby offering the potential to exhibit some form of low dimensional magnetism or long range magnetic order. Notably within the series **29** – **31** subtle changes to the size of the carbon chain dramatically affect the structural topology. Thus **29** adopts a π^*-π^* dimer motif, **30** adopts a regular π-stacked motif and **31** displays a herringbone motif. Further work is required to optimize recovered yields for further physical characterization, e.g. through changing reaction time, solvent and reducing agent. An alternative strategy would be to undertake salt metathesis to generate a more ionic salt in which alternative counter-ions may assist a cleaner reduction due to an increase in solubility.

5.4 Experimental

5.4.1 Crystallographic studies

Crystals of **30** and **31** were mounted on a cryoloop in paratone oil and data collected on a Bruker Duo APEX-II single crystal X-ray diffractometer using Mo-Kα (**30**) or Cu-Kα (**31**) radiation and equipped with an Oxford cryostream cooler which maintained a constant temperature of -100 °C. Data were integrated using SAINT[20] corrected for absorption using sadabs[21] and the structure solved using direct methods and refined against F^2 within the SHELXTL package.[22]

5.4.2 General Experimental Procedures

Salts **26** and **27** as well as radicals **30 and 31** were prepared following the established literature methodology.[10] CH_2Cl_2 was dried and deoxygenated using an Innovative Technology Solvent Purification System and manipulation of air-sensitive materials carried out under an atmosphere of dry nitrogen using standard Schlenk techniques and a dry-nitrogen glove box (MBraun Labmaster). All glassware was oven dried (~ 120°C) prior to use.

NMR spectra were recorded on a Bruker DPX300 UltraShield 300 MHz spectrometer with a Broadband AX Probe using $CDCl_3$ (^{1}H δ = 7.26 ppm, s) as an internal reference point relative to Me_4Si (δ = 0 ppm). IR spectra were obtained using a Bruker Alpha FT-IR spectrometer equipped with a Platinum single reflection diamond ATR module. Elemental compositions were determined on a PerkinElmer 2400 Series II Elemental Analyzer. EPR spectra were observed using a Bruker EMXplus X-Band EPR spectrometer equipped with variable temperature control unit and high precision microwave frequency counter.

The tetrathiocines **12** and **13** were prepared using the methodology described in Chapter 4.

5.4.3 Preparation of [DOXBDTA]Cl, (26).

Tetrathiocine **12** (2.93 g, 14.8 mmol) was suspended in 30 mL of dry CH_2Cl_2 under nitrogen. SO_2Cl_2 (1.5 mL, 18.5 mmol) was added dropwise to the cloudy yellow solution while monitoring gas evolution after each drop. With the addition of each drop a green precipitate began to form. After complete addition the solution was lightly refluxed (45 °C) until no further gas evolution was observed (~ 1 hour). Solvent was removed in *vacuo* and a dark green oil was afforded. The oil was then redissolved in 30 mL of dry CH_2Cl_2 and the dark black/yellow solution was treated with Me_3SiN_3 (1.2 mL, 9.12 mmol) dropwise at room temperature, while monitoring gas evolution between each drop and adding further Me_3SiN_3 only when evolution of SO_2 from the previous drop had ceased. A yellow precipitate began to form in a red solution and this was left to stir overnight to ensure complete reaction. The yellow/orange solid was isolated by filtration using a cannula and dried in *vacuo* (2.34 g, 80% yield).

Elemental Analysis Calc. for $C_8H_6O_2S_2NCl{\cdot}\frac{2}{3}CH_2Cl_2$: C 34.20; H= 2.43; N= 4.60%; found: C 34.15; H 2.07; N 4.96%.

IR ν_{max} (cm^{-1}): 3015(w), 1515(m), 1468(vs), 1348(m), 1285(vs), 1256(vs), 1059(s), 934(m), 904(vs), 768(m), 739(m), 694(m), 549(m), 494(m), 420(s).

5.4.4 Synthesis of DOXBDTA$^{\bullet}$, (30).

Solid **26** (0.96 g, 3.81 mmol) and triphenylantimony (0.67 g, 1.90 mmol) were heated at 40 ^{o}C for 1 hour under nitrogen allowing the triphenylantimony to melt. The mixture was removed from heat and 10 mL of dry CH_2Cl_2 was added affording an immediate dark solution which was left to stir for a few minutes under nitrogen. The dark solution was filtered *via* cannula into a dry Schlenk and evaporated *in vacuo* to afford a dark black residue. Purification by sublimation at 60 ^{o}C onto a cold finger under dynamic vacuum afforded a dark film of crystalline **30** suitable for X-ray diffraction (0.022 g, 3% yield).

EPR(X-band, MeCN, 298K): g = 2.007, a_N = 11.15G.

Elemental Analysis calc. for $C_8H_6O_2S_2N$: C 45.26; H 2.81; N 6.60%; found: C 44.24; H 3.05; 5.99%.

5.4.5 Preparation of [DOXEBDTA]Cl, (27).

Tetrathiocine **13** (3.41 g, 4.88 mmol) was suspended in 25 mL of dry CH_2Cl_2 under nitrogen. SO_2Cl_2 (1.70 mL, 12.61 mmol) was added dropwise to the cloudy solution while watching gas evolution after each drop to afford a dark green solution. The mixture was then brought to a light reflux (50 °C) until gas evolution ceased (~ 1 hour). Solvent was removed in *vacuo*, and the dark green oil was redissolved in 20 mL of dry CH_2Cl_2. The solution was filtered into a dry Schlenk *via* cannula to afford a dark green-yellow solution. Me_3SiN_3 (2.13 mL, 16.06 mmol) was added dropwise at 0 ^oC, watching gas evolution between each drop and adding only when bubbling of solution ceased. The solution turned from a brown/red colour to an orange colour with a yellow precipitate present after complete addition. The solution was left to stir at room temperature for 72 hours to ensure complete reaction. The orange-yellow solid was isolated by cannula filtration and dried thoroughly in *vacuo* (0.616 g, 39% yield).

Elemental Analysis calc. for $C_9H_8O_2S_2NCl \cdot \frac{1}{3}\ CH_2Cl_2$: C 38.64; H= 3.02; N= 4.83%; found: C 38.49; H 2.78; N 4.99%.

IR ν_{max} (cm^{-1}): 3063(w), 3014(s), 1442(vs), 1259(s), 1022(s), 922(m), 884(m), 767(s), 548(m), 438(m).

5.4.6 Synthesis of DOXEBDTA˙, (31)

Solid **27** (0.616 g, 2.72 mmol) and $SbPh_3$ (0.48 g, 1.34 mmol) were heated at 40 °C for 1 hour under nitrogen. Dry CH_2Cl_2 (10 mL) was added under nitrogen and immediately afforded a dark solution. The dark solution was evaporated *in vacuo* to afford a dark residue and purified by sublimation onto a cold-finger at 60 °C under dynamic vacuum producing a dark film of crystalline powder containing a small number of crystals suitable for X-ray diffraction (0.013 g, 2%).

EPR (X-band, THF, 298 K): g = 2.006, a_N = 11.25G.

MS (EI+): *m/z* (%) = 226.0 (100)

5.5 References

1. G. Wolmershäuser, M. Schnauber and T. Wilhelm, *J. Chem. Soc., Chem. Commun*. 1984, 573.

2. E. G. Awere, N. Burford, C. Mailer, J. Passmore, M. J. Schriver, P. S. White, A. J. Banister, M. Oberhammer and L. H. Sutcliffe, *J. Chem. Soc., Chem. Commun*. 1987, **2**, 66.

3. W. Fujita, K. Awaga, Y. Nakazawa, K. Saito and M. Sorai, *Chem. Phys. Lett*. 2002, **352**, 348-352.

4. A. Alberola, R. J. Collis, R. J. Less and J. M. Rawson, *J. Organomet. Chem.* 2007, **692**, 2743.

5. G. D. McManus, J. M. Rawson, N. Feeder, F. Palacio and P. Oliete, *J. Mater. Chem.* 2000, **10**, 2001.

6. A. Alberola, R. J. Collis, S. M. Humphrey, R. J. Less and J. M. Rawson, *Inorg. Chem.* 2006, **45**, 1903.

7. J. M. Rawson, A. Alberola and A. Whalley, *J. Mater. Chem*. 2006, **16**, 2560.

8. A. Alberola, J. Burley, R. J. Collis, R. J. Less and J. M. Rawson, *J. Organomet. Chem*. 2007, **692**, 2750.

9. T. M. Barclay, A. W. Cordes, N. A. George, R. C. Haddon, M. E. Itkis, M. S. Mashuta, R. T. Oakley, G. W. Patenaude, R. W. Reed, J. F. Richardson and H. Zhang, *J. Am. Chem. Soc.*, 1998, **120**, 352.

10. E. Navarro-Moratalla, ERASMUS Report. University of Cambridge. 2007.

11. K. W. Stender, N. Wolki, G. Klar, *Phosphorus, Sulfur, and Silicon Relat. Elem*., 1989, **42**, 111.

12. J. M. Rawson, A. Alberola, D. Eisler, R. J. Less and E. Navarro-Moratalla, *Chem. Comm.* 2010, **46**, 6114.

13. Removal of the solvent along with trace dissolved SO_2 or Cl_2 or unreacted SO_2Cl_2 is essential; The presence of trace water may generate acidic solutions which may react with Me_3SiN_3 to form HN_3 which is a potential explosive hazard. In our hands, using this approach, no evidence for HN_3 formation has been observed.

14. E. G. Awere, N. Burford, R. C. Haddon, S. Parsons, J. Passmore, J. V. Waszczak and P. S. White, *Inorg. Chem.* 1990, **29**, 4821.

15. G. D. McManus, PhD thesis, University of Cambridge, 2001.

16. A. Alberola-Catalan, PhD thesis, University of Cambridge, 2004.

17. The synthesis and purification of C.4 was carried out by Osman Raza as part of his Undergraduate Research Project under my guidance.

18. G. D. McManus and J. M. Rawson, *Coord. Chem. Rev.*, 1999, **189**, 135.

19. J. N. B. Smith, Ph.D. thesis, University of Cambridge, 1998.

20. SAINT, Bruker AXS, Madison, Wisconsin, USA

21. Sadabs, Bruker AXS Inc., Madison, Wisconsin, USA.

22. SHELXTL package for crystal structure solution and refinement, Bruker AXS Inc., Madison, Wisconsin, USA.

CHAPTER 6

Conclusions and Future Work

6.1 Conclusion

Previous work on the chemistry of tetrathiocines (see Chapter 1) broadly focused on the inter-relationship between 'dimeric' 1,2,5,6-tetrathiocines, 'monomeric' dithietes and higher oligomers. The organic chemistry of 1,2-dithietes appears to mimic that of *ortho*-quino-dimethanes in their capacity to undergo [4+2] cycloaddition reactions. Other studies have shown that the chelate nature of the dithiolate favours a redox-coupled ligand exchange whereby a tetrathiocine can react with a metal bis(thiolate) to afford a metal dithiolate complex and a disulfide. Thus, despite the strength of the S-S bond, the 1,2,5,6-tetrathiocine ring system seems to exhibit a rich chemistry in which S-S bond cleavage occurs readily in conjunction with redox reactions. In Chapters 2 – 4 of this thesis the oxidative addition chemistry of the tetrathiocine ligand is explored for the first time. These studies have shown that such processes occur readily under microwave conditions to afford dithiolate complexes of the group 10 metals in good yield. The reaction product appears sensitive to the nature of the phosphine and a range of mono- , di- and hexa-nuclear complexes have been isolated. In these oxidative addition reactions the S-S bond is cleaved with the tetrathiocine acting as an electron acceptor being *reduced* to a dithiolate anion. In Chapter 5 the *oxidation* of tetrathiocines by sulfuryl chloride provides a route to bis(sulfenyl chlorides) which have been utilised to access two new dithiazolyl radicals. In addition the synthetic methodology initially reported by Stender *et al.* to access simple 1,2,5,6-tetrathiocines bearing O-donor groups has been extended to access a range of novel tetrathiocines including crown ether derivatives and π-donor N substituents.

6.2 Future Work

There are several pathways of which the research in this thesis can be expanded in the future. Current research in the Rawson group has expanded the synthesis of dithiolate ligands to include N donor co-ligands rather than P donor ligands which were the primary focus of this thesis and oxidative addition reactions of tetrathiocines to $Ni(COD)_2$ in the presence of *N,N′*-chelate ligands appears to be a successful route to generate 'push-pull' dithiolate complexes which have attracted attention in both solar-cell technology[1] and non-linear optics.[2] The oxidative addition reactions under microwave conditions can be applied to other low oxidation state metals such as Wilkinson's catalyst, $RhCl(PPh_3)_3$. However experiments to access to other derivatives *via* microwave-mediated oxidative addition will need to be carefully designed as metal carbonyls, for example, are not expected to be good precursors due to the elimination of gaseous CO in a sealed microwave reaction vessel. An alternative strategy is to reduce the tetrathiocine to a dithiolate using electropositive metals such as those of the *s*-block and use these sodium salts as precursors to metal complexes via simple ligand exchange reactions. The oxidative addition chemistry of these tetrathiocines to a variety of Main Group metals such as indium(I), tin(II) or antimony(III) could further extend this reaction chemistry.

The current studies have revealed several new avenues for further pursuit. For example a whole series of crown ether derivatives should be readily accessible using this synthetic methodology and offer the potential to develop selective binding for a range of 'hard' metals including the alkali and alkaline earth metals as well as lanthanides. Here the spectroscopic properties of the metal-dithiolate component may act as a reporter to reflect metal binding or the redox properties of the metal-dithiolate or dppf ancilliary ligand could be used in a similar fashion. Notably the role of the phosphine seems to play a decisive role in the degree of aggregation of the metal-dithiolate and a more careful examination of other phosphines may lead to other oligomers of formulation $M_x(L)_x(PR_3)_y$ where L is a dithiolate ligand. In this context $Ni_3(bdt)_3(PPh_3)_2$ and $Ni_3(bdt)_3(PMePh_2)_2$ has been reported[3] as well as a tetranuclear disulfide Ni_4L_4.[4]

Further work is needed to pursue the potential range of dithiazolyl radicals which can be derived from these tetrathiocines. This chemistry appears synthetically more demanding

but the results presented in Chapter 5, coupled with previous work by Navarro-Moratalla in this group,[5] clearly demonstrate the efficacy of this method. The opportunity to prepare benzo-crown-functionalised radicals offers interesting opportunities for the design of new metal-radical systems in which there is communication between *d*- or *f*-based electrons on the metal and *p*-based radical electrons.

Finally, the tetrathiocines are prepared by the electrophilic addition of S_2Cl_2 to activated aromatics. The heavier *p*-block congener Se_2Cl_2 is likely to exhibit similar reaction chemistry and could provide a versatile synthetic route to the less well studied diselenide complexes. In addition other *p*-block elements such as PCl_3 can undergo electrophilic addition to aromatics[6] and use of activated aromatics such as veratrole could provide access to 1,2-diphosphines which are less readily accessible by conventional routes.

6.3 References

1. See for example: **(a)** C.L. Linfoot, P. Richardson, K.L. McCall, J.R. Durrant, A. Morandeira and N. Robertson, *Solar Energy*, 2011,**85**, 1195; **(b)** S. Dalgleish, J.G. Labram, Z. Li, J. Wang, C.R. McNeill, T.D. Anthopoulos, N. C. Greenham and N. Robertson, *J. Mater. Chem.*, 2011,**21**, 15422.

2. L. Pilia, M. Pizzotti, F. Tessore and N. Robertson, *Inorg. Chem.*, 2014, **53**, 4517.

3. **(a)** M. Cha, J. Sletten, S. Critchlow and J.A.Kovacs, *Inorg. Chim. Acta.*, 1997, **263**, 153; **(b)** E. Cerrada, A. Moreno and M. Laguna, *Dalton Trans.*, 2009, 6825.

4. M.Kockerling and G.Henkel, *Inorg. Chem. Commun.*, 2000, **3**, 117.

5. E. Navarro-Moratalla, ERASMUS report, University of Cambridge, 2007.

6. *Studies in Organic Chemistry*, Electrophilic Additions to Organic Systems, 1982, **9**, 247 (P.B. de la Mere and R. Bolton, Eds).

APPENDIX

Crystallographic Information

** Note that any hydrogen atoms or solvate molecules within each diagram have been removed for clarity.Where more than one molecule exists in the asymmetric unit, just one molecule is illustrated.*

Structure: JW002

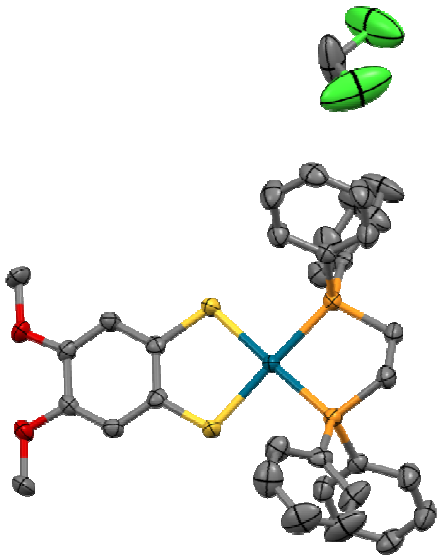

Table 1. Crystal data and structure refinement for JW002

Identification code	jw002	
Empirical formula	C35 H34 Cl2 O2 P2 Pd S2	
Formula weight	789.98	
Temperature	150(2) K	
Wavelength	0.71073 Å	
Crystal system	Tetragonal	
Space group	I-42d	
Unit cell dimensions	a = 20.8660(21) Å	α= 90°
	b = 20.8660(21) Å	β= 90°
	c = 15.5435(16) Å	γ = 90°
Volume	6767.5(15) $Å^3$	
Z	8	
Density (calculated)	1.551 Mg/m^3	
Absorption coefficient	0.956 mm^{-1}	
F(000)	3216	
Crystal size	0.20 x 0.18 x 0.14 mm^3	
Theta range for data collection	1.95 to 24.99°	
Index ranges	-24<=h<=24, -24<=k<=24, -18<=l<=18	
Reflections collected	32531	
Independent reflections	2984 [R(int) = 0.0456]	
Completeness to theta = 28.31°	99.1 %	
Absorption correction	Semi-empirical from equivalents	
Max. and min. transmission	0.8778 and 0.8318	
Refinement method	Full-matrix least-squares on F^2	
Data / restraints / parameters	4126 / 6 / 205	
Goodness-of-fit on F2	1.064	
Final R indices [I>2sigma(I)]	R1 = 0.0289, wR2 = 0.0666	
R indices (all data)	R1 = 0.0325, wR2 = 0.0688	
Absolute structure parameter	0.0(4)	
Largest diff. peak and hole	0.596 and -0.538 e.$Å^{-3}$	

Structure: JW003

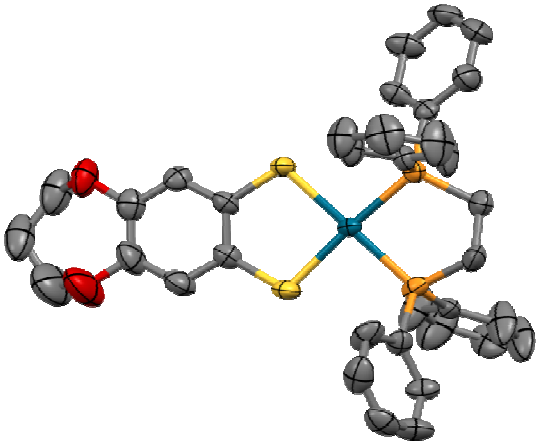

Table 1. Crystal data and structure refinement for JW003

Identification code	jw003	
Empirical formula	C35 H32 O2 P2 Pd S2	
Formula weight	717.07	
Temperature	150(2) K	
Wavelength	0.71073 Å	
Crystal system	Orthorhombic	
Space group	$P2_12_12_1$	
Unit cell dimensions	a = 11.4906(12) Å	α= 90°
	b = 12.9099(14) Å	β= 90°
	c = 21.333(2) Å	γ = 90°
Volume	3164.6(6) $Å^3$	
Z	4	
Density (calculated)	1.505 Mg/m^3	
Absorption coefficient	0.851 mm^{-1}	
F(000)	1464	
Crystal size	0.16 x 0.06 x 0.05 mm^3	
Theta range for data collection	1.84 to 27.50°	
Index ranges	-14<=h<=14, -16<=k<=16, -27<=l<=27	
Reflections collected	36543	
Independent reflections	7243 [R(int) = 0.0465]	
Completeness to theta = 27.50°	100.0 %	
Absorption correction	Empirical	
Max. and min. transmission	0.9587 and 0.8759	
Refinement method	Full-matrix least-squares on F^2	
Data / restraints / parameters	7243 / 68 / 434	
Goodness-of-fit on F2	1.095	
Final R indices [I>2sigma(I)]	R1 = 0.0350, wR2 = 0.0762	
R indices (all data)	R1 = 0.0402, wR2 = 0.0791	
Absolute structure parameter	0.00	
Largest diff. peak and hole	1.029 and -0.639 e.$Å^{-3}$	

Structure: JW004

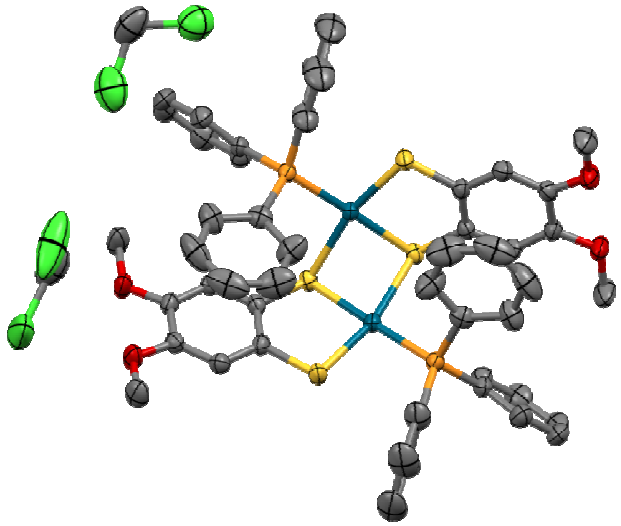

Table 1. Crystal data and structure refinement for JW004

Identification code	jw004	
Empirical formula	C55 H52 Cl6 O4 P2 Pd2 S4	
Formula weight	1392.714	
Temperature	150(2) K	
Wavelength	0.71073 Å	
Crystal system	Orthorhombic	
Space group	$P2_12_12$	
Unit cell dimensions	*a* = 16.9591(17) Å	α= 90°
	b = 20.351(2) Å	β= 90°
	c = 8.4374(8) Å	γ = 90°
Volume	2912.1(5) Å^3	
Z	2	
Density (calculated)	1.588 Mg/m^3	
Absorption coefficient	1.135 mm^{-1}	
F(000)	1404	
Crystal size	0.31 x 0.22 x 0.19 mm^3	
Theta range for data collection	2.33 to 27.52°	
Index ranges	-21<=h<=22, -25<=k<=26, 10<=l<=10	
Reflections collected	33406	
Independent reflections	6634 [R(int) = 0.0230]	
Completeness to theta = 27.52°	99.6 %	
Absorption correction	Empirical	
Max. and min. transmission	0.8132 and 0.7198	
Refinement method	Full-matrix least-squares on F^2	
Data / restraints / parameters	6634 / 7 / 339	
Goodness-of-fit on F^2	1.061	
Final R indices [I>2sigma(I)]	R1 = 0.0197, wR2 = 0.0489	
R indices (all data)	R1 = 0.0201, wR2 = 0.0491	
Absolute structure parameter	0.00(13)	
Largest diff. peak and hole	0.940 and -0.485 e.Å^{-3}	

Structure: JW005a

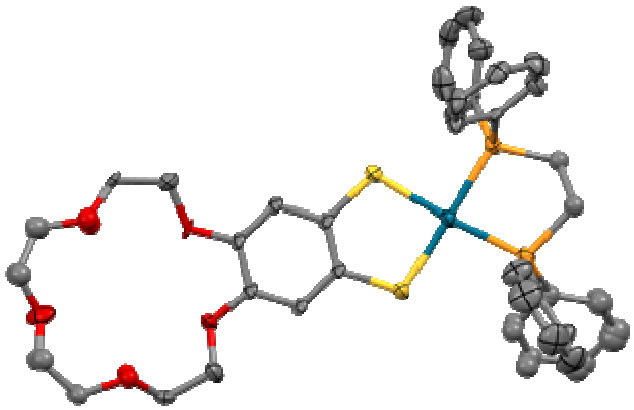

Table 1. Crystal data and structure refinement for JW005

Identification code	jw005	
Empirical formula	C42 H45 O5 P2 Pd S2 N	
Formula weight	876.25	
Temperature	150(2) K	
Wavelength	0.71073 Å	
Crystal system	Monoclinic	
Space group	$P2_1/c$	
Unit cell dimensions	a = 11.8434(12) Å	α = 90°
	b = 13.561(3) Å	β = 101.568(14)°
	c = 24.616(7) Å	γ = 90°
Volume	3873.2(15) Å^3	
Z	4	
Density (calculated)	1.503 Mg/m^3	
Absorption coefficient	0.716 mm^{-1}	
F(000)	1748	
Crystal size	0.34 x 0.16 x 0.14 mm^3	
Theta range for data collection	1.689 to 27.537°	
Index ranges	-6<=h<=6, 0<=k<=17, -31<=l<=0	
Reflections collected	24776	
Independent reflections	4810 [R(int) = 0.0228]	
Completeness to theta = 27.50°	57.8 %	
Absorption correction	Empirical	
Max. and min. transmission	0.9069 and 0.7939	
Refinement method	Full-matrix least-squares on F^2	
Data / restraints / parameters	4810 / 5 / 404	
Goodness-of-fit on F2	1.140	
Final R indices [I>2sigma(I)]	R1 = 0.0316, wR2 = 0.0871	
R indices (all data)	R1 = 0.0341, wR2 = 0.0953	
Largest diff. peak and hole	1.152 and -0.756 e.Å^{-3}	

Structure: JW006

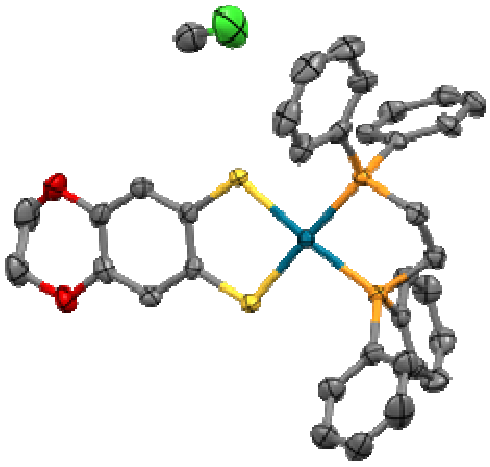

Table 1. Crystal data and structure refinement for JW006

Identification code	jw006	
Empirical formula	C34.50 H31 Cl O2 P2 Pd S2	
Formula weight	745.50	
Temperature	150(2) K	
Wavelength	0.71073 Å	
Crystal system	Monoclinic	
Space group	$P2_1/n$	
Unit cell dimensions	*a* = 17.797(7) Å	α = 90°
	b = 20.004(7) Å	β = 92.047(4)°
	c = 17.816(7) Å	γ = 90°
Volume	6338(4) $Å^3$	
Z	8	
Density (calculated)	1.562 Mg/m^3	
Absorption coefficient	0.934 mm^{-1}	
F(000)	3032	
Crystal size	0.16 x 0.09 x 0.07 mm^3	
Theta range for data collection	1.02 to 26.71°	
Index ranges	-22<=h<=22, -25<=k<=25, -22<=l<=22	
Reflections collected	70375	
Independent reflections	13391 [R(int) = 0.0470]	
Completeness to theta = 26.71°	99.6 %	
Absorption correction	Empirical	
Max. and min. transmission	0.9375 and 0.8649	
Refinement method	Full-matrix least-squares on F^2	
Data / restraints / parameters	13391 / 0 / 764	
Goodness-of-fit on F2	1.102	
Final R indices [I>2sigma(I)]	R1 = 0.0304, wR2 = 0.0694	
R indices (all data)	R1 = 0.0321, wR2 = 0.0704	
Largest diff. peak and hole	1.197 and -0.447 e.$Å^{-3}$	

Structure: JW007

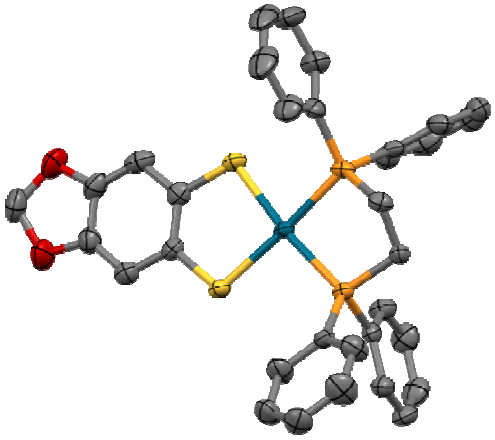

Table 1. Crystal data and structure refinement for JW007

Identification code	jw007	
Empirical formula	C33 H28 O2 P2 Pd S2	
Formula weight	689.01	
Temperature	150(2) K	
Wavelength	0.71073 Å	
Crystal system	Monoclinic	
Space group	$P2_1/n$	
Unit cell dimensions	a = 11.053(5) Å	α = 90°
	b = 12.788(6) Å	β = 97.308(6)°
	c = 20.727(9) Å	γ = 90°
Volume	2906(2) $Å^3$	
Z	4	
Density (calculated)	1.575 Mg/m^3	
Absorption coefficient	0.923 mm^{-1}	
F(000)	1400	
Crystal size	0.18 x 0.04 x 0.04 mm^3	
Theta range for data collection	1.88 to 27.70°	
Index ranges	-14<=h<=14, -16<=k<=16, -27<=l<=26	
Reflections collected	32920	
Independent reflections	6655 [R(int) = 0.0718]	
Completeness to theta = 27.70°	97.7 %	
Absorption correction	Empirical	
Max. and min. transmission	0.9640 and 0.8515	
Refinement method	Full-matrix least-squares on F^2	
Data / restraints / parameters	6655 / 0 / 361	
Goodness-of-fit on F2	1.080	
Final R indices [I>2sigma(I)]	R1 = 0.0439, wR2 = 0.0921	
R indices (all data)	R1 = 0.0621, wR2 = 0.0997	
Largest diff. peak and hole	0.646 and -0.712 e.$Å^{-3}$	

Structure: JW008

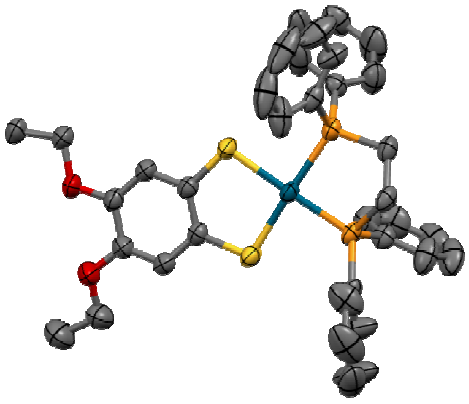

Table 1. Crystal data and structure refinement for JW008

Identification code	jw008	
Empirical formula	C36 H36 O2 P2 Pd S2	
Formula weight	733.11	
Temperature	150(2) K	
Wavelength	0.71073 Å	
Crystal system	Monoclinic	
Space group	$P2_1/c$	
Unit cell dimensions	a = 12.247(3) Å	α= 90°
	b = 13.509(4) Å	β= 91.730(3)°
	c = 23.332(7) Å	γ = 90°
Volume	3858.5(19) $Å^3$	
Z	4	
Density (calculated)	1.262 Mg/m^3	
Absorption coefficient	0.699 mm^{-1}	
F(000)	1504	
Crystal size	0.16 x 0.09 x 0.07 mm^3	
Theta range for data collection	1.66 to 27.57°	
Index ranges	-15<=h<=15, 0<=k<=17, 0<=l<=30	
Reflections collected	8828	
Independent reflections	8828 [R(int) = 0.0000]	
Completeness to theta = 27.57°	98.9 %	
Absorption correction	Empirical	
Max. and min. transmission	0.9527 and 0.8963	
Refinement method	Full-matrix least-squares on F^2	
Data / restraints / parameters	8828 / 0 / 391	
Goodness-of-fit on F2	1.107	
Final R indices [I>2sigma(I)]	R1 = 0.0298, wR2 = 0.0820	
R indices (all data)	R1 = 0.0336, wR2 = 0.0846	
Extinction coefficient	0.00051(9)	
Largest diff. peak and hole	0.688 and -0.316 e.$Å^{-3}$	

Structure: JW009b_0m

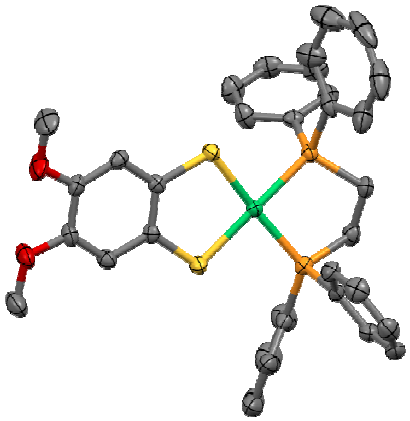

Table 1. Crystal data and structure refinement for JW009b_0m.

Identification code	jw009b_0m	
Empirical formula	C34 H32 Ni O2 P2 S2	
Formula weight	657.37	
Temperature	150(2) K	
Wavelength	0.71073 Å	
Crystal system	Orthorhombic	
Space group	$P2_12_12_1$	
Unit cell dimensions	*a* = 11.9151(12) Å	α = 90°
	b = 12.7964(11) Å	β = 90°
	c = 20.0546(19) Å	γ = 90°
Volume	3057.7(5) $Å^3$	
Z	4	
Density (calculated)	1.428 Mg/m^3	
Absorption coefficient	0.907 mm^{-1}	
F(000)	1368	
Crystal size	0.50 x 0.17 x 0.07 mm^3	
Theta range for data collection	2.55 to 30.03°	
Index ranges	-15<=h<=16, -17<=k<=15, -28<=l<=25	
Reflections collected	20051	
Independent reflections	8721 [R(int) = 0.0353]	
Completeness to theta = 30.03°	99.6 %	
Absorption correction	Semi-empirical from equivalents	
Max. and min. transmission	0.9393 and 0.6599	
Refinement method	Full-matrix least-squares on F^2	
Data / restraints / parameters	8721 / 0 / 373	
Goodness-of-fit on F2	1.086	
Final R indices [I>2sigma(I)]	R1 = 0.0426, wR2 = 0.0881	
R indices (all data)	R1 = 0.0482, wR2 = 0.0903	
Absolute structure parameter	0.094(10)	
Largest diff. peak and hole	0.527 and -0.346 e.$Å^{-3}$	

Structure: JW010

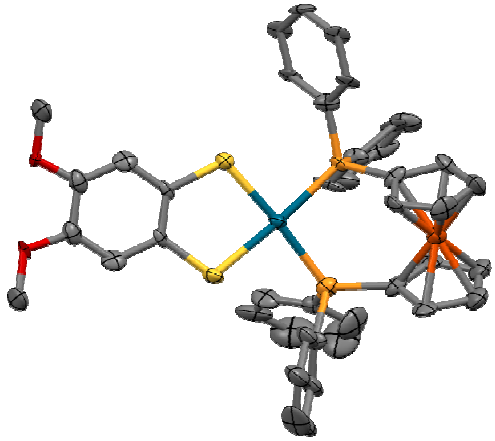

Table 1. Crystal data and structure refinement for JW010

Identification code	jw010	
Empirical formula	C42 H36 Fe O2 P2 Pd S2	
Formula weight	861.02	
Temperature	150(2) K	
Wavelength	0.71073 Å	
Crystal system	Triclinic	
Space group	P-1	
Unit cell dimensions	*a* = 15.232(5) Å	α = 64.850(4)°
	b = 21.963(7) Å	β = 76.688(4)°
	c = 22.470(7) Å	γ = 76.738(4)°
Volume	6547(3) $Å^3$	
Z	6	
Density (calculated)	1.310 Mg/m^3	
Absorption coefficient	0.944 mm^{-1}	
F(000)	2628	
Crystal size	0.27 x 0.06 x 0.02 mm^3	
Theta range for data collection	1.01 to 20.25°	
Index ranges	-14<=h<=14, -18<=k<=21, 0<=l<=21	
Reflections collected	12586	
Independent reflections	12586 [R(int) = 0.0000]	
Completeness to theta = 20.25°	99.2 %	
Absorption correction	Semi-empirical from equivalents	
Max. and min. transmission	0.9814 and 0.7846	
Refinement method	Full-matrix least-squares on F^2	
Data / restraints / parameters	12586 / 325 / 1093	
Goodness-of-fit on F^2	1.077	
Final R indices [I>2sigma(I)]	R1 = 0.0632, wR2 = 0.1659	
R indices (all data)	R1 = 0.0831, wR2 = 0.1735	
Largest diff. peak and hole	0.643 and -0.746 e.$Å^{-3}$	

Structure: JW011

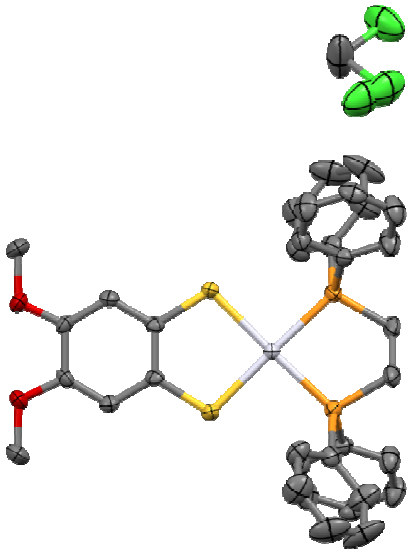

Table 1. Crystal data and structure refinement for JW011

Identification code	jw011	
Empirical formula	C35 H34 Cl2 O2 P2 Pt S2	
Formula weight	878.67	
Temperature	150(2) K	
Wavelength	0.71073 Å	
Crystal system	Tetragonal	
Space group	I-42*d*	
Unit cell dimensions	a = 20.864(6) Å	α= 90°
	b = 20.864(6) Å	β= 90°
	c = 15.544(5) Å	γ = 90°
Volume	6766(3) $Å^3$	
Z	8	
Density (calculated)	1.725 Mg/m^3	
Absorption coefficient	4.556 mm^{-1}	
F(000)	3472	
Crystal size	0.22 x 0.15 x 0.15 mm^3	
Theta range for data collection	1.38 to 28.46°	
Index ranges	-26<=h<=27, -27<=k<=27, -20<=l<=20	
Reflections collected	39594	
Independent reflections	4142 [R(int) = 0.0420]	
Completeness to theta = 20.25°	98.4 %	
Absorption correction	Semi-empirical from equivalents	
Max. and min. transmission	0.5482 and 0.4339	
Refinement method	Full-matrix least-squares on F^2	
Data / restraints / parameters	4142/0/205	
Goodness-of-fit on F^2	1.086	
Final R indices [I>2sigma(I)]	R1 = 0.0172, wR2 = 0.0407	
R indices (all data)	R1 = 0.0181, wR2 = 0.0411	
Largest diff. peak and hole	0.647 and -0.487 e.$Å^{-3}$	

Structure: JW014

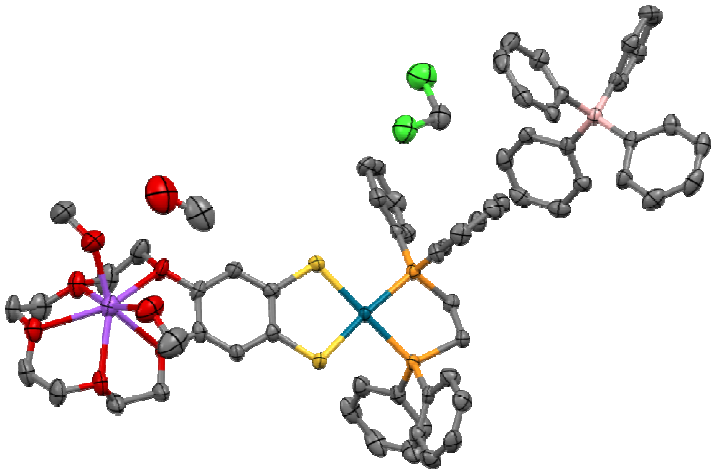

Table 1. Crystal data and structure refinement for JW014

Identification code	jw014	
Empirical formula	C68 H76 B Cl2 Na O8 P2 Pd S2	
Formula weight	1358.45	
Temperature	150(2) K	
Wavelength	0.71073 Å	
Crystal system	Triclinic	
Space group	P-1	
Unit cell dimensions	*a* = 9.565(7) Å	α = 95.318(9)°
	b = 17.558(12) Å	β = 98.525(9)°
	c = 20.088(14) Å	γ = 100.269(9)°
Volume	3258(4) Å^3	
Z	2	
Density (calculated)	1.385 Mg/m^3	
Absorption coefficient	0.541 mm^{-1}	
F(000)	1412	
Crystal size	0.27 x 0.12 x 0.05 mm^3	
Theta range for data collection	2.07 to 27.60°	
Index ranges	-12<=h<=12, -22<=k<=22, -25<=l<=26	
Reflections collected	36253	
Independent reflections	14503 [R(int) = 0.0410]	
Completeness to theta = 27.60°	95.9 %	
Absorption correction	Semi-empirical from equivalents	
Max. and min. transmission	0.9735 and 0.8677	
Refinement method	Full-matrix least-squares on F^2	
Data / restraints / parameters	14503 / 3 / 779	
Goodness-of-fit on F2	1.054	
Final R indices [I>2sigma(I)]	R1 = 0.0489, wR2 = 0.1115	
R indices (all data)	R1 = 0.0642, wR2 = 0.1207	
Largest diff. peak and hole	1.316 and -0.719 e.Å^{-3}	

Structure: JW016

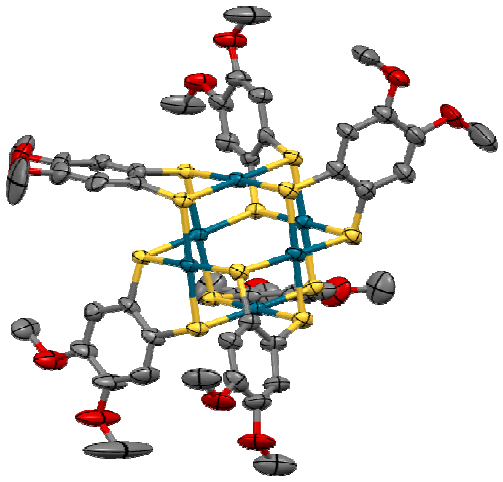

Table 1. Crystal data and structure refinement for JW016

Identification code	jw016	
Empirical formula	C48 H48 O12 Pd6 S12	
Formula weight	1839.98	
Temperature	150(2) K	
Wavelength	0.71073 Å	
Crystal system	Orthorhombic	
Space group	$P2_12_12$	
Unit cell dimensions	a = 21.721(6) Å	α = 90°
	b = 22.370(6) Å	β = 90°
	c = 16.448(4) Å	γ = 90°
Volume	7992(4) Å^3	
Z	4	
Density (calculated)	1.529 Mg/m^3	
Absorption coefficient	1.677 mm^{-1}	
F(000)	3600	
Crystal size	0.37 x 0.21 x 0.18 mm^3	
Theta range for data collection	1.80 to 27.58°	
Index ranges	-28<=h<=28, 0<=k<=29, 0<=l<=21	
Reflections collected	18317	
Independent reflections	18317 [R(int) = 0.0000]	
Completeness to theta = 27.58°	99.4 %	
Absorption correction	Semi-empirical from equivalents	
Max. and min. transmission	0.7522 and 0.5757	
Refinement method	Full-matrix least-squares on F^2	
Data / restraints / parameters	18317 / 0 / 715	
Goodness-of-fit on F2	1.035	
Final R indices [I>2sigma(I)]	R1 = 0.0291, wR2 = 0.0782	
R indices (all data)	R1 = 0.0319, wR2 = 0.0799	
Absolute structure parameter	0.016(17)	
Largest diff. peak and hole	0.923 and -0.579 e.Å^{-3}	

Structure: JW017

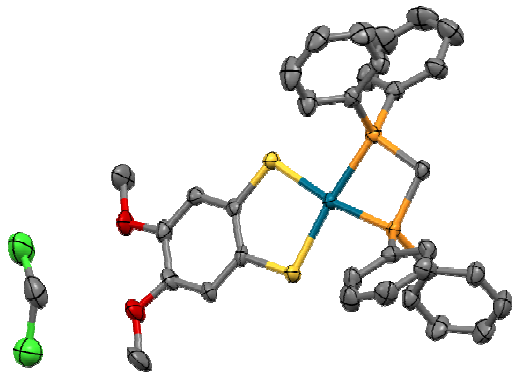

Table 1. Crystal data and structure refinement for JW017

Identification code	JW017	
Empirical formula	C34 H32 Cl2 O2 P2 Pd S2	
Formula weight	775.95	
Temperature	150(2) K	
Wavelength	0.71073 Å	
Crystal system	Monoclinic	
Space group	$P2_1/c$	
Unit cell dimensions	*a* = 12.136(5) Å	α = 90°
	b = 23.488(9) Å	β = 102.527(5)°
	c = 24.456(10) Å	γ = 90°
Volume	6805(5) $Å^3$	
Z	8	
Density (calculated)	1.515 Mg/m^3	
Absorption coefficient	0.949 mm^{-1}	
F(000)	3152	
Crystal size	0.200 x 0.150 x 0.100 mm^3	
Theta range for data collection	1.216 to 26.526°	
Index ranges	-15<=h<=15, -29<=k<=29, -30<=l<=30	
Reflections collected	72349	
Independent reflections	14081 [R(int) = 0.0638]	
Completeness to theta = 25.242°	99.9 %	
Absorption correction	Empirical	
Max. and min. transmission	0.745 and 0.625	
Refinement method	Full-matrix least-squares on F^2	
Data / restraints / parameters	14081 / 0 / 779	
Goodness-of-fit on F2	1.147	
Final R indices [I>2sigma(I)]	R1 = 0.0557, wR2 = 0.1159	
R indices (all data)	R1 = 0.0705, wR2 = 0.1219	
Extinction coefficient	n/a	
Largest diff. peak and hole	1.862 and -1.363 e.$Å^{-3}$	

Structure: JW018

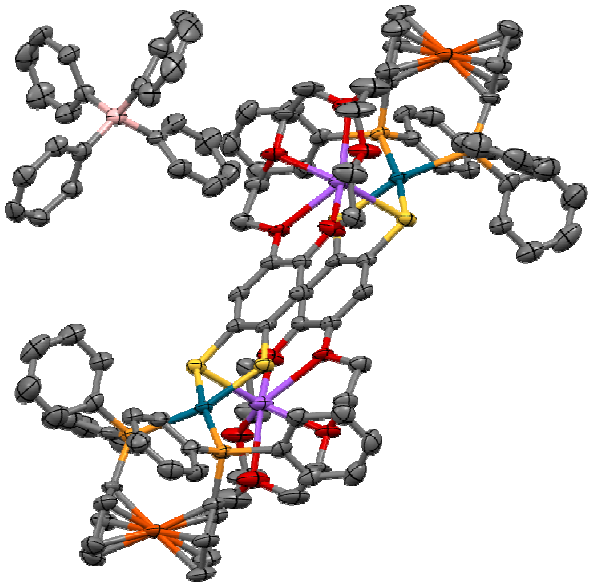

Table 1. Crystal data and structure refinement for JW018

Identification code	jw018presq_sq	
Empirical formula	C144 H132 B2 Fe2 Na2 O10 P4 Pd2 S4	
Formula weight	2666.70	
Temperature	150(2) K	
Wavelength	0.71073 Å	
Crystal system	Triclinic	
Space group	P-1	
Unit cell dimensions	a = 17.450(4) Å	α= 82.45(3)°
	b = 18.650(4) Å	β= 89.97(3)°
	c = 22.080(4) Å	γ = 88.92(3)°
Volume	7122(3) $Å^3$	
Z	2	
Density (calculated)	1.243 Mg/m^3	
Absorption coefficient	0.612 mm^{-1}	
F(000)	2752	
Crystal size	0.160 x 0.130 x 0.070 mm^3	
Theta range for data collection	0.930 to 27.499°	
Index ranges	-22<=h<=22, -22<=k<=22, -28<=l<=28	
Reflections collected	78176	
Independent reflections	29815 [R(int) = 0.0451]	
Completeness to theta = 25.242°	98.6 %	
Absorption correction	Semi-empirical from equivalents	
Max. and min. transmission	0.978 and 0.912	
Refinement method	Full-matrix least-squares on F^2	
Data / restraints / parameters	29813 / 292 / 1279	
Goodness-of-fit on F^2	1.050	
Final R indices [I>2sigma(I)]	R1 = 0.0972, wR2 = 0.2418	
R indices (all data)	R1 = 0.1208, wR2 = 0.2656	
Extinction coefficient	n/a	
Largest diff. peak and hole	2.516 and -1.999 e.$Å^{-3}$	

Structure: JW019

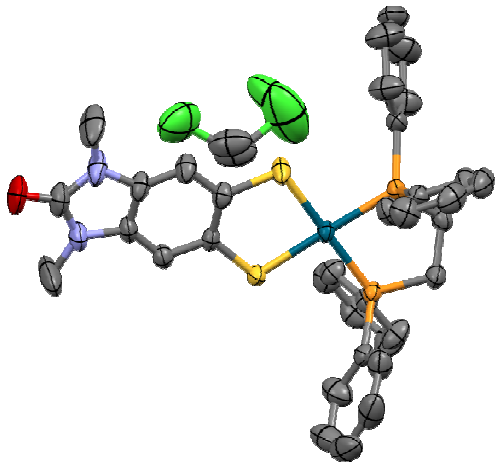

Table 1. Crystal data and structure refinement for JW019

Identification code	JW019	
Empirical formula	C36 H34 Cl2 N2 O P2 Pd S2	
Formula weight	814.01	
Temperature	173(2) K	
Wavelength	0.71073 Å	
Crystal system	Monoclinic	
Space group	$P2_1/c$	
Unit cell dimensions	a = 14.1330(5) Å	α= 90°
	b = 24.2766(10) Å	β= 106.2705(15)°
	c = 22.0469(9) Å	γ = 90°
Volume	7261.4(5) $Å^3$	
Z	8	
Density (calculated)	1.489 Mg/m^3	
Absorption coefficient	0.893 mm^{-1}	
F(000)	3312	
Crystal size	0.511 x 0.200 x 0.062 mm^3	
Theta range for data collection	2.931 to 28.312°	
Index ranges	-18<=h<=18, -32<=k<=32, -29<=l<=29	
Reflections collected	135287	
Independent reflections	18020 [R(int) = 0.0641]	
Completeness to theta = 25.242°	99.8 %	
Absorption correction	Empirical	
Max. and min. transmission	0.7457 and 0.6577	
Refinement method	Full-matrix least-squares on F^2	
Data / restraints / parameters	18020 / 19 / 845	
Goodness-of-fit on F^2	1.055	
Final R indices [I>2sigma(I)]	R1 = 0.0408, wR2 = 0.0837	
R indices (all data)	R1 = 0.0661, wR2 = 0.1001	
Extinction coefficient	n/a	
Largest diff. peak and hole	1.293 and -1.505 e.$Å^{-3}$	

Structure: JW020

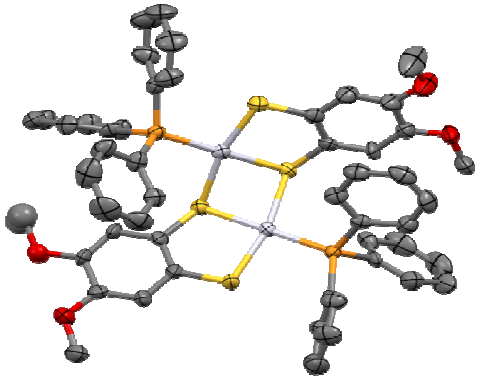

Table 1. Crystal data and structure refinement for JW020

Identification code	jw020_a_sq	
Empirical formula	C52 H46 O4 P2 Pt2 S4	
Formula weight	1315.25	
Temperature	173(2) K	
Wavelength	0.71073 Å	
Crystal system	Monoclinic	
Space group	$P2_1/c$	
Unit cell dimensions	a = 18.3891(8) Å	α= 90°
	b = 16.3542(8) Å	β= 105.6010(16)°
	c = 18.1252(9) Å	γ = 90°
Volume	5250.1(4) $Å^3$	
Z	4	
Density (calculated)	1.664 Mg/m^3	
Absorption coefficient	5.585 mm^{-1}	
F(000)	2560	
Crystal size	0.370 x 0.140 x 0.110 mm^3	
Theta range for data collection	2.858 to 26.373°	
Index ranges	-22<=h<=20, -20<=k<=20, -22<=l<=22	
Reflections collected	105199	
Independent reflections	10737 [R(int) = 0.0738]	
Completeness to theta = 25.242°	99.8 %	
Absorption correction	Empirical	
Max. and min. transmission	0.7461 and 0.4241	
Refinement method	Full-matrix least-squares on F^2	
Data / restraints / parameters	10737 / 1 / 578	
Goodness-of-fit on F^2	1.084	
Final R indices [I>2sigma(I)]	R1 = 0.0389, wR2 = 0.0832	
R indices (all data)	R1 = 0.0521, wR2 = 0.0925	
Extinction coefficient	n/a	
Largest diff. peak and hole	3.363 and -1.158 e.$Å^{-3}$	

Structure: JW022

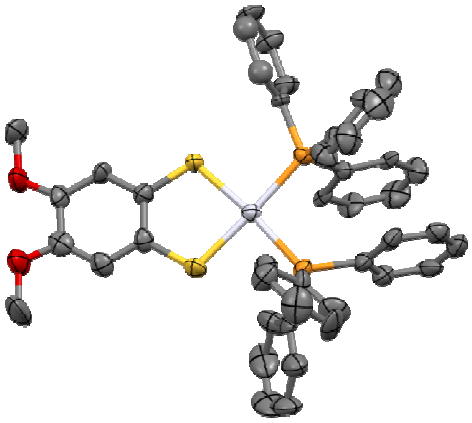

Table 1. Crystal data and structure refinement for mo_jw022_0m_a_sq.

Identification code	mo_jw022_0m_a_sq	
Empirical formula	C44 H38 O2 P2 Pt S2	
Formula weight	919.89	
Temperature	173(2) K	
Wavelength	0.71073 Å	
Crystal system	Monoclinic	
Space group	$P2_1/n$	
Unit cell dimensions	a = 11.1383(8) Å	α= 90°.
	b = 25.343(2) Å	β= 104.980(3)°.
	c = 18.1408(13) Å	γ = 90°.
Volume	4946.6(7) $Å^3$	
Z	4	
Density (calculated)	1.235 Mg/m^3	
Absorption coefficient	3.014 mm^{-1}	
F(000)	1832	
Crystal size	0.500 x 0.160 x 0.130 mm^3	
Theta range for data collection	2.942 to 30.530°	
Index ranges	-15<=h<=15, -36<=k<=36, -24<=l<=25	
Reflections collected	194807	
Independent reflections	15048 [R(int) = 0.0940]	
Completeness to theta = 25.242°	99.5 %	
Absorption correction	Semi-empirical from equivalents	
Max. and min. transmission	0.7461 and 0.4964	
Refinement method	Full-matrix least-squares on F^2	
Data / restraints / parameters	15048 / 0 / 447	
Goodness-of-fit on F2	1.103	
Final R indices [I>2sigma(I)]	R1 = 0.1148, wR2 = 0.2868	
R indices (all data)	R1 = 0.1237, wR2 = 0.2913	
Extinction coefficient	0.0077(4)	
Largest diff. peak and hole	5.671 and -8.009 e.$Å^{-3}$	

Structure: MH6

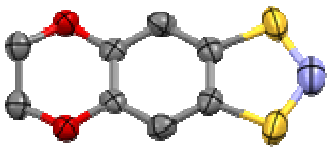

Table 1. Crystal data and structure refinement for MH6

Identification code	MH6	
Empirical formula	C8 H6 N O2 S2	
Formula weight	212.26	
Temperature	170(2) K	
Wavelength	1.54178 Å	
Crystal system	Orthorhombic	
Space group	$C222_1$	
Unit cell dimensions	a = 3.8382(3) Å	α= 90°.
	b = 19.7534(12) Å	β= 90°.
	c = 10.7869(7) Å	γ = 90°.
Volume	817.84(10) $Å^3$	
Z	4	
Density (calculated)	1.724 Mg/m^3	
Absorption coefficient	5.597 mm^{-1}	
F(000)	436	
Crystal size	0.260 x 0.120 x 0.030 mm^3	
Theta range for data collection	4.098 to 58.903°.	
Index ranges	-4<=h<=4, -21<=k<=20, -11<=l<=10	
Reflections collected	2123	
Independent reflections	585 [R(int) = 0.0456]	
Completeness to theta = 67.679°	80.4 %	
Absorption correction	Empirical	
Max. and min. transmission	0.7515 and 0.5069	
Refinement method	Full-matrix least-squares on F^2	
Data / restraints / parameters	585 / 11 / 61	
Goodness-of-fit on F^2	1.128	
Final R indices [I>2sigma(I)]	R1 = 0.0381, wR2 = 0.1001	
R indices (all data)	R1 = 0.0399, wR2 = 0.1013	
Absolute structure parameter	0.34(6)	
Extinction coefficient	n/a	
Largest diff. peak and hole	0.346 and -0.261 $e.Å^{-3}$	

Structure: MH007

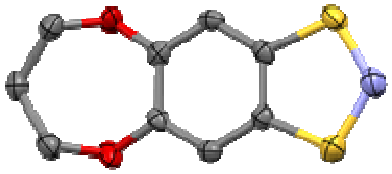

Table 1. Crystal data and structure refinement for MH007

Identification code	MH007_a	
Empirical formula	C9 H8 N O2 S2	
Formula weight	226.28	
Temperature	173(2) K	
Wavelength	0.71073 Å	
Crystal system	Orthorhombic	
Space group	Pbca	
Unit cell dimensions	a = 11.5892(4) Å	α= 90°
	b = 7.9390(3) Å	β= 90°
	c = 20.1201(7) Å	γ = 90°
Volume	1851.18(11) $Å^3$	
Z	8	
Density (calculated)	1.624 Mg/m^3	
Absorption coefficient	0.543 mm^{-1}	
F(000)	936	
Crystal size	0.403 x 0.240 x 0.046 mm^3	
Theta range for data collection	3.271 to 26.423°	
Index ranges	-14<=h<=14, -9<=k<=9, -25<=l<=25	
Reflections collected	21654	
Independent reflections	1901 [R(int) = 0.0384]	
Completeness to theta = 25.242°	99.8 %	
Absorption correction	Semi-empirical from equivalents	
Max. and min. transmission	0.7454 and 0.6662	
Refinement method	Full-matrix least-squares on F^2	
Data / restraints / parameters	1901 / 0 / 127	
Goodness-of-fit on F^2	1.069	
Final R indices [I>2sigma(I)]	R1 = 0.0300, wR2 = 0.0717	
R indices (all data)	R1 = 0.0369, wR2 = 0.0762	
Extinction coefficient	n/a	
Largest diff. peak and hole	0.282 and -0.280 $e.Å^{-3}$	

VITA AUCTORIS

Name: Justin David Wrixon

Education: St. Thomas of Villanova Catholic Secondary School, LaSalle, ON, 2007.

University of Windsor, Windsor, ON, 2012, B.Sc.[H] Chemistry with Thesis.

University of Windsor, Windsor, ON, 2015, M.Sc. Chemistry.

Publications: J. D. Wrixon, J. J. Hayward, O. Raza and J. M. Rawson, *Dalton Trans.*, 2014, **43**, 2134.

J. D. Wrixon, J. J. Hayward and J. M. Rawson, *Inorg. Chem.*, 2015, accepted.

J. D. Wrixon, Z. Ahmed, M. U. Anwar, Y. Beldjoudi, N. Hamidouche, J. J. Hayward and J. M. Rawson, *Polyhedron*, 2015, accepted.

Conferences: 13th International Symposium on Inorganic Ring Systems, Victoria, BC, July 28 – August 2, 2012 (***Poster Presentation***)

46th Inorganic Discussion Weekend, Toronto, ON, November 8 – 10, 2013. (***Poster Presentation***)